Alma Mater Studiorum – Università di Bologna

DOTTORATO DI RICERCA IN

ONCOLOGIA, EMATOLOGIA e PATOLOGIA

Ciclo XXXII

**Settore Concorsuale: 06/F4**

**Settore Scientifico Disciplinare: MED/33**

# ABC TRANSPORTERS OF THE A SUBFAMILY: POTENTIAL PROGNOSTIC MARKERS AND CANDIDATES FOR ANTIBODY SELECTION FROM PHAGE-DISPLAY LIBRARIES FOR THERAPEUTIC USE IN EWING SARCOMA

**Presentata da: Giudice Anna Maria**

**Coordinatore Dottorato**

**Prof. Pier-Luigi Lollini**

**Supervisore**

**Prof.ssa Katia Scotlandi**

**Co-supervisori**

**Prof. Davide Maria Donati**
**Prof. Mauro Magnani**

**Esame finale anno 2020**

*A mia madre*

# Table of contents

# Abstract

In Ewing sarcoma the association of ATP-binding cassette (ABC) transporters with patient outcomes is still poorly explored and controversial. In this study, for the first time, the investigation of associations with prognosis has been extended to numerous ABC transporters belonging to different subfamilies; unexpected associations with favourable outcomes were observed for two ABC transporters belonging to the A subfamily, ABCA6 and ABCA7, in primary tumors, whereas no associations with the canonical multidrug ABC transporters were identified.

The ABC members of the A subfamily are involved in lipid transportation and efflux from cells, particularly cholesterol and phospholipids. Our clinical data support the drug-efflux independent contribution to cancer progression of the ABCAs, which has been further confirmed in Ewing sarcoma PDX-derived cell lines. The overexpression of ABCA6 and ABCA7 impaired the *in vitro* migratory ability of Ewing sarcoma cells and increased the chemosensitivity to doxorubicin; the impact of these ABCA transporters on tumor progression seems to be mediated by low intracellular cholesterol accumulation, supporting the role of these proteins in lipid transport. In addition, ABCA6 and ABCA7 are in turn regulated by transcription factors involved in cellular regulation of lipid metabolism: the expression of ABCA6 was found to be induced by the direct binding of FoxO1/FoxO3a to its promoter and was repressed by IGF1R/Akt signaling, whereas the expression of ABCA7 was regulated by p53.

The data point to ABCA6 and ABCA7 as potential prognostic markers in Ewing sarcoma and suggest the IGF1/ABCA/lipid axis as an intriguing therapeutic target. Agonist monoclonal antibodies towards ABCA6/7 or inhibitors of cell cholesterol biosynthesis, such as statins or aminobiphoshonates, may be investigated as therapeutic options in combination with conventional chemotherapy for patients who express low levels of both transporters.

Considering that no monoclonal antibodies selectively targeting extracellular domains of ABCA6 and ABCA7 are currently available, the second part of the project has been dedicated to the generation of human antibody phage-display libraries as tools for selecting monoclonal antibodies in scFv format. Particularly, a novel synthetic naïve human antibody phage-display library has been designed, cloned and characterized, whereas a disease-specific library using the antibody genes repertoire of Ewing sarcoma patients is currently being developed. The first library takes advantages of the high variability of a rationally designed naïve repertoire to be a useful tool for isolating antibodies towards all potential antigens, including the ABCAs, while the Ewing sarcoma-specific library may present the benefit of an enrichment in antibodies specific for tumor-associated antigens.

# 1. Introduction

## 1.1. Ewing Sarcoma

### 1.1.1. Classification

Sarcomas are a heterogeneous group of mesenchymal neoplasms that account for 1-2% of all adult malignancies. There are more than 50 different subtypes which are divided into two broad categories: soft-tissue sarcomas and bone sarcomas [1].
Primary bone sarcomas are rare, accounting for less than 0.2% of malignant neoplasms registered in the EUROCARE (European Cancer Registry based study on survival and care of cancer patients) database [2], with distinct patterns of incidence associated to different bone tumour subtypes. Osteosarcoma and Ewing sarcoma have a relatively high incidence in the second decade of life, whereas chondrosarcoma is more common in older age [3] [4].

Ewing sarcoma is a very aggressive bone tumor of mesenchymal origin [5], described for the first time in 1921 by James Ewing as a "diffuse endothelioma of bone" [6]. Because of its highly undifferentiated small round cell phenotype, for many years the distinction between Ewing sarcoma and others small round blue cell tumors of childhood was essentially a diagnosis of exclusion until the advancements in molecular and genetic techniques led to the identification of Ewing sarcoma-specific chromosome aberrations.
Historically, it belongs to the Ewing's sarcoma family tumors (ESFT) comprehending osseous and extra-skeletal Ewing sarcoma, Askin tumor and peripheral primitive neuroectodermal tumor (PNET) [7, 8]. However, the 2013 WHO classification of sarcomas uniformly defined these tumours as 'Ewing sarcoma' [9], which are characterized by pathognomonic FET–ETS chimeric gene fusions [10] [11]. The WHO classification also includes the term 'Ewing-like sarcomas', which are small round cell sarcomas with morphologically similar appearances to Ewing sarcoma but are characterized by different fusion genes and clinical and pathological features, such as CIC-fused and BCOR-rearranged sarcomas [12] [13, 14].

### 1.1.2. Epidemiology and risk factors

Ewing sarcoma is the second most frequent bone tumour of childhood and adolescence after osteosarcoma, with an annual incidence rate of three per million and a peak incidence at the age of 15 years; boys are slightly more affected than girls with a ratio of 3:2 [15].

No environmental factor has been identified as a risk factor for this tumor [16] and there is no evidence regarding familiar predisposition [17] beside some studies reported an increased risk of neuroectodermal tumors and stomach cancer in family members of ES patients [18] or congenital mesenchymal defects in ES patients [19].

Ethnicity represents an important epidemiologic factor with striking disparities in Ewing sarcoma incidence across populations. Specifically, Ewing sarcoma is predominantly observed in Caucasians, with an estimated incidence of ~1.5 cases per million children and young adults, more than in Africans and Asians accounting for annual rates of ~0.8 and ~0.2 cases per million children, respectively, implying that genetic variants specific to European ancestry could influence the tumor risk [20] [21] [15] [22].

### 1.1.3. Localization and histopathology

Ewing sarcoma is a highly aggressive and poor differentiated disease composed by small round cells. It mostly affects bone, occurring predominantly in the pelvis, femur, tibia and ribs, but can also involve soft tissues including kidney, lung, bladder and prostate.

Microscopically this cancer is characterized by sheets of small rounded cells closely packed, without matrix and rich in glycogen: the cytoplasm is scarce, pale, granular and with poorly defined limits; nuclei, on the other hand, present a distinct nuclear membrane and they represent the bigger part of the cell, with a distinct nuclear membrane and powder-like chromatin (Figure 1).

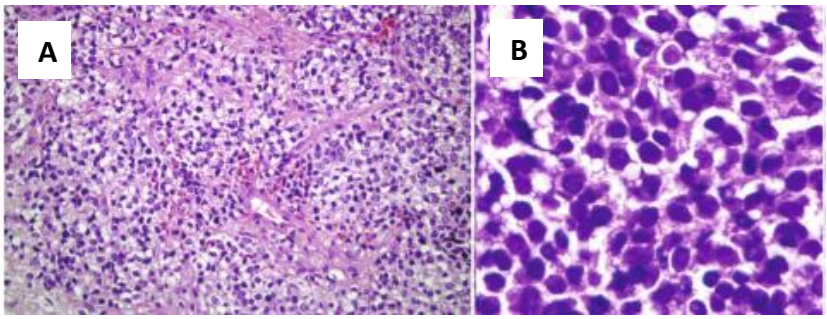

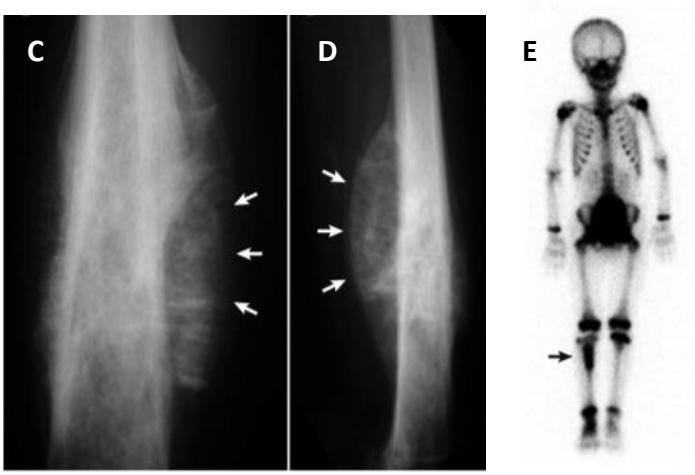


**Figure 1.** Histologic and radiographic appearance of Ewing sarcoma. The panels A) and B) are haemotoxylin and eosin stained sections. Conventional Ewing sarcoma showing a diffuse and vaguely lobular appearance at low-power magnification in (A) (magnification ×10); characteristic fairly monotonous arrangement of small round cells in (B) (magnification ×40); anteroposterior (C) and lateral (D) X-ray images showing an osteolytic lesion of a Ewing sarcoma and involvement of the periosteal soft tissue (arrows) in the right femur of a 14-year-old boy; E) Bone scintigraphy of a 6-year-old male patient highlighting a Ewing sarcoma tumour mass comprising his right tibia. Adapted from Grunewald TGP et al., 2018 [23].

### 1.1.4. Molecular biology and genomic landscape

Conventionally, bone sarcomas or soft tissues can be cytogenetically distinguished in two groups: one group characterized by simple near-diploid karyotype with few chromosome rearrangements and one group with a complex karyotype and a severe disturbance in genomic stability [24]. Ewing sarcoma belongs to the simple karyotype sarcomas group as it carries a tumor-specific recurrent chromosome aberration leading to the fusion of the *EWSR1* gene with one of several members of the *ETS* family of transcription factor [25]. In 85% of the cases, patients express the t(11;22)(q24;q12) translocation which produces the **EWS-FLI1** chimeric protein, the main patognomonic alteration of Ewing sarcoma. In other 10-15% of the cases, the translocation t(21;12)(22;12) leads to the fusion of *EWSR*1 gene to *ERG*, while others translocations account only 1 to 5% of the cases and result in the *EWSR1* gene fused with other *ETS* transcription factors including *ETV1*, *ETV4*, or *FEV* or rarely by *EWSR1* being replaced by another member of the *FET* family of transcription factors, *FUS* [11] (Table 1).

| Translocation | Fusion gene | Frequency (%) |
|---|---|---|
| t(11;22)(q24;q12) | *EWSR1-FLI1* | ≈ 85 |
| t(21;22)(q22;q12) | *EWSR1-ERG* | ≈ 10 |
| t(7;22)(p22;q12) | *EWSR1-ETV1* | <1 |
| t(17;22)(q21;q12) | *EWSR1-ETV4* | <1 |
| t(2;22)(q33;q12) | *EWSR1-FEV* | <1 |
| t(16;21)(p11;q22) | *FUS–ERG* | <1 |
| t(2;16)(q35;p11) | *FUS–FEV* | <1 |

**Table 1.** Current *FET–ETS* fusion pairings identified in Ewing sarcoma.

The chimera holds the amino terminus of *EWSR1* gene and the carboxy terminus of the *ETS* gene acting as an aberrant transcription factor. The *EWSR1* gene, located on chromosome 22, belongs to a subgroup of RNA-binding proteins called FET family and is ubiquitously expressed [26]. EWS is a nuclear protein involved in transcriptional regulation and RNA processing since it seems to be recruited to promoter regions acting as a promoter-specific transactivator upon association with other factors [16], such as RNA polymerase II, TFIID and CBP/p300 [11]. The glutamine-rich N-terminal portion stimulates transcription if fused with DNA-binding domains, as described in Ewing sarcoma [27]. Protein members of ETS family are transcription factors whose DNA binding domain is part of the EWS-ETS chimeric product causing its aberrant transcriptional activity.

In the *EWS-FLI1* fusion gene, breakpoints most commonly interest exon 7 of *EWSR1* and exon 6 of *FLI1* (fusion type I); this chimeric protein shows a lower transactivation potential than a second variant, interesting instead *EWSR1* exon 7 and *FLI1* exon 5 (fusion type II) [26]. This lower transactivation potential appears to correlate with a higher relapse-free survival of Ewing sarcoma patients [28].

Since the cloning of the *EWS-FLI1* fusion oncogene [26], the predominant point of view has been that *EWS-FLI1* plays a central role in Ewing sarcomagenesis [5, 29-32]. The EWS-FLI1 gene product indeed regulates the expression of several genes critical for cancer progression (e.g. C-MYC) [33], drives widespread epigenetic reprogramming by inducing *de novo* (Ewing-specific) enhancers and by repressing enhancers that are instead active in many normal cell types, including those of mesenchymal origin [34, 35]. Accordingly, the chimeric protein expression can transform murine fibroblasts such as NIH3T3 [27] and C3H10T1/2 [36]; it is necessary for proliferation and

tumorigenicity of Ewing sarcoma cells [5, 29-32], while its silencing causes apoptosis and decreases tumoral growth both *in vitro* and *in vivo* [37-40], suggesting a role for EWS-FLI1 as principal oncogenic driver.

However, a variety of evidence also suggest that EWS-FLI1 alone cannot fully explain the Ewing sarcomagenesis: (i) EWS-FLI1 alone cannot transform any human cell types including mesenchymal stem cells (MSCs) which are the putative cells of origin of Ewing sarcoma [29, 31]; (ii) generating a transgenic mouse model of Ewing sarcoma by using EWS-FLI1 alone has been unsuccessful [31, 41]; and (iii) other genetic alterations, although far less common than EWS-FLI1 translocation, confer worse clinical outcome [29, 30]; for instance, inactivating mutations of TP53 occur in ~ 10% of cases and are associated with poor outcome when compared to patients with wild type TP53 [42].

These latter results underlie the importance of a specific cellular context for EWS-FLI1-mediated oncogenesis [43], suggesting that further factors are needed to create a permissive background to induce oncogenic transformation.

Critical factors include the presence of an intact insulin-like growth factors (IGF) system and the expression of CD99, a 32kDa integral membrane glycoprotein expressed in 90% of the cases. EWS-FLI1 directly affects at transcriptional level the expression of components of the **IGF system**, thus creating a major autocrine loop IGF-1/IGF-1R that sustains cell growth, pathogenesis and malignant behaviour of Ewing sarcoma [44]. Particularly, the aberrant chimeric transcription factor enhances IGF1 promoter activation [45] and the expression of cell surface protease (*i.e.* pappalysin-1 (PAPPA)) which degrades IGF binding proteins (IGFBPs) with the consequence of increased IGF bioavailability [46].

**CD99** is a protein highly expressed in Ewing sarcoma; it is required for the oncogenic phenotype by blocking differentiation whilst supporting growth and cell migration [47, 48]. Because of its high expression, CD99 is used as reliable diagnostic biomarker of Ewing Sarcoma, together with the specific *EWS-ETS* chromosomal translocations [7, 49] (Figure 2).

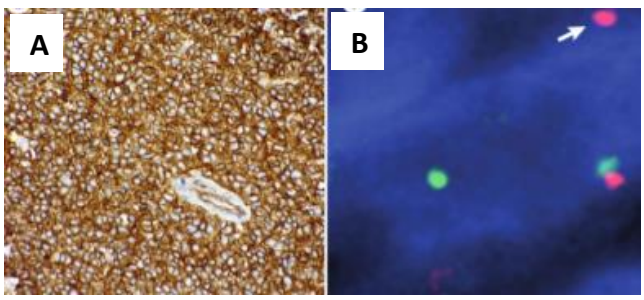


**Figure 2.** Diagnostic biomarker expression. A) Biopsy specimen of a 16-year-old boy showing diffuse and intense plasma membrane expression of CD99 by immunohistochemical staining (magnification ×10); B)

EWSR1 gene rearrangements by fluorescence in situ hybridization (arrow) with a break-apart EWSR1 probe (magnification ×600). Adapted from Grunewald TGP et al., 2018 [23].

### 1.1.5. Diagnosis and course

Routinely, Ewing sarcoma diagnosis requires a multidisciplinary approach involving (i) histochemical and immunohistochemical reactions to test different biological markers expression, (ii) molecular genetic and (iii) imaging techniques.

Lack of exclusive morphologic characteristics made the diagnosis of this tumor difficult up to the 90's when EWS-FLI1 fusion gene was discovered and, consequently, the molecular analysis was introduced in the clinical practice. Biopsy from at least two sites of the tumor should be obtained for pathological, cytogenetic and molecular studies. In addition, as Ewing sarcoma metastasize to bone marrow in ~10% of cases, patients must undergo bone marrow aspiration and biopsy [50]. Currently, no blood or urine markers are available for the routine diagnostics of Ewing sarcoma.

(i) Immunohistochemistry markers routinely used for Ewing sarcoma diagnosis include: CD99, FLI1 (whose sensitivity is however reduced by the occurrence of variant translocations involving other ETS-family genes), Caveolin 1 (whose expression has been demonstrated to be useful to diagnose Ewing sarcomas negative for CD99 expression) and NKX-2.2. Particularly, CD99 expression appears diffuse and intense at plasma membrane level by immunohistochemical staining in ~95% of Ewing sarcomas [51] (Figure 2A). Recently, innovative genomics-based combinations of immunohistochemical markers, such as B cell lymphoma/leukaemia 11B (BCL-11B) and Golgi apparatus protein 1 (GLG1), have been described as highly specific for Ewing sarcoma but require validation in prospective studies [52].

(ii) Currently, the diagnosis of Ewing sarcoma can be confirmed only by molecular pathology, which is mandatory when cases have unusual clinical and pathological features. Fluorescence *in situ* hybridization (FISH) and/or reverse transcription PCR (RT-PCR) detection of FET–ETS gene rearrangements, specific for Ewing sarcoma, are used as diagnostic tools [53].

(iii) Imaging for diagnosis include magnetic resonance imaging (MRI) of the entire bone or compartment of the suspected primary tumour, computed tomography (CT) or $^{18}$F-fluorodeoxyglucose (FDG) PET–CT of lungs, whole-body imaging and echography for evaluation of organ function [54]. Imaging studies are the central tool for detection of metastases.

The clinical stage at diagnosis is one of the major predictors of survival. The accurate determination of tumour burden at diagnosis is a critical factor for planning treatment and predicting outcome.

Currently, patients with localized disease generally have a 5-year overall survival of ~70–80%, which may be lower in patients presenting with pelvic tumours, large tumours and/or incomplete tumour regression after neoadjuvant or adjuvant chemotherapy. Despite an overall improvement in sarcoma-related deaths over the last two decades, patients presenting with metastasis at diagnosis generally continue to have a significantly lower overall survival of < 30%, whereas patients with isolated pulmonary metastasis have an overall survival of ~50% [55]. Ewing sarcoma predominantly spreads via the bloodstream, and the most common metastatic sites are the lungs, bones or bone marrow, whereas other sites are rare.

Moreover, Ewing sarcoma relapse is associated with very poor outcomes; patients who relapse within 24 months after diagnosis have a 5-year survival of < 10% [56]. A potential source of relapse may be a highly resistant clone of tumour cells that either existed *a priori* or developed under anticancer treatment.

### 1.1.6. Treatment

Patients with newly diagnosed Ewing sarcoma are treated with a combination of multi-agent chemotherapy and local control measures, including surgery and/or radiotherapy [57]. The standard approach is given by local treatment of the tumor and cycles of systemic chemotherapy (pre- and post-operatively). Surgery plays an essential role in treatment of primary tumor, especially to avoid radiotherapy, but it is not always feasible. Conventionally, in case of localized disease neo-adjuvant chemotherapy is applied for a local control and to facilitate surgery. Chemotherapy response is than monitored to evaluate clinical response and modulate adjuvant chemotherapy. Six standard chemotherapy drugs are active against Ewing sarcoma: cyclophosphamide, ifosfamide, doxorubicin, vincristine, actinomycin D and etoposide. Multicentric clinical studies demonstrated a higher efficacy for the association of 4 drugs (vincristin, cyclophosphamide, doxorubicin and actinomycin D) if compared to an association of 3 drugs or to the utilization of the single drugs alone.

Patients with metastatic disease remain a therapeutic challenge. The presence of metastasis at diagnosis determines a worse prognosis for these patients when treated with the same regimen utilized for localized disease. Indeed, a more aggressive treatment is necessary for these patients, consisting of higher doses and a reduced time between cycles of treatment followed by myeloablative therapy and stem-cells transplantation [50]. Overall, such aggressive treatment causes severe side effects.

Therefore, therapy amelioration represents an urgent need, particularly, for Ewing sarcoma patients with metastatic and recurrent disease.

### 1.1.7. Targeted therapy opportunities

*Potential use of monoclonal antibodies and small molecule inhibitors*

Despite recent advances in genetic profiling of Ewing sarcoma and in the biological and molecular understanding of this tumor, the translation of knowledge into novel targeted therapeutic opportunities has been more challenging and no new therapies have been approved by the FDA specifically for Ewing sarcoma in the last 30 years.

Considering that Ewing sarcoma is characterized by a unique aberrant protein expressed by a tumor-specific translocation, **EWS-FLI1** is an intriguing candidate with a great potential as a molecular target for therapy. Indeed, the chimeric protein is only expressed in tumor cells, does not exist in any normal cell of the body and is essential for tumor survival, which makes it an ideal target for developing specific inhibitors. However, unlike kinase fusions, the transcription factor fusions, such as *EWSR1–FLI1*, are currently not directly druggable for inhibition due to the lack of any enzymatic activity. An indirect approach to targeting this aberrant transcription factor would comprise disruption of its transcriptional complex. RNA helicase A (RHA) is a crucial part of the complex and the blockage of its binding to EWSR1–FLI1 by a small-molecule inhibitor, YK-4-279, has been shown to effectively reduce proliferation of Ewing sarcoma cells [58]. The analogue TK-216 is currently under investigation in a first-in-human phase I clinical trial (NCT02657005).
As alternative to the inhibition of EWS-FLI1 transcriptional activity, targeting downstream effectors of the fusion protein represented by downregulated/upregulated gene pathways as well as epigenetic deregulation are suitable novel approaches [59-61].

Considering its elevated expression in Ewing sarcoma cells and its key role in tumor malignancy, **CD99** glycoprotein has been considered as potential therapeutic target. As a cell surface molecule, the antigen is a suitable target for the development of therapeutic monoclonal antibodies (mAbs) [47]. Triggering CD99 with the specific murine 0662 mAb induces cell death in Ewing sarcoma cells [62] [63] and, when combined with doxorubicin, inhibits tumor growth and metastasis formation in a xenograft model [64]. Subsequently, based on these promising results, a full human anti-CD99 mAb (scFvC7) was isolated from the semi-synthetic ETH-2 antibody phage library by selections toward the extracellular portion of recombinant human CD99 protein [65]. Preclinical studies with scFvC7 confirmed the previous results of efficient delivery of cell death signal in Ewing sarcoma cells induced by specific triggering of CD99 [63]. Despite these potentialities, antibodies directed against CD99 have not reached the clinics yet. A limitation on the clinical use could be represented by the fact that, even if it is highly expressed in tumor cells, CD99 is not a proper tumor-associated antigen and it is broadly expressed in many normal cells at low levels with some notable exceptions of high

expression in immature T lymphocytes, thus representing a possible source of side effects. However, normal stem cells seem to be spared from the cell death induced by CD99 engagement *in vitro*, suggesting the need for an aberrant genetic background in order to accomplish the CD99-mediated function [63].

Anti-CD99 still remains an interesting therapeutic perspectives for all tumors in which the expression of CD99 is maintained at high levels, such as acute lymphoblastic leukemia [66] thymic tumors, some spindle cell tumors (*e.g.*, synovial sarcoma), hemangiopericytoma, meningioma, and malignant glioma [67], in which it confers high invasiveness and low survival rates.

Recently also small molecule inhibitors have been proposed, Çelik et al. demonstrated that the small molecule clofarabine was able to bind the extracellular portion of CD99, inhibiting the biological properties of Ewing sarcoma cells both *in vitro* and *in vivo* [68], thus suggesting a drug repurposing of an already developed drug for a targeted use.

Since the **IGF1R pathway** is deregulated by EWS–FLI1 and it plays a key role in maintaining malignant behavior and pathogenesis of Ewing sarcoma, as well as in many other cancers, numerous therapeutic agents targeting the IGF1R have been developed and also tested for Ewing sarcoma [44]; they include: mAbs specifically inhibiting the receptor (dalotuzumab, figitumumab, cixutumumab, ganitumab, R1507 and AVE1642), IGF1R/IR tyrosine kinase inhibitors (TKIs) (linsitinib), and more recently monoclonal antibodies against IGF1 and IGF2 (MEDI-573 and BI 836845) [69, 70].

These agents showed good preclinical results and good tolerability by several Phase I studies [71, 72], however clinical effects in Phase II were poor; just a 10% of patients experienced relevant benefits from anti-IGF1R mAbs as single therapy [73]; mainly for the rapid development of mechanisms of resistance [74], suggesting the need for the identification of predictive markers of response and combination therapies as possibility to overcome resistance. An overview of new potential targeted therapy approaches is schematized in Figure 3.

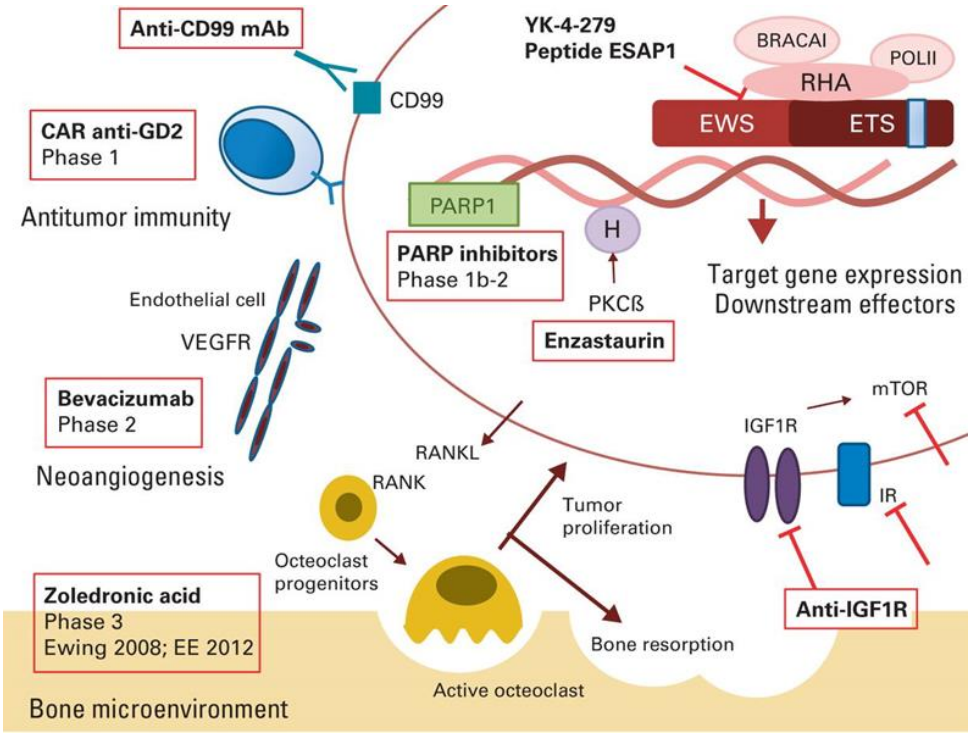


**Figure 3.** Some new potential targeted therapy approaches in Ewing sarcoma. *CAR, chimeric receptor gene-modified T cell; EE 2012, Euro-Ewing 2012; H, histone; IGF1R, insulin-like growth factor receptor-1; mAb, monoclonal antibody; mTOR, mammalian target of rapamycin; PARP, poly (ADP-ribose) polymerase; PKC, protein kinase C; RANKL, RANK ligand; RHA, RNA helicase; VEGFR, vascular endothelial growth factor receptor*. Image from Gaspar N et al., 2015 [55].

**Immunotherapy** breakthroughs in many adult cancer types have sparked the interest in investigating this approach in Ewing sarcoma as well. Unfortunately, the success with the use of immune-checkpoint inhibitors has been very limited [75], probably due to the low mutational burden, rare presence of infiltrating T cells and absence of PD-L1 expression in tumor [76] (Figure 4). Recently, chimeric antigen receptor (CAR) T cells targeting IGF1R or ROR1 are also being investigated for their use in Ewing sarcoma. Thus far, there has been success in mouse models leading to a prolonged overall survival, but results have been limited to preclinical studies [77].

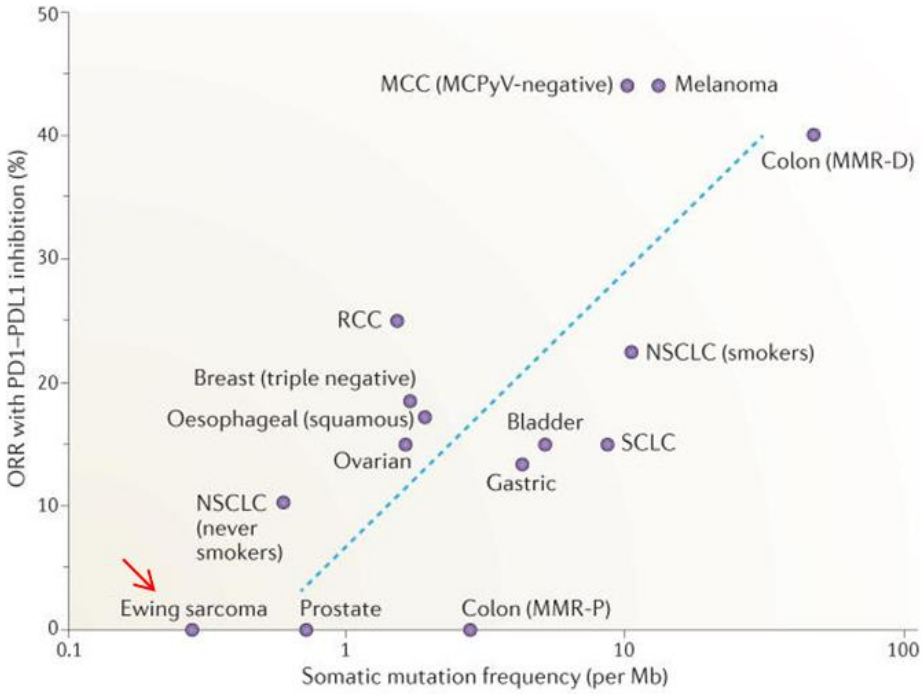


**Figure 4.** Correlation of tumour somatic mutation frequency with objective response rates to immune checkpoint blockade. Available clinical data showed a positive correlation between tumour somatic mutation frequency and clinical benefit, measured by the objective response rate (ORR). The ORR is defined in the context of these clinical studies as the proportion of patients who achieved 30% decrease in the sum of the longest diameters of target tumours based on modified Response Evaluation Criteria in Solid Tumours (RECIST). Here, the somatic mutation frequency (per megabase) and ORR to single-agent PD1 or PDL1 inhibition are shown across multiple solid tumours of non-viral origin for which clinical and sequencing data are available. Adapted from Yarchoan M et al., 2017 [78].

## 1.2. ABCA transporters

### 1.2.1 General characteristics of ABC transporters

The ATP-binding cassette (ABC) transporters are essential proteins found across all living organisms [79] that harness the energy of ATP hydrolysis to drive the import of nutrients inside prokaryotic and eukaryotic cells [80-82] or the export of toxic compounds or essential lipids across membranes [81, 83]. Encoded by 48 genes in human genome, the ABC transporters are subdivided into seven subfamilies, identified by the letters A through G. Typically, the structure of a full ABC transporter consists of four domains: two transmembrane domains (TMDs), which form the pore in the membrane and dictate which substrate can be translocated across it, and two nucleotide-binding domains (NBDs) that carry out ATP binding and hydrolysis. Located in both the plasma membrane and the membranes of intracellular compartments (mitochondria, Golgi and endoplasmic reticulum), ABC transporters translocate specific substrates against the concentration gradient [82, 84]. A wide range of ligands is

transported by ABC members, with different specificities according to the subfamily of belonging (Figure 5); the substrates include steroids, phospholipids, glycolipids, fatty acids, cholesterol, peptides or xenobiotics, therefore ABC transporters are engaged in numerous physiological processes such as membrane homeostasis, lipid trafficking, cell signalling, cell detoxification and drug resistance [85]. Despite the fact that a lot of emphasis has been placed on investigating the role of ABC transporters as protective pumps from exogenous compounds, xenobiotic excretion has been recently suggested not to be the primary function of these proteins [86, 87]. Various other physiological roles have been assigned to ABC transporters; inter alia translocation of cholesterol and other lipids (through export or floppase activity), as well as defence against oxidative stress and antigen presentation [88]. Notably, it has been shown that some members of the superfamily, such as ABCAs, are able to translocate endogenous lipids maintaining their asymmetric distribution at plasma membrane and actively influencing lipid homeostasis, trafficking and signalling. These are crucial processes for cell functioning and, more importantly, they are involved in the development of multiple pathologies [89].

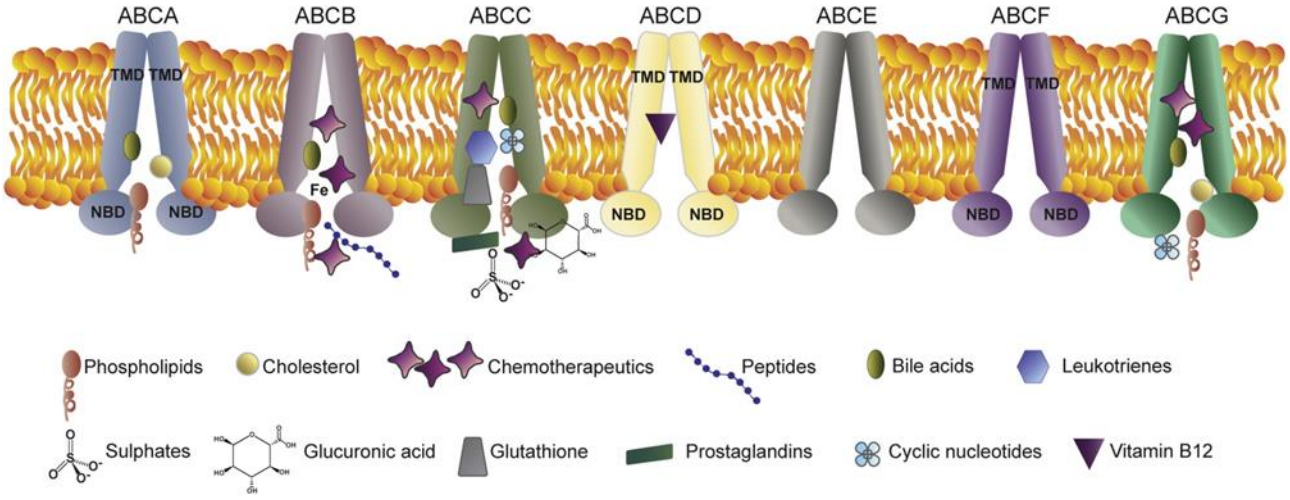


**Figure 5.** ATP-binding cassette family of transporters utilize the energy derived from the hydrolysis of ATP to translocate a variety of lipophilic endogenous substrates outside the cells. *TMD, transmembrane domain; NBD, nucleotide-binding domain; Fe, iron.* Reprinted with permission from Domenichini A et al., 2019 [90].

### 1.2.2. Role of ABC transporters in cancer

The role of some ABC transporters, particularly of ABCB1 (P-glycoprotein/MDR1), ABCC1 (Multidrug Resistance Protein 1/MRP1) and ABCG2 (Breast Cancer Resistance Protein/BCRP), has

been extensively documented in cancer multidrug resistance (MDR). These proteins act as drug efflux pumps with broad substrate specificity at plasma membrane level, decreasing drug accumulation inside the cells and thus often mediating the development of resistance to anticancer drugs. Numerous clinical studies demonstrate associations between overexpression of these ABCs and worst outcomes in a plethora of tumors, supporting their value as prognostic biomarkers [91-95]. Compelling evidence supports roles for ABCB1, ABCG2 and ABCC1 in chemoresistance *in vivo*. The emergence of MDR is one of the causes for the failure of chemotherapy in the treatment of cancer. Once MDR appears, chemotherapy is not effective even when using high doses of drugs enough to overcome resistance, toxic effects are brought about, and the resistance mechanism could be further stimulated. One of the therapeutic strategies attempted to overcome MDR in cancer, has been the inhibition of the ABC-mediated drug efflux; P-glycoprotein, particularly, has been the object of extensive efforts to develop small molecule inhibitors over several decades. However, despite the promising successes obtained in preclinical studies [96, 97], the strategy to reverse drug resistance by targeting ABC transporters with specific inhibitors has not been successful in clinical studies as initially hoped. Clinical trials, conducted thus far, have shown that the tested ABC modulators added limited benefits to cancer patients, as some of them induced unwanted drug–drug interactions and others were merely toxic [98]. They caused severe side effects due to their impact on normal cell functions, particularly in brain, where ABCs are physiologically involved in xenobiotic efflux at the level of the blood–brain barrier [99, 100]. A main limitation in the translation of *in vitro* findings to clinical evidence may be likely due to the fact that most studies testing ABC inhibition failed to take into consideration the physiological functions of the transporters in a whole organism and the possible co-expression of many ABC transporters, with high protein homology, within tumours and neighbouring tissues [101]. Nevertheless, improvement in both inhibitor properties and clinical trial design may overcome many of these limitations [102, 103].

Beyond the well-established role in MDR phenomenon, a less known but emerging theme is the drug efflux-independent role of ABC transporters in cancer biology [98, 104]; this concerns also some neglected members of ABC family, such as those of A subfamily [105]. Increasing awareness has revealed that the loss or inhibition of some ABC transporters impacts cellular phenotypes closely linked to differentiation, migration/invasion and malignant potential in a variety of cancers [106, 107], suggesting a potential role in cancer development and progression. Moreover, the loss of several ABC transporters in both xenograft and transgenic mouse cancer models can impact tumorigenesis and tumour progression [106, 108, 109]. These contributions are likely related to the normal physiological function of ABCs of exporting endogenous metabolites (which are not known for all the members) as well as signalling molecules [110, 111]. However, the mechanisms by which ABC

transporters affect the proliferation, differentiation, migration and invasion of cancer cells are still poorly defined, particularly for the less studied members of ABC family such as ABCAs, and thus need further investigation.

### 1.2.3 ABC transporters belonging to A subfamily

The ABCA subfamily of transporters consists of 12 members denoted ABCA1 to ABCA13 (originally, a non-functional human gene was erroneously named ABCA11), which are divided into two subgroups according to their chromosomal location and phylogenetic analysis. One subgroup is formed by five genes, *ABCA5, A6, A8, A9,* and *A10,* which are located in a compact cluster on human chromosome 17 (named "ABCA6-like transporters"), while the other members map to six different chromosomes [112]. Proteins of subfamily A are characterized by two large extracellular domains (ECD1 and ECD2) and an overall molecular weight greater than 200 kDa for most of the components. The structure of a typical ABCA transporter is depicted in Figure 6.

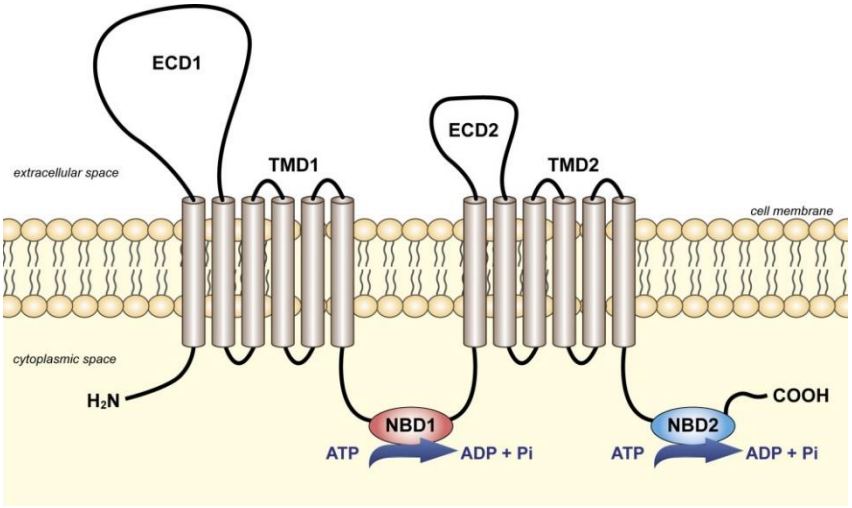


**Figure 6.** Schematic representation of a typical ABCA transporter structure. Full-length ABCA transporters are composed of two hydrophobic transmembrane domains (TMD1 and TMD2) and two nucleotide-binding domains (NBD1 and NBD2). ATP binds to each of the NBDs. Members of subfamily A are characterized by two large extracellular domains (ECD1 and ECD2) with a molecular weight greater than 200 kDa. Reprinted from Pasello M et al., 2019 [105].

*Functions in lipid transportation:*

Many members of the ABCA subfamily play important roles in lipid transport and trafficking, including the maintenance of plasma high-density lipoprotein (HDL) and cholesterol levels, and the regulation of efflux from cells.

The contribution of ABCAs in regulation and maintenance of cellular lipid homeostasis is supported by many evidences. (i.) Mutations in ABCA transporters have been identified as the cause of severe disorders associated with impaired lipid transport, such as harlequin ichthyosis, a disease arising from defective lipid transport in the skin [113] caused by loss of ABCA12 function [114]; the macular dystrophy Stargardt disease [115] associated with disease-causing sequence variants in the *ABCA4* gene [116]; and Tangier disease, which is a recessive disorder caused by loss-of-function variants in the *ABCA1* gene resulting in reduced cholesterol efflux from cells and lack of circulating HDL [117]. By disrupting the outflow of free cholesterol, mutations of the *ABCA1* gene also cause a toxic accumulation of cholesteryl esters within cells; evidence confirmed also in *ABCA1* knockout mice [118]. The translatability of this finding was confirmed in humans, in which mutations in *ABCA1* result in significantly lower plasma HDL and have a role in metabolic syndrome and diabetes [119]. In addition, functional and genetic association studies suggest either a putative preventive function (*e.g.*, for ABCA1, ABCA5 and ABCA7) or a predisposing role (*e.g.*, for ABCA2) in Alzheimer's disease pathophysiology, and this characteristic may be once more related with cellular cholesterol trafficking [120].

(ii.) The expression of many ABCAs is regulated by the transcription factors, liver X receptor (LXR) and sterol regulatory element-binding protein 2 (SREBP2), which are defined master regulators of cholesterol and lipid homeostasis [121, 122]. Particularly, both LXR and SREBP2 act as sensors of intracellular cholesterol levels and consequently regulate the expression of genes involved in cholesterol biosynthesis pathway and cholesterol efflux (*e.g.*, *ABCA*s); indeed, under high cellular cholesterol content, LXR interacts with the heterodimeric partner RXR (retinoid X receptor) in the nucleus, inducing *ABCA1* expression with the consequence of increased cholesterol efflux ABCA1-mediated [123, 124] (Figure 7A). Under low-cholesterol conditions or after exposure to cholesterol-lowering drugs, such as statins, the mRNA expression of ABCAs is mainly regulated by SREBP2 (Figure 7B). In particular, SREBP2 translocates to the nucleus and negatively influences *ABCA1* expression [125, 126], while activates expression of *ABCA7* as well as that of genes involved in cholesterol biosynthesis, such as the *Hydroxy-methyl-glutaryl co-enzyme A reductase* (HMGCR) [127, 128].

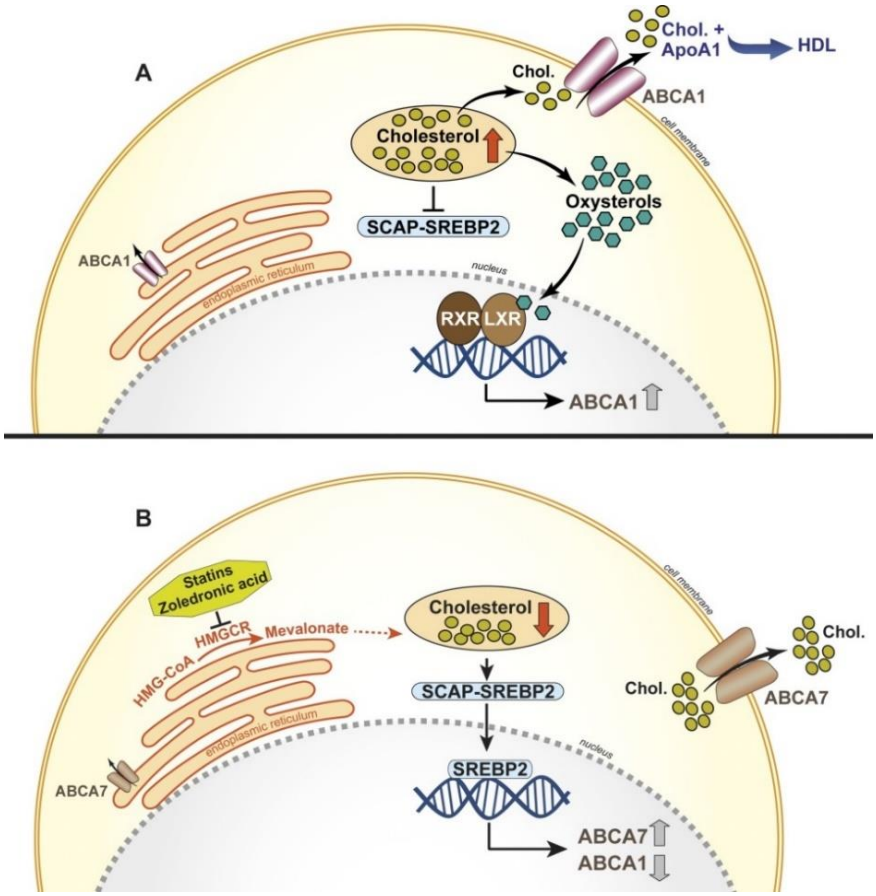


**Figure 7.** Model for the transcriptional regulation of ABCA1 and ABCA7 in response to cellular cholesterol levels. *ApoA1: apolipoprotein A1; Chol: cholesterol; HDL: high-density lipoprotein; HMG-CoA: 3-hydroxy-3-methylglutaryl-CoA; HMGCR: HMG-CoA reductase; LXR: liver X receptor; RXR: retinoid X receptor; SCAP: SREBP cleavage-activating protein; SREBP2: sterol regulatory element-binding protein 2.* Reprinted from Pasello M et al. 2019 [105].

For some ABCA transporters, the lipid substrates are well defined, for instance ABCA1, ABCA3, and ABCA7 export cholesterol and phospholipids from the plasma membrane [89, 129]. **ABCA1** is the most studied and characterized ABCA transporter; it exports free (unesterified) cholesterol and phospholipids from cells to ApoA1 to generate HDLs, which are the main cholesterol vehicle in bloodstream. The molecular mechanism by which ABCA1 mediates the cellular binding of ApoA1 and the nascent HDL assembly is not precisely determined. Two principal models have been proposed to explain ABCA1-mediated HDL formation: in the direct loading model, ApoA1 acquires lipids directly from ABCA1 while it is bound to the transporter; whereas in the indirect model, ApoA1 acquires lipids from specific membrane domains created by the phospholipid floppase activity of ABCA1 [130]. Indeed ABCA1, as well as ABCA7, is not only a mediator of lipid-efflux but it can also "flop" phosphatidylserine (PS) and phosphatidylinositol (4,5) bis-phosphate (PIP2) from the cytoplasmic to the exocytoplasmic leaflet of membranes, thus maintaining the asymmetry distribution of these lipids at membrane [81].

Despite showing the highest homology with ABCA1 (54%), **ABCA7** transporter exhibits a distinctive tissue expression patterns, with high expression in myelolymphatic tissues, and is regulated by SREBP2 in the opposite way compared to ABCA1 (as previously described). Accordingly, ABCA7 function as mediator of cholesterol and phospholipids efflux seem to be mostly related to stimulate phagocytic capacity of macrophages, as demonstrated both *in vivo* and *in vitro*, rather than mediating HDL biogenesis [127, 131, 132]. **ABCA4** is the only member of the subfamily acting as an importer, transporting N-retinylidene-phosphatidylethanolamine [82].

Regarding the role in regulation of cholesterol homeostasis in cells, ABCAs are not only involved in the efflux from cells; **ABCA2** and **ABCA3** take part in the uptake and consequent intracellular trafficking of low-density lipoprotein (LDL), a major source of cholesterol for cells of peripheral tissues. Both the transporters are localized in late endosomes/lysosomes, where they directly regulate intracellular processing of LDL content [133, 134]. For other ABCAs, the data reported thus far are scarce and the endogenous substrates are not univocally defined, for example **ABCA5** and **ABCA8** were described to stimulate cholesterol efflux in neurons or in fibroblasts [135], but definitive evidence is lacking.

Cholesterol homeostasis in cells rely not only on ABCA-mediated transport and regulation but it is the result of concerted processes, involving *de novo* cholesterol biosynthesis, metabolic conversion to cholesteryl ester/oxysterols/bile acids/steroid hormones and uptake of cholesterol-containing lipoprotein particles (such as LDL) from the extracellular milieu.

All the mechanisms are fine-tuned modulated in response to fluctuations in cell cholesterol levels and lipid homeostasis alterations are now increasingly recognized as a hallmark of cancer cells [136-139].

*Impact on cancer biology through altered lipid homeostasis:*

The specific roles of the ABCA transporters in tumors are multifaceted, and their associations with tumor malignancy are more complex than those reported for the conventional ABC members which act as drug pumps. The overall scenario is complicated by the fact that the available clinical information of associations with prognosis is heterogeneous and variable in different tumors, indicating controversial and complex relationships that may be influenced by the disparate cellular context. The topic has been extensively addressed in the review *Pasello M et al., 2019* [105].

Probably, the biologic roles of ABCA transporters in cancer may be an indirect consequence of their capabilities to export and/or flop signaling lipids such as (i.) cholesterol, (ii.) PIP2 and other phospholipids, maintaining their asymmetric distribution at plasma membrane and thus regulating lipid rafts composition. Lipid rafts are microdomains of cellular membranes enriched in transmembrane or glycosylphosphatidylinisotol-anchored proteins and lipids (cholesterol and

sphingolipids). These highly dynamic raft domains are essential platforms in triggering intracellular signaling processes and protein endocytosis. Radically alterations of lipid raft composition occur in cancer cells, thus affecting cell proliferation, signaling, protein trafficking, adhesion, migration and apoptosis.

(i.) Membrane cholesterol modulates the functionality of growth factor receptors, integrins and cell surface glycoproteins [140]. For example, the ligand-binding ability of the cell surface adhesion receptor CD44 to hyaluronan is governed by its cholesterol-dependent localization into cell membrane microdomains [141], while growth factor receptor (i.e., IGF1R, EGFR and HER2) signaling events are dependent on the cholesterol content of lipid rafts [142-144]. In addition, cholesterol can directly bind and activate specific proteins, such as the oncogenic smoothened protein. Both cholesterol and smoothened can work in concert in Hedgehog signaling, a pathway that plays a critical role in embryonic development and tumorigenesis [145, 146]. Also the complex signalling machine of several G-protein-coupled receptors (GPCRs) is modulated by cholesterol, particularly in terms of ligand-binding properties, stability and function [147].

Accordingly, cancer cells have a distinctive plasma membrane lipid composition characterized by the loss of lipid asymmetry, which differs from that of normal cells and allows discrimination between different tumor types, from benign to malignant cancers and from localized to metastatic tumors [138, 148]. In addition, altered lipid composition of cancer cells results in an altered permeability to chemotherapy drugs, such as cisplatin, in comparison to the membranes of normal cells [148].

(ii.) Any modulation in the levels or activity of ABCA1 may vary the quantity of phosphatidylinositol phosphates (PIPs), particularly PIP2, in the inner leaflet of the plasma membrane, wherein they can act as scaffolds for the recruitment of proteins with a specific PIP binding domain. PIP2 is linked to a diverse set of signaling functions, such as actin polymerization and cytoskeletal dynamics [149] and the downstream protein kinase B (PKB)/AKT signaling pathway, which is important for cell growth, survival, proliferation, and motility and provides crosstalk between different signaling pathways. In addition, increased cellular PIP2 levels lead to increased rates of receptor-mediated endocytosis [150]. Therefore, as a consequence of ABCA1-PIP2 floppase activity, AKT phosphorylation or endocytic vesicle formation may decrease [151, 152] and tumor cell behavior may be significantly altered.

### 1.2.4 ABC transporters in Ewing sarcoma

To date only associations of conventional ABC transporters with clinical outcome have been investigated in Ewing sarcoma. Whereas the prognostic value of the multidrug resistance mediator ABCB1/ P-

glycoprotein is well recognized in Osteosarcoma [153], in which many therapeutic strategies targeting the ABC have been attempted in order to reverse MDR [154]; not the same has been highlighted in Ewing sarcoma. Regarding this transporter, the results are contradictory: one study described a significant association between protein expression and poorer response to therapy in pre- and post-therapeutic Ewing sarcoma [155], while the majority reported that ABCB1 mRNA and protein expression were not predictive of prognosis [156-158]. No significant correlation with prognosis for ABCG2 has been found in Ewing sarcoma [159], but some evidences indicated a predictive value for survival of ABCC1/MRP-1 [158].

## 1.3. Antibodies

### 1.3.1. Structure and formats

Monoclonal antibodies are universal binding molecules with a high specificity for their targets and are indispensable tools in research, diagnostics and therapy of cancer.

Antibodies are the major components of humoral adaptive immunity towards pathogens. They are produced by plasma cells and are able to specifically recognize antigens, thereby activating other components of the immune system against the pathogen.

The structure of a prototypic IgG antibody consists of four polypeptide chains: two identical light (L) and two identical heavy (H) chains which are linked by disulfide bonds. In addition to the type γ of IgG, there are other four main types of heavy chain isotypes, denoted: α, δ, ε and μ (in IgA, IgD, IgE, and IgM antibodies, respectively), some of which have several subtypes, and these determine the effector function of the antibody molecule. Instead, the light chains in mammals are only of two types, λ and κ [160].

The 110 amino-terminal residues of each heavy and light chain are characterized by extensive variability in the amino acid sequence and are referred to as variable (V) regions (VH and VL, respectively). The variable domains contain three hypervariable loops, named complementarity determining regions (CDRs) that account for different binding specificity of antibodies, and highly conserved framework regions. The carboxy-terminal part of the immunoglobulin molecule, referred to as the constant (C) region (CH and CL), is less variable and differs only between distinct immunoglobulin isotypes and subtypes [161].

Two sophisticated genetic mechanisms generate the genetic diversification of V regions, accounting for the wide antibody repertoire: V (variable), D (diversity) and J (joining) recombination and somatic hypermutation.

In germline DNA of B cell precursors, the immunoglobulin encoding gene segments are organized into three genetic loci (κ, λ, and heavy chain loci), arranged on different chromosomes. Each genetic locus contains numerous gene segments, for example the heavy chain locus has separate clusters of VH, DH, JH multiple gene segments and of CH genes (Figure 8A). During B cell development in the bone marrow, one variable gene segment of each type (V, D, J for heavy chain and V, J for light chain) is randomly selected and they are joined to assemble a functional V region. CDR1 and CDR2 of both H and L chains are encoded by V segments. CDR3 of the light chain is produced by the combination of V and D segments, whereas CDR3 of the heavy chain is formed by the combination of V, D, and J segments [162] (Figure 8B).

After antigenic stimulation, diversity is further enhanced by the process of somatic hypermutation that introduces point mutations into the rearranged V-region genes in mature activated B cells. Thereby the antibody repertoire further increases.

Theoretically, the human immune system can generate $10^{26}$ different antibody molecules, however the size of the Ig repertoire present at any time is limited by the total number of B cells in an individual ($\sim 2 \times 10^{12}$). The human antibody repertoire is, thus, a small sampling of the wide potential repertoire.

**A**

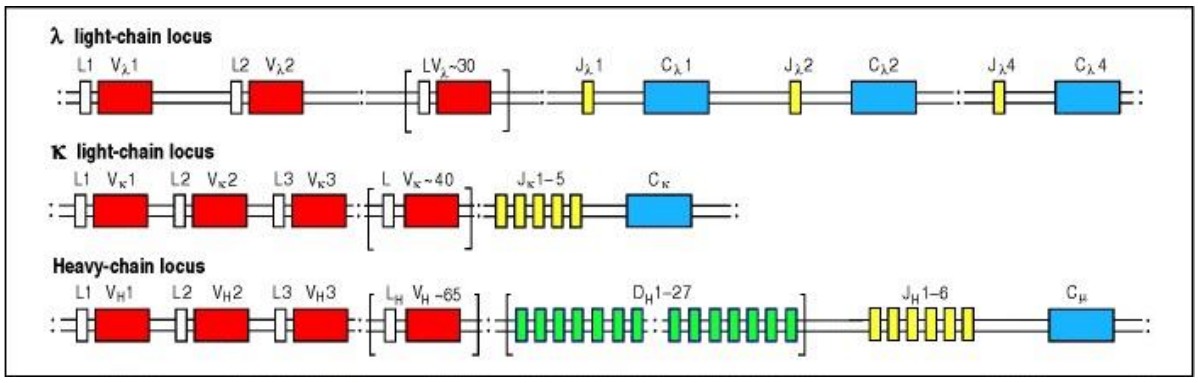

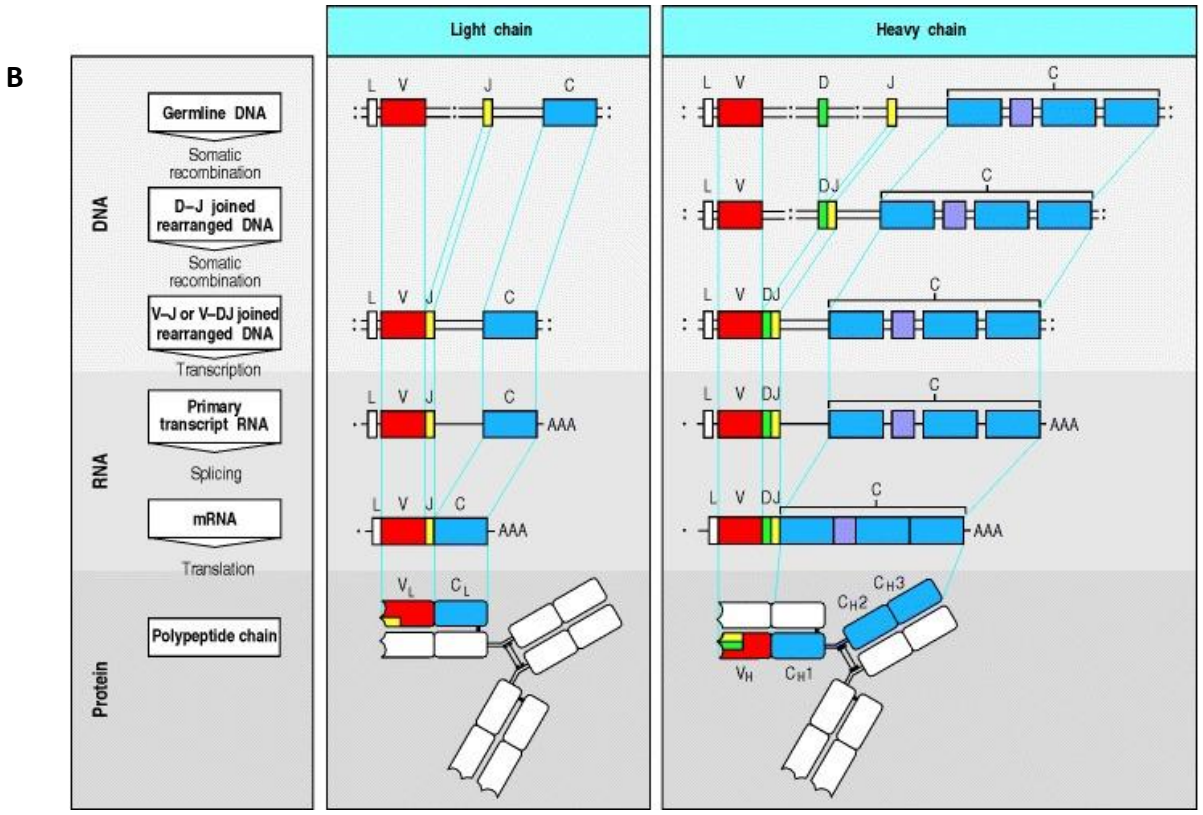


**Figure 8.** *In vivo* antibody gene rearrangement and genetic diversification of variable regions. A) Organization of Immunoglobulin locus in the gene segments: C, constant chain; D, diversity segment; J, joining chain; V, variable chain; B) V(D)J somatic recombination of antibody gene and protein assembly *in vivo.* Note that while only single V, J, D, and C regions are shown for simplicity, these are selected from a large number of genes. The major processes leading to the next step in antibody assembly are noted on the left. *RNA transcripts are noted by "AAA" designating the poly-A tails; L indicated the Leader sequence.*

### 1.3.2. Antibodies for pharmaceutical applications

*Therapeutic use*

The idea that antibodies could serve as 'magic bullets' in diagnosis and target therapy for selectively killing cancer cells while sparing normal tissue has a long history, which started soon after their discovery in the late nineteenth century.

Human monoclonal antibodies (mAbs) and their derivatives represent, nowadays, the largest and fastest growing group of biopharmaceutical products (therapeutic proteins). More than 50 antibody drugs have obtained market approval by the FDA and EMA for clinical use [163] and furthermore, more than 500 therapeutic antibodies and derivatives are currently tested in clinical trials with a focus on the treatment of cancer and autoimmune diseases [164].

The use of antibodies as therapeutic agents has been made possible only after the introduction of hybridoma technology for mAbs production by Köhler and Milstein in 1975. This technology consists in the immortalization of murine antibody-secreting B cells by fusion with a myeloma cell to obtain

the hybridoma, a hybrid cell line that has both the antibody-producing ability of the murine B-cell and the high longevity of myeloma.

The first marketing approved therapeutic mAb, muromonab-CD3 (anti-CD3), used for preventing kidney transplant rejection, [165] was obtained by mouse hybridoma technology [166]. However, the main limitation for therapeutic applications of murine antibodies was their immunogenicity in humans, making them unsuitable for repeated administration required for cancer treatment.

A solution to overcome this problem was only brought by recombinant DNA technology. Using genetic engineering, the murine sequences were partially replaced by the homologous human sequences. The result was the production of 'chimeric' antibodies, where the murine constant domains were replaced by human constant regions, and 'humanized' antibodies, where the complementarity determining regions (CDRs) of a parental murine antibody were transferred to human variable region frameworks [167] (Figure 9). Traditionally, mAbs were obtained by immunization of mice (or other laboratory animals) with the desired antigen, followed by their conversion into chimeric or humanized analogues. These engineered mouse antibodies dominated the first decade of therapeutic antibody approvals, while today, to further reduce the immunogenicity, it is preferred to use fully human mAbs. To date, several methods to generate fully human mAbs have been established. These include (i.) transgenic mice carrying human immunoglobulin loci [168], (ii.) *in vitro* immunization of Epstein–Barr virus (EBV)-immortalized B cells [169] and (iii.) selection of antibodies from phage-display libraries of human antibody fragments [170, 171]. Display of mAbs on filamentous phage offered the possibility of producing efficiently mAbs or their fragments using only *in vitro* procedures for naïve libraries, thus overcoming major limitations of conventional hybridoma technology. In 2002 in USA, and one year later in Europe, the first fully human antibody (adalimumab, anti-TNFα), generated *in vitro* using phage-display technology, received marketing authorization. As of the beginning of 2016, six human antibodies discovered or further developed by phage display were approved for therapy.

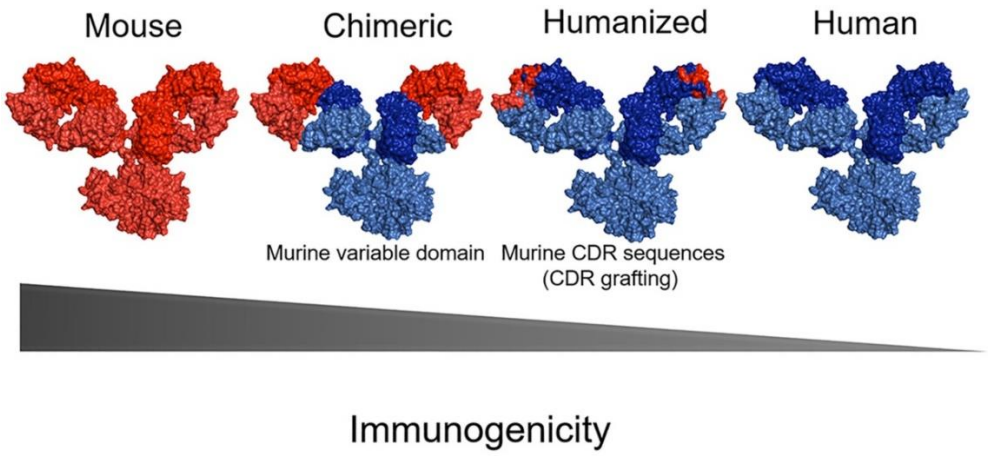


**Figure 9.** Progressive humanization of antibodies by recombinant DNA technology. Schematic overview of antibody humanization from murine antibodies (red domains) to fully human antibodies (blue domains). Chimeric antibodies are produced by combining sequences of a murine variable domain with human constant region domains. The murine CDR sequences transplanted to a human framework sequence produce humanized antibodies by the technique known as CDR grafting. The images of the immunoglobulin structure (PDB code 1IGY) were created using PYMOL (The PyMOL Molecular Graphics System, Version 2.0 Schrödinger, LLC). Reprinted from Santos Mariana Lopes dos et al., 2018.

Therapeutic anticancer mAbs function through various mechanisms and strategies, including (i.) directly targeting the malignant cells, (ii.) modifying the host response and retargeting cellular immunity towards the malignant cells, (iii.) delivering cytotoxic moieties.

(i.) mAbs have been extensively used to target a wide variety of functionally-relevant target antigens expressed specifically on the surface of cancer cells (Figure 10A). Characteristics that make antigens attractive as targets for mAb therapy include high level of expression by malignant cells and, on the other hand, limited expression on normal cells, lack of high levels of soluble target and limited tendency of antigen-negative tumour variants to develop.

Mechanisms of action carried out by IgG mAbs directly targeting cancer cell antigens include inducing Fcγ-mediated antibody-dependent cellular cytotoxicity (ADCC), complement-mediated cytotoxicity (CMC) or direct signalling-induced death of cancer cells (e.g. trastuzumab (anti-HER2) for HER2-positive breast cancer and rituximab (anti-CD20) for non-Hodgkin's lymphomas). mAbs can also have direct effects on target cells by blocking the binding of growth factors , responsible for the survival of the cancer cell, such as anti-EGFR (Cetuximab) or anti-IGF1R (Dalotuzumab). These mAbs can act by competitively inhibiting the binding of the growth factor ligand to the receptor, thereby blocking its dimerization and the downstream signaling pathway or inducing an apoptotic signal by crosslinking the receptor [172].

Therapeutic antibodies could also act as agonists of receptors or transporters, essentially replacing the activity of the normal ligand. The agonist activity can occur when the mAb binds the receptor/transporter in a manner that mimics the binding of the physiological ligand resulting in antibody-mediated activation.

(ii.) mAbs can also be used to affect the tumor microenvironment, such as inhibiting angiogenesis (Figure 10B) (e.g., bevacizumab) or to block inhibitory signals on immune cells (Figure 10C), thereby resulting in a stronger antitumour T cell response (checkpoint inhibitors, such as anti-CTLA-4 (ipilimumab) and anti-PD-1 (nivolumab, pembrolizumab)/anti-PD-L1 (avelumab). Other approaches to enhancing T cell-specific immunity against tumor cells aim to activate co-stimulatory signals with agonist antibodies acting on CD28, CD40, inducible T cell co-stimulator (ICOS), OX40, CD27 and DR3 [173]. Although the manipulation of T cells is currently a primary focus, other approaches may leverage the innate immune system, such as targeting NK cells or macrophages.

(iii.) The previous functional mechanisms can be carried out directly by mAbs (i.e. based on Fc-mediated events) or exploiting only their intrinsic high-affinity binding ability for a tumoral target and committing the functional effect to conjugated molecules, such as radioactive (Figure 10D) molecules and cytotoxic small molecules (Figure 10E). In these cases, Abs are used as modular building blocks for the selective pharmaco-delivery of payloads at the tumor site. This approach can also be used to selectively activate immunity against cancer by delivering cytokines to primary/metastatic tumor lesions using antibody–cytokine fusion proteins, also named "immunocytokines" [174]. The antibody-based delivery of certain proinflammatory payloads (such as IL2, IL12, and TNF) to the tumor microenvironment can lead to a dramatic potentiation of their anticancer activity and meanwhile to a reduction of systemic toxicity, which represents a common issue of cytokine-based therapeutics.

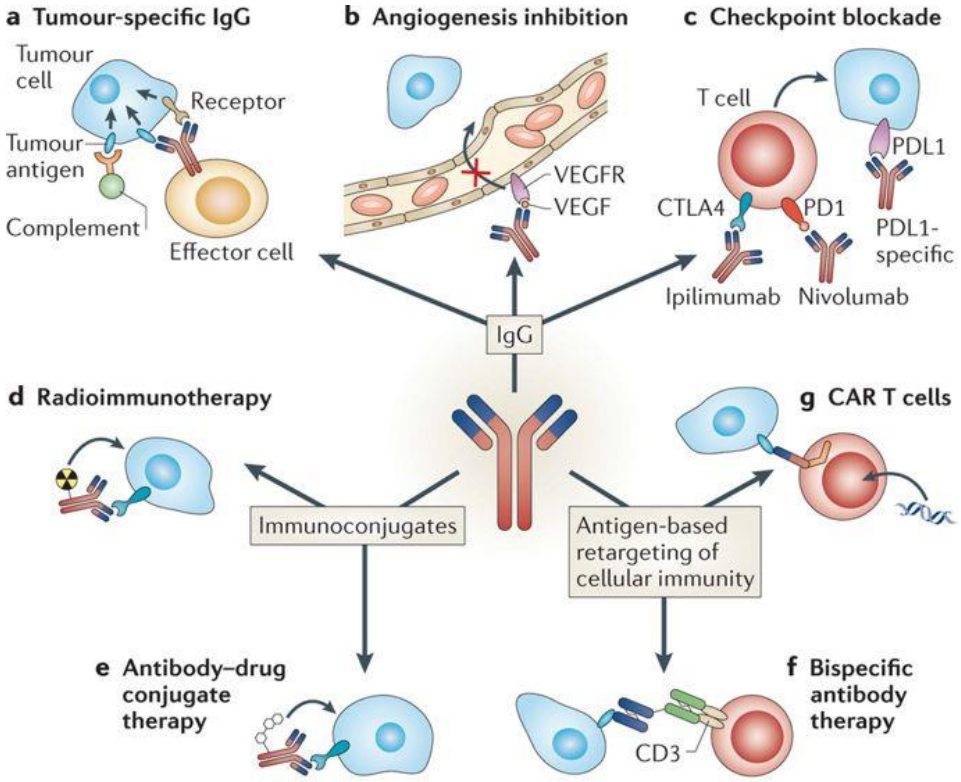


**Figure 10.** Monoclonal antibody-based cancer therapeutic strategies. A) Immunoglobulin G (IgG) molecules that bind to target cancer cells can mediate antibody-dependent cellular cytotoxicity (ADCC) by immune effector cells, induce complement-mediated cytotoxicity (CMC) or result in the direct signalling-induced death of cancer cells (for example, herceptin and rituximab). B) IgG mAbs can also be used to inhibit angiogenesis (for example, bevacizumab) or to block inhibitory signals (C), thereby resulting in a stronger antitumour T cell response (for example, ipilimumab and nivolumab). D) Radioimmunoconjugates (for example, 131I tositumomab and ibritumomab tiuxetan) deliver radioisotopes to the cancer cells; E) antibody–drug conjugates (for example, brentuximab vedotin and trastuzumab emtansine) deliver highly potent toxic drugs to the cancer cells. mAb variable regions are also used to retarget immune effector cells towards cancer cells through the use of bispecific mAbs that recognize cancer cells with one arm and activating antigens on immune effector cells with the other arm (for example, blinatumomab) (F) or through a gene therapy approach in which DNA for a mAb variable region fused to signalling peptides is transferred to T cells, thereby rendering them chimeric antigen receptor (CAR) T cells specific for the tumour (G). *CD3, T cell surface glycoprotein CD3 ε-chain; CTLA4, cytotoxic T lymphocyte-associated antigen 4; PD1, programmed cell death protein 1; PDL1, PD1 ligand; VEGF, vascular endothelial growth factor; VEGFR, VEGF receptor.* Reprinted with permission from Weiner GJ, 2015 [172].

Most of these mechanisms are not necessarily optimally mediated by a whole IgG Ab; clearly, in the case of ADCC or CMC, Fc is required to accomplish the function. However, the advances in protein engineering allowed to exploit the modular nature of antibodies, both structurally and functionally, for the generation of smaller mAb fragments with several advantages over full-length mAbs, particularly improved binding avidity, access to challenging epitopes, pharmacological properties, tumor penetration resulting from their small size and lower costs of production. Indeed, Ab fragments

are not generally glycosylated, therefore they can be easily produced using microbial expression systems (e.g. *E. Coli*, *S. Cerevisiae*) [175]; whereas whole Abs, because of an N-linked glycosylation site in the CH2 domain of the H chain that is important for stability, preventing aggregation, and effector function, require expression in mammalian cell lines (*e.g*. Chinese hamster ovary (CHO) cells) [176].

On the other hand, their smaller size results in faster renal clearance, which may require higher doses and/or more frequent dosing regimens *in vivo* unless confined by the addition of half-life extension moieties such as polyethylene glycol or albumin binding fragments [177, 178].

Different formats of recombinant antibody fragments can be displayed on phage surface in Ab libraries, including Fab, scFv, diabody, SIP (Figure 11, for a schematic overview of antibody formats).


**Figure 11.** Schematic representation of various antibody formats. Fragment formats include the antigen-binding (Fab) and single-chain variable (scFv) fragments. The small immune protein (SIP) has the CH4 domain of an IgE coupled to a scFv, forming stable dimers by disulphide bridges. Multispecific fragment formats include the $Fab_2$ bispecific and Bis-scFv.

The antigen-binding fragment (Fab) is composed of an antibody light chain (VL + CL domain) linked by a disulphide bond to the antibody heavy chain VH and CH1 domains; the molecular format is monovalent and monospecific and retains the parental antibody's ability to bind the antigen. Resulting from the removal of the Fc portion of an IgG molecule, it has been traditionally prepared by proteolytic digestion of a whole antibody, but in more recent times it was expressed using recombinant DNA technology. With a molecular mass of ~50 kDa they are much smaller than mAbs (MW of IgG is ~150 kDa), therefore they have an improved tissue penetration, but also lower stability and shorter half-life. Fab was the first therapeutic antibody format adopted and still remains one of the most successful, comprising ~49% of all antibody fragments that have entered clinical trials [179, 180].

F(ab')2 fragments are composed of two Fab fragments held together by an Ig hinge region and have a MW of ~110 kDa. They are bivalent, giving them increased avidity compared to Fabs [181], but their larger size may lead to reduced tumor penetration, which however is still superior to that of a full-size mAb [182]. They can be generated by the enzymatic digestion of whole antibodies or by recombinant expression in mammalian cells.

The single chain fragment variable (scFv) consists of a single polypeptide chain, including the VH domain linked to the VL by a flexible polypeptide linker, which is most commonly glycine- and serine-rich with dispersed hydrophilic residues; the affinity for its antigen is comparable to that of the parental mAb. The sequence and length of the linker may differ between scFvs in order to optimise affinity for the antigen and thermostability. The format linker sequence $(Gly_4Ser)_3$ has been frequently used for the construction of many phage libraries [183-185].

The scFvs have several advantages over a conventional mAb. Firstly, the small size of ~27 kDa and the lack of glycosylation makes scFvs ideal for large-scale production in microbial systems. In addition, the size also facilities tumor penetration and access to cryptic epitopes. The lack of an Fc region excludes the risk of immune cell activation and antibody effector functions, allowing the molecule to bind its target without activation of the host's immune system. This may be advantageous or disadvantageous depending on the context. Nevertheless, the lack of an Fc domain also brings about several disadvantages, mainly low thermostability compared to a full-size mAb, a greater propensity for aggregation, therefore increasing the risk of immunogenicity, and a shorter half-life. This can require higher and more frequent dosing. Fusion of the scFv to albumin or polyethylene glycol (PEG) can be used to improve half-life. An example of scFv in clinical trial is gancotamab, an HER2-targeted PEGylated antibody-liposomal doxorubicin conjugate, for therapeutic use in HER2-positive locally advanced/metastatic breast cancer [186].

Antibody fragments can be used on their own or linked to other molecules or fragments with a different antigen-specificity to generate bispecific, multi-specific or multifunctional molecules to achieve a variety of biological effects.

*Non-therapeutic uses of monoclonal antibodies: Diagnostics and Imaging*

The new therapeutic options available for cancer in the era of target-therapy, immunotherapy and personalized medicine are requiring in parallel the boosting of new specific diagnostic and predictive tests aimed to provide, respectively, a deep molecular characterization of the disease and the identification of biomarkers to define the best therapeutic option. The high affinity and specificity of mAbs make them ideal probes for the detection of a specific surface protein *in vivo* or *in vitro*.

They can be conjugated to radioisotopes, fluorescent molecules or enzymes without inhibiting

binding to the target, becoming thereby useful for many *in vitro* applications such as ELISA (Enzyme-linked immunosorbent assay), Immunohistochemistry, flow cytometry. Many Ab-based laboratory tests have been standardized and validated for routine clinical use [187]; for example, HercepTest™ (semi-quantitative HER2-specific IHC) is used to guide decisions on the use of trastuzumab, pertuzumab, and ado-trastuzumab emtansine [188].

For *in vivo* molecular imaging and noninvasive PET, instead, scFv and other small-size mAb formats, particularly diabodies, minibodies and nanobodies, are more suitable compared to full-size mAbs because of their shorter half-lives and high rates of clearance resulting in reduced radiation exposure. Additionally, the lack of Fc domain eliminates the immune activating potential of the Ab and prevents recycling through the neonatal Fc receptor (FcRn) pathway, facilitating visualization of targeted tissues via rapid blood clearance and improved contrast [188].

In addition, the small size of mAb fragments allows a better tissue distribution and provides more options regarding epitope choice [182]. Nanobodies targeting Carbonic anhydrase IX (CAIX) and HER2 have been used for optical imaging of pre-invasive breast cancer, which requires a high tumour/background ratio [189, 190]. Diabodies, tribodies, and tetrabodies also have potential uses in applications such as radioimmunotherapy and diagnostic *in vivo* imaging [191]. In addition, fluorescently labelled nanobodies have been used for real-time analysis of epithelial mesenchymal transition [192].

### 1.3.3. Antibody phage-display technology for antibody discovery

*Concept of Antibody phage-display technology*

Phage display is the most widely used *in vitro* antibody selection technology from wide repertoires of proteins displayed on phages. It has proven to be a robust, versatile platform method for the discovery of human antibodies and a powerful engineering tool to improve antibody properties.

The technology is based on the display of a protein, with a desired binding phenotype, on the surface of filamentous phage by introducing the corresponding gene coding into the phage genome by fusion with a phage protein coat. Therefore, the phage particle contains, packaged into the capsid, the genetic information coding for the displayed protein directly linking genotype to the specific desired phenotype. When combined with large combinatorial antibody libraries in which each antibody is slightly different from the others, phage display allows for rapid *in vitro* selection of antigen-specific antibodies and recovery of their corresponding coding sequence.

The technology was originally described in 1985 by Smith [193] for the display of properly folded peptides on phage envelope through fusion with phage coat protein III. After the breakthrough of smaller recombinant antibody formats like scFv [194] and their secretory periplasmic expression *in E. coli* [195], the technology was independently pursued for the phage display of antibody fragments by the groups of Winter and Lerner, in the early 1990s [170, 183, 196]. For their work on phage display of peptides and antibodies, George P. Smith and Sir Gregory P. Winter were jointly awarded one half of the 2018 Nobel Prize in Chemistry.

Phage display technology relies on filamentous bacteriophage, frequently M13 phage, which naturally infects bacteria by attaching to the tip of F pilus thus translocating its genome (circular single-stranded DNA molecule) into the bacterial cytoplasm (Figure 12). During M13 life cycle, the phage genome is replicated exploiting both phage and host proteins and then is packaged into mature progeny virions which are released from bacteria. The phage capsid is composed of 2700 copies of pVIII, the major coat protein, and few copies of minor coat proteins: 3-5 copies of the pIII and pVI proteins at one extremity of the phage, and 3-5 copies of pVII and pIX proteins at the other end, which begin the assembly process [197].

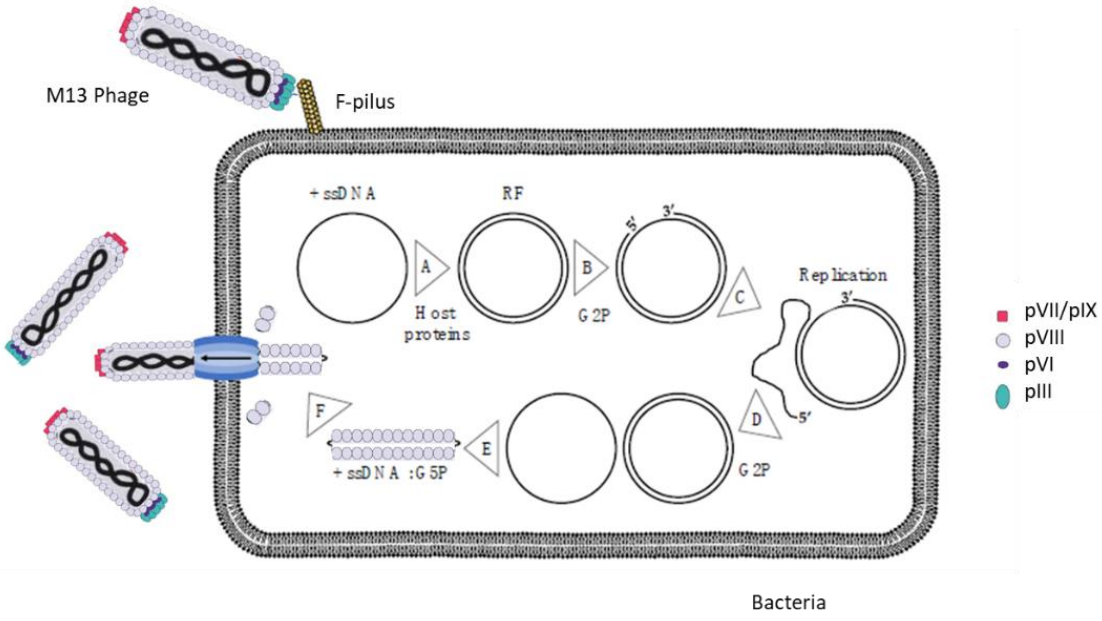


***Figure 12.*** Infection cycle of the M13 phage. A) Upon infection, the single stranded (+) chromosome of the M13 phage is converted into the double-stranded replicative form (RF); B) the G2P protein nicks the (+) strand in the RF and binds covalently to the 5′-end; C) the genome is then replicated from the 3′ end of the nick, using the (−) strand as a template. The original G2P-bound (+) strand is physically displaced by the Rep helicase throughout the elongation process; D) The old (+) strand is re-circularized by the bound G2P after dissociation, ready to be converted into an RF or to be packaged into new M13 phages; genome replication continues until the concentration of G5P has accumulated to sufficient levels to sequester the ssDNA; E) G5Ps will bind the ssDNA in a back-to-back dimeric conformation, causing the more rod-shaped appearance of the ssDNA; F) a pore is formed in the membrane, and the phage genome is translocated through this pore, while the phage coat is assembled. Adapted from Ledsgaard L et al., 2018 [198].

Peptides and/or proteins have been displayed on phage as fusion products with the minor coat protein pIII or, especially for short peptides, with the pVIII (Figure 13). Display of proteins encoded by a cDNA library as carboxy-terminal fusion with the minor coat protein pVI has also been reported [199].

Phage display libraries can be produced using (i.) phage vectors or (ii.) phagemid vectors; in both, the antibody coding sequence is cloned in-frame upstream of the gene encoding the pIII protein. In the earliest examples, (i.) antibody genes were cloned as antibody-pIII fusion directly into the phage genome, which carries all the genes needed for a complete virus life cycle, including the F1 phage origin of replication and generally also an antibiotic resistance marker for selection of infected bacteria (ampicillin resistance gene). Since each phage particle normally incorporates three to five copies of pIII, the use of phage vectors potentially results in a multivalent display of antibody-pIII fusion proteins [198]. As an alternative, (ii.) phagemid vectors based on smaller "minimal plasmids" (~4000 bp) may be used. Phagemids have, additionally to the previous phage characteristics, a plasmid origin allowing the replication and propagation of the plasmid in E. coli (Figure 13). Since the phagemid does not contain all the information required for a complete viral life cycle, the bacteria, transformed with the phagemid, have to be superinfected with helper phage particles containing a complete phage genome in order to allow the production of functional phage particles displaying antibody-pIII. Phagemid vectors encoding the antibody fusion product are preferentially packaged into the phage particles, because the typically used helper phages (M13K07 or VCS-M13) have a slightly defective origin of replication, which also serves as packaging signal.

However, the mature phage particles released from bacteria may display pIII protein derived from both the helper phage and the phagemid vector. The pIII proteins derived from the phagemid vector are fused to the antibody that will be displayed on the surface of the phage, while those from the helper phage are unmodified. Therefore, phage particles from phagemid libraries do not usually display more than one copy of the antibody, since a considerable portion of minor coat protein corresponds to unmodified pIII from the helper phage.

Phagemid vectors are more typically used in library construction than phage vectors because higher transformation efficiencies can be achieved facilitating the construction of larger libraries.

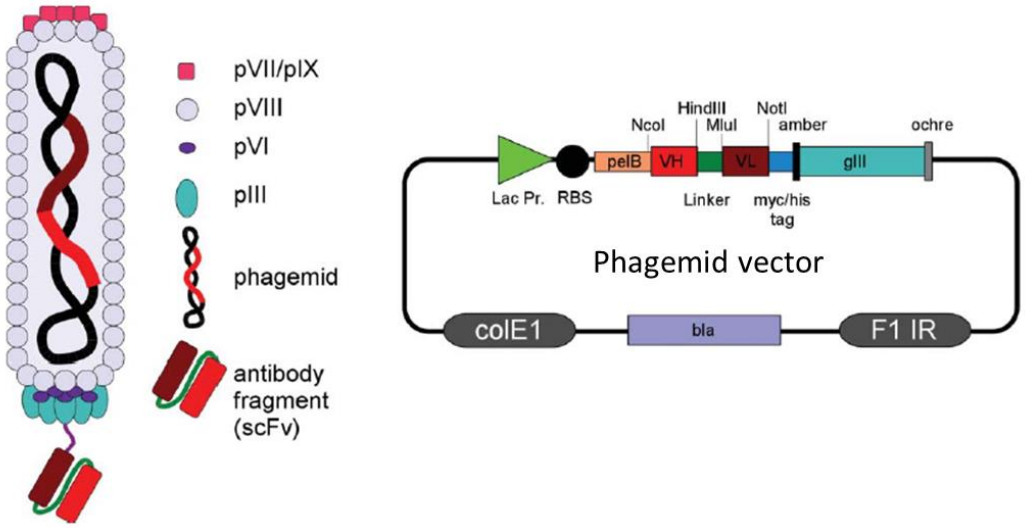


**Figure 13.** Schema of an antibody (scFv) displayed on a phage surface on the left, and phage display vector (phagemid) on the right. *Bla: β-lactamase, ampicillin resistance; ColE1: bacterial origin of DNA replication; F1 IR: intergenic region of phage f1, phagemid packaging signal; gIII: phage gene encoding pIII; Lac Pro: promoter of lacZ; pIII, pVI, pVII, pVIII, pVIX: phage protein III, VI, VII, VIII, VIX; pelB: Erwinia carotovora pectate lyase B leader peptide; scFv: single chain fragment variable; VH: variable domain heavy chain; VL: variable domain light chain.* Adapted from Frenzel A et al., 2016 [200].

While phage display represents the most widely used methodology for selection of antibody repertoires, other additional display platforms have been developed and are used to discover therapeutic antibodies, including ribosome [201], yeast, bacteria [202] and mammalian [203] display methods.

### 1.3.4. Antibody phage-display libraries

Antibody phage libraries are huge collections of mAbs with unknown properties, displayed on phage particles, which carry inside the correspondent antibody gene sequence. The mAbs displayed on each phage are slightly different from each other thanks to the introduction of variation, by random mutations, in fixed regions along the V antibody sequence.

*Library size*

Intuitively, the likelihood of isolating high affinity antibodies correlates with the library size [204, 205]. Considering the Kabat's definition of CDRs [206] and the most frequent CDR lengths in humans [207], if each position of each of the six CDRs were diversified with the 20 natural amino acids, the corresponding theoretical repertoire would contain $10^{78}$ unique antibody variants. Obviously, only a very small fraction of this universe of $10^{78}$ unique variants can be sampled in a

phage display antibody library [208]. Several practical factors further limit the maximum size of a phage display antibody library to $10^{10}$–$10^{11}$ antibody variants, such as the transformation efficiency of *E. coli* ($10^{10}$-$10^{11}$ colony transforming units (cfu) per μg of DNA), solubility of phage particles (typically $\leq 10^{13}$ transforming units/ml) and the need to use small volume (ml) of phage preparation for antigen selection procedures. Additionally, the quality of gene synthesis, either using RT-PCR (Reverse transcription polymerase chain reaction) for naïve libraries [184] or exploiting random PCR mutagenesis/ chemical means for synthetic [209, 210], affects the effective size of the library. Nucleotide sequences with insertions or deletions of one or two nucleotides change the reading frame of the gene sequence leading to aberrant products. Moreover, some in-frame antibody genes have low expression due to suboptimal codon usage in *E. coli* and/or inefficient translocation in the cell compartments [211], thus generate variants displayed in low proportion with respect to others further reducing the effective size of the libraries. Precision DNA synthesis platforms can be applied to avoid frameshifts, redundant and/or unwanted amino acids in the targeted positions for diversification. In order to improve the quality of the antibodies, these precise synthesis methods may be coupled with *in silico* tools for the prediction of the developability profile, named therapeutic antibody profiling (TAP); by generating a structural model for each possible variant of an antibody library *in silico* and filtering out those with poor TAP, non-developable antibody variants can be replaced with developable ones during the design phase of the libraries [212].

*Types of antibody libraries*

Based on the source of antibody genes, the libraries can be divided into three main classes: Immune, Naïve and Synthetic. The latter two have been considered as "single-pot" libraries, as they are designed to isolate, theoretically, antibodies binding to every possible antigen.

**Immune libraries** use, as source of variable immunoglobulin genes, B-cells from donors immunized with the antigen of interest in order to obtain mAb repertoire enriched in antigen-specific immunoglobulins. Frequently, immune libraries are generated from immunized animals [213-215]; including macaques which have antibodies that are very similar to those of humans [216]. Immune libraries already contain affinity-matured antibodies, because they are generated from antibody repertoires that underwent antigen driven *in vivo* selection, therefore they generally yield high-affinity clones even if the size is usually not very extensive (e.g. $10^7$ clones). However, the main limitation of animal immune libraries remains that the isolating antibodies are not human and thereby potentially immunogenic. Use of transgenic animals containing human antibody gene repertoire can overcome the limit allowing the discovery of full human antibody [217].

In addition, immune human libraries can be generated starting from B cells of patients who have suffered of infection/disease or donors who received vaccination. Lymphocytes from individuals with cancer may also represent a valuable source of high affinity human mAbs toward tumor-associated antigens; phage libraries can be generated using the antibody genes repertoire of cancer patients thus representing a potential useful tool for the discovery of novel tumor markers. For example, an antibody library of scFv was developed from melanoma patients immunized with genetically modified autologous tumor cells [218]; other Fab/scFv libraries were constructed from patients with colorectal cancer [219], osteosarcoma [220], gastric cancer [221].

**Naïve libraries** are constructed from V genes of B cells from non-immunized donors, (*i.e.*, human IgM repertoire) combinatorially rearranged to create large repertoires of antibodies. These antibodies have already undergone *in vivo* selection for functional B cell receptors, therefore have a low risk of immunogenicity; on the other hand, they may be depleted for clones reacting against self-antigens, thus being potentially less effective for isolation of mAbs towards these antigens.
The advantage of naïve libraries is that contain a very broad repertoire of antibody specificities ($>10^9$ clones), potentially towards every possible antigen; however, the discovered antibody fragments may generally have lower affinities than antibodies discovered from an immunized source [222, 223]. Nevertheless, antibody fragments isolated from universal antibody libraries can be further modified to improve affinity or avidity for the target through *in vitro* affinity maturation or multimerization, respectively [184].
Several naïve human antibody phage libraries have been cloned thus far. In our laboratory, a human naïve single-chain variable fragment library, named IORISS1 and comprising $1.2 \times 10^9$ individual clones, has been generated [224].

In addition to naïve universal libraries, taking advantage of the ability of the immune system to generate diversity, there are **semi-synthetic or fully-synthetic universal libraries**. These are constructed using designed synthetic DNA that exploits the use of highly optimized human frameworks to maintain folding of the V regions, and the introduction of chemical diversity at positions that are most likely to contribute to antigen recognition (usually CDRs).
Semi-synthetic libraries were the first to be made; they typically consist of frameworks sourced from naturally occurring antibodies and CDR regions synthesized using degenerate oligonucleotides [204, 225]. In many instances, to simplify the construction, the randomization is confined to the VH CDR3 region, the loop where most of the sequence diversity naturally occur.

Subsequently, libraries with fully synthetic variable sequences were introduced; frameworks are based on consensus sequences from natural antibodies but optimized for high expression in *E. coli* and display on phages.

Synthetic libraries can generate very high genetic diversity in order to facilitate binding diversity to any potential target. However, while naïve repertoires have been proofread *in vivo* by the immune system, synthetic libraries have not been selected for functionality. Therefore, the strategy of design, i.e. the choice of the germline V genes as scaffolds as well as the choice of position, length and frequency of randomization, is fundamental to maximize the functional diversity. On the other hand, the unbiased nature against self-antigens makes synthetic repertoire suitable for selection, in combination with phage-display technique, of antibodies towards tumor-associated markers for therapeutic purpose. Other advantages of synthetic libraries are the possibility to choose frameworks which possess useful properties including, for example, high stability and binding affinities exploited to facilitate the purification step. Further modification in scaffold sequence may be added to improve other antibody properties such as phage elution, selection for in-frame clones, optimization for expression in mammalian cell culture through removal of undesired potential post-translational modification sites.

Functional diversity can be enhanced and optimized by choosing the germline V genes which compose the framework scaffold. In human *in vivo* antibody repertoire, variable regions of human antibodies are assembled from 51 different VH germline genes [226] and 70 different functional VL segments (40 Vκ and 30 Vλ) [227, 228]. A possibility is to use only a single type of framework scaffold [229, 230], or keep one of the VH or VL constant and use different scaffolds of the other one [231], or take full advantage of the diversity of the scaffolds by combinatorial assembly of many different VH and VL segments, such as in HuCAL PLATINUM, built with 7 VH and 7 VL scaffolds that were combined to yield 49 antibody sub-libraries [232]. However, using such a great variation of scaffolds is not necessarily indicative of improved functionality of the library. Indeed, there is evidence that not all the V variants are equally represented in the functional repertoire, which is instead dominated only by a few germline V genes [227, 233]. By using scaffolds that are not often represented among the binders, library diversity would be wasted. Therefore, limiting the choice of scaffolds to the few V domains that are more frequently found in human antibodies (*e.g.*, DP47 for the heavy chain) can be advantageous. For instances, highly functional synthetic human libraries of scFv antibodies (such as ETH-2, ETH2-Gold, PHILO library and PHILO Diamond) have been constructed by choosing the most common V germlines segments in the human functional repertoire as scaffold: one VH segment (DP47) and one Vk (DPK22) or Vλ (DPL16) segment, respectively

[171, 234-236]; similar rationale has been applied for the new synthetic library described in this thesis, with the addition of an alternative Vk segment (DPK9).

### 1.3.5. Panning for antibody selection

The process of *in vitro* selection of phages displaying monoclonal antibodies with desired binding specificities for a target antigen from libraries is referred to as "(bio)panning" (Figure 14). This procedure basically mimics the B-cell clonal selection system by specifically enriching phage particles that display antibodies with the desired specificity.

The *in vitro* selection process is extremely critical to successfully isolate antigen-specific antibodies, particularly for universal libraries, in which there might be one specific binder in $10^7$–$10^9$ non-antigen specific antibodies [200]. The process requires the immobilization of the target antigen to a solid surface, such as magnetic beads [237], column matrices [238] or plastic surfaces with high protein binding capacity as polystyrene tubes or plates [239]. The latter system is the most widely used [234, 235]. The antigen coated surface is subsequentially incubated with phages from the antibody library. Panning in solution, which involves the use of biotinylated antigens followed by a "pull-down" with streptavidin beads [240], can also be used. The large amount of unbound antibody phage is removed by stringent washing steps. Subsequently, the bound antibody phage will be eluted and reamplified by infection of *E. coli* with helper phage to produce a new antibody phage sub-library, which will be used for another panning round until a significant enrichment of antigen specific antibody phages is achieved. Usually 2-4 panning rounds are required to enrich antibodies even from the largest available libraries. As result, even very rare phenotypes present in large repertoires can be selected and amplified. The optimal selection strategy depends on many parameters, including the target antigen, the optimal antigen immobilization strategy, the quality of the library (particularly the frequency of antigen specific antibodies therein) and the binding and washing conditions. The phage pool with the binding phenotype of interest can be further screened for binding to antigen using enzyme-linked immunosorbent assay (phage ELISA) or other screening assays.

ELISA tests can easily and rapidly be performed using unpurified antibody fragments, either solubly expressed or displayed on phages. Soluble antibodies fragments can be directly produced from the panning output colonies using an amber-suppressor bacterial strain, if the phagemid vector has an amber stop codon between the genes coding for the recombinant antibody and the *pIII* [241].

The binding affinity for the target antigen of the isolated antibody can be further improved by *in vitro* affinity maturation, a process mimicking the natural process of somatic hypermutation occurring *in vivo* in germinal centers, through multiple cycles of random mutation followed by selection [242].

Affinity maturation libraries can be constructed by introducing sequence variability into the CDRs by PCR using partially degenerated primers; for instance, when the antibody clone has been isolated from a synthetic parental library with randomization in the CDR3 region, an efficient strategy can be site-directed mutagenesis either in the CDR1 loop or in the CDR2 loop of VH and VL [235, 243, 244]. Further diversification methods used for *in vitro* affinity maturation of antibody fragments are the introduction of random mutation into the antibody V genes using an error-prone polymerase [245] or chain shuffling [184]. The resulting antibody affinity-maturation library undergoes new rounds of phage display selections, through antigen panning, to select for potential ultra-high-affinity binders. Isolated antibody fragment can be directly used or converted into other antibody formats (antibody reformatting) for therapeutic development, *e.g.*, IgG or antibody-drug conjugates (Figure 14) [246].

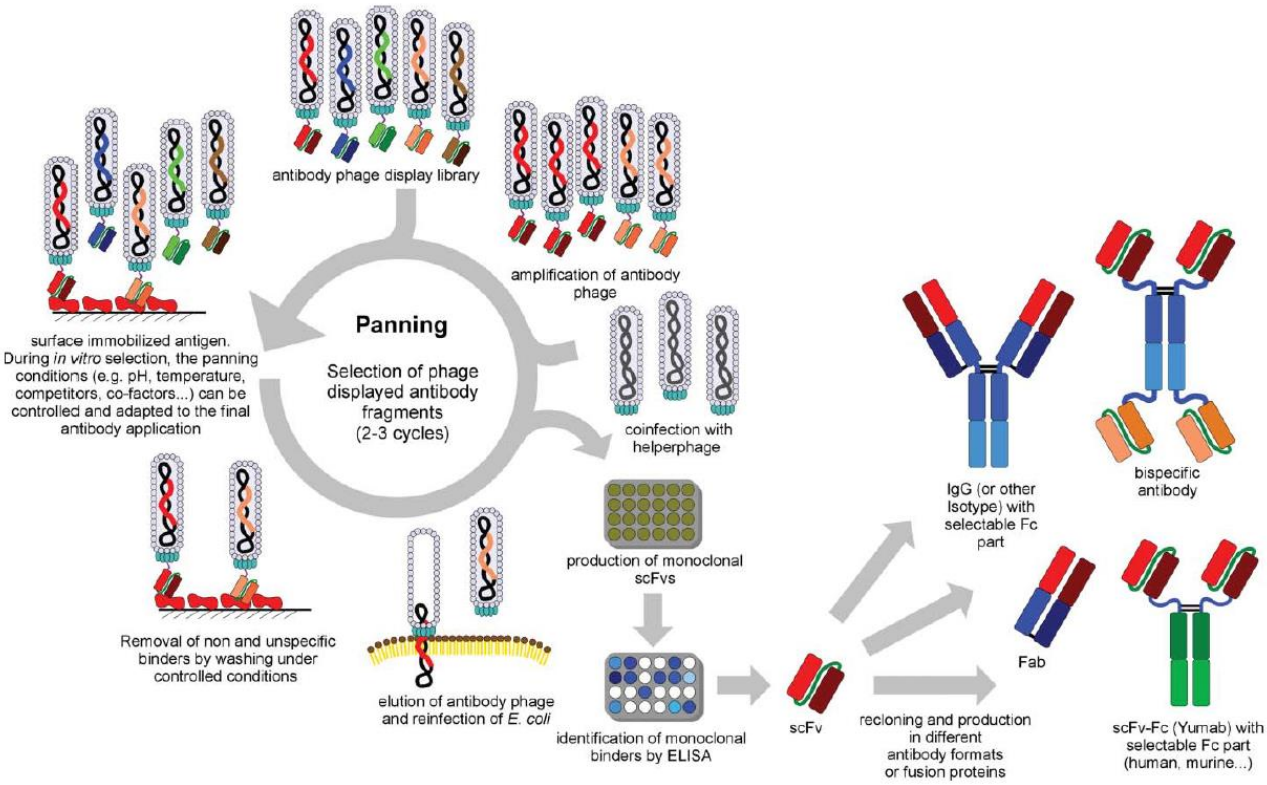


**Figure 14.** Schema of antibody (scFv) phage display selection, screening and reformatting/production of other antibody formats. Reprinted with permission from Frenzel A et al., 2016 [200].

# 2. Aim of the study

Advancements in molecular and genetic techniques have significantly furthered our biological understanding of Ewing sarcoma. While there have been clear advancements in the use of genetic profiling for the diagnosis of Ewing sarcoma, the translation of genomic knowledge into therapeutic advances has been more challenging. The low mutational burden, the general stability of the genome and the low rate of neoantigens are distinctive of Ewing sarcoma, as other paediatric sarcomas, and have limited the role of targeted therapy with mAbs compared to other malignancies. The identification of suitable antigens to be used as targets for antibody development is indeed a major critical step.

ABC transporters have been investigated as one of the causes of drug resistance in a plethora of tumors. Beyond this well-established role in multidrug resistance, less known but an emerging theme is the drug efflux-independent role of ABC transporters in cancer biology; this particularly concerns some neglected members of the ABC family, such as those of the A subfamily [105].
Whereas the association with prognosis of some ABC transporters, such as ABCB1, is well recognized in osteosarcoma, the same has not been highlighted in Ewing sarcoma, in which information regarding the transporters are scattered and controversial.

This PhD project evaluates the clinical relevance of ABC transporters in Ewing sarcoma, looking for potential novel markers to better refine the prognosis and suitable target candidates for novel mAb therapeutic approaches to be used in combination with conventional chemotherapy.
The first aim of the thesis was to perform a retrospective study of correlation of ABC transporter expression in primary tumors with patient outcomes and further investigate the functions and mechanisms of these transporters in *in vitro* models of Ewing sarcoma.
The second aim of the study was to clone and characterize novel human antibody libraries as available tools for the selection of antibodies with specificities towards antigens of interest, such as the ABC transporters identified in the first part of the study.

# 3. Results

## 3.1. ABC transporters of the A subfamily: association with prognosis and implication in cholesterol/lipid homeostasis in Ewing sarcoma

### 3.1.1. Gene expression of ABC transporters and associations with prognosis

We performed an explorative analysis of gene expression of 16 ABCs, belonging to different subfamilies and characterized by a broad range of various functions (Table 2), in order to establish novel relationships with disease outcome in Ewing sarcoma.

| | | Localization | Function |
|---|---|---|---|
| A | **ABCA2** | Lysosomal membrane | Cholesterol homeostasis and lipid transport; drug resistance |
| | **ABCA6** | Plasma membrane | Sterol transport |
| | **ABCA7** | Plasma membrane, endoplasmic reticulum | Phospholipid and ceramide transport, cholesterol transport |
| B | **ABCB1** | Plasma membrane | Multidrug-resistant; transporter in the blood-brain barrier |
| | **ABCB9** | Endoplasmic reticulum and plasma membrane | Peptide transport |
| | **ABCB10** | Mitochondrial membrane | - |
| C | **ABCC1** | Plasma membrane | Multidrug resistance, multispecific organic anion transporter |
| | **ABCC2** | Plasma membrane | Multidrug resistance and detoxification, transport of conjugates of lipophilic substances with glutathione, glucuronate and sulfate |
| | **ABCC4** | Plasma membrane | Multidrug resistance, regulation of cAMP |
| | **ABCC5** | Plasma membrane | Multidrug resistance, export of cyclic nucleotides |
| | **ABCC11** | Plasma membrane | Multidrug resistance, efflux pump for variety of lipophilic anions including the cyclic nucleotides cAMP and cGMP, glutathione conjugates, steroid sulfates, bile acids |
| E | **ABCE1** | Cytoplasmatic localization | Endoribonuclease activity, ribosomal recycling |
| F | **ABCF1** | Cytoplasmatic and nuclear localization | involved in translation of mRNA, potentially involved in inflammatory process |
| | **ABCF2** | Cytoplasmatic localization | - |
| | **ABCF3** | Cytoplasmatic localization | - |
| G | **ABCG2** | Plasma membrane | Multidrug resistance, may play an important role in the exclusion of xenobiotics from the brain; significant expression in the placenta |

**Table 2.** Sixteen ABC transporters of different subfamilies whose gene expression has been evaluated by quantitative reverse transcription PCR (RT-qPCR) in the explorative retrospective analysis on 27 primary Ewing sarcoma samples.

The gene expression was evaluated by quantitative reverse transcription PCR (RT-qPCR) in a training set of 27 tumor samples from patients with primary localized Ewing sarcoma. Subsequently, correlations between ABC expression and prognosis, in terms of event-free survival (EFS) and overall survival (OVS), were investigated. For each ABC, the median expression value was calculated, and patients were stratified as ‘‘high-expressors’’ or ‘‘low-expressors’’ relative to the median value. Kaplan-Meier and univariate analysis (log-rank test) were applied in order to evaluate the prognosis role. Unexpectedly, we found that high levels of three genes, *ABCA6* (EFS, p = 0.049; OVS, p = 0.037) *ABCA7* (EFS, p = 0.033) and *ABCB9* (EFS, p = 0.031; OVS, p= 0.025), were significantly associated with better prognosis (Figure 15).

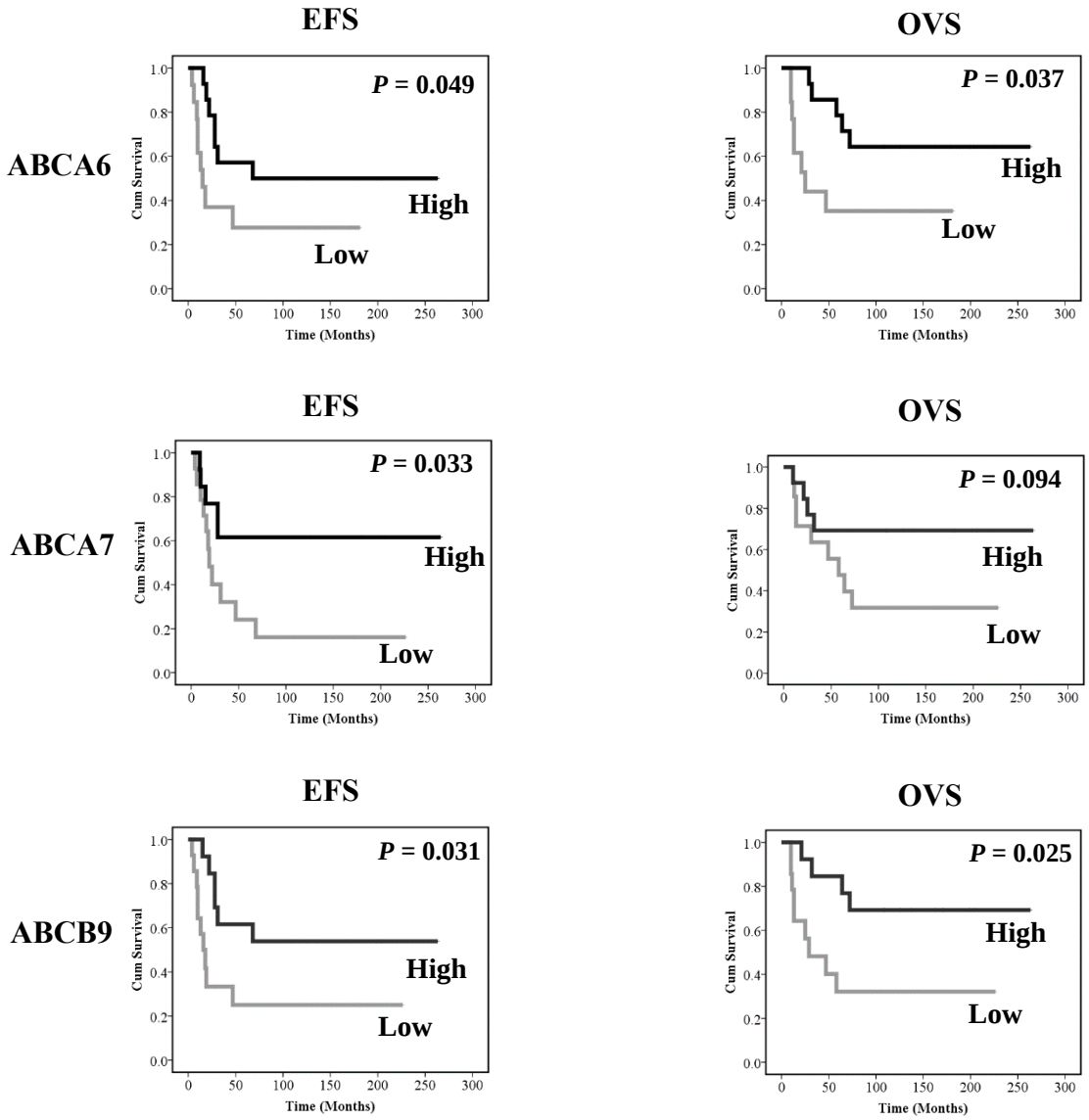


**Figure 15**. Prognostic value of *ABCA6*, *ABCA7* and *ABCB9* in primary Ewing Sarcoma patients. Prognostic impact of *ABCA6*, *ABCA7* and *ABCB9* expression according to Kaplan-Meier curves and log-rank test in 27 Ewing Sarcoma cases analyzed by qRT-PCR. Samples with high (H) and low (L) expression were defined according to the median values. EFS and OVS were evaluated. Time scale refers to months from diagnosis.

To confirm the prognostic relevance, we examined the gene expression of the three transporters on other 103 clinical samples from patients with primary localized Ewing sarcoma. In this set, the relationship between high gene expression and the improved outcome of patients was confirmed only for *ABCA6* (EFS, $p < 0.001$; OVS, $p = 0.002$) and *ABCA7* (EFS, $p = 0.027$; OVS $p = 0.017$) but not for *ABCB9*.

In addition, because Spearman's test indicated a significant correlation between ABCA6 and ABCA7 in the 103 cases (test $r = 0.42$; $p < 0.0001$), the prognostic impact of a model evaluating the combined expression of both genes was evaluated (Figure 16). Patients with low expression of both *ABCA6* and *ABCA7* exhibited a markedly worse OVS with respect to patients classified as ''high-expressors'' for at least one of them ($p = 0.001$). Accordingly, multivariate analysis of the variables associated with OVS by univariate analysis, confirmed the statistical significance of the combined evaluation: the low expression of both *ABCA6* and *ABCA7* emerged as an independent risk factor related to a poor prognosis ($p = 0.030$). Taken together, these findings identified, among the 16 ABCs originally assessed, ABCA6 and ABCA7 as potential indicator of good prognosis in Ewing sarcoma. The association with favorable outcome of patients suggests that the contribution of these ABCA transporters is different from that of "canonical" ABC transporters involved in MDR in cancer. Therefore, we decided to focus our attention on the investigation of the biological functions of ABCA6 and ABCA7 in Ewing sarcoma.

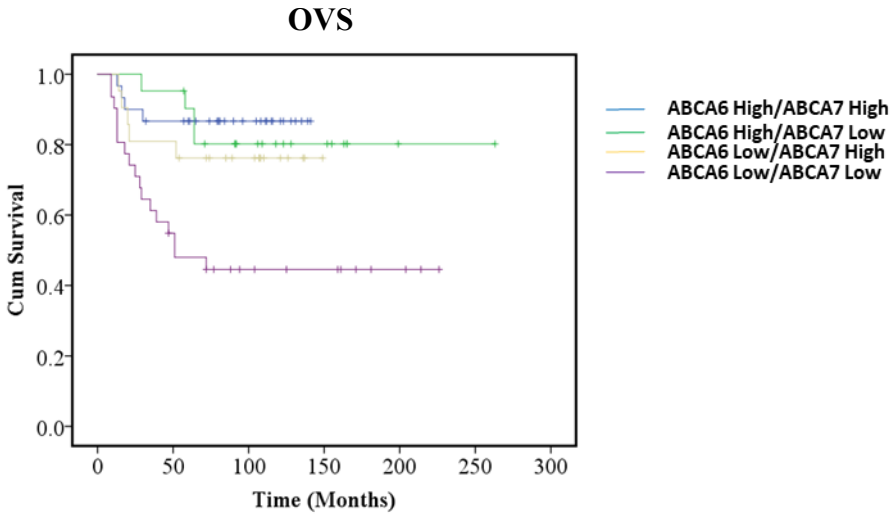


**Figure 16.** Prognostic value of *ABCA6* and *ABCA7* in primary Ewing Sarcoma patients. Prognostic impact of *ABCA6* expression in combination with *ABCA7* expression according to Kaplan-Meier curves and log-rank test in 103 Ewing sarcoma cases analyzed by qRT-PCR. Samples with high (H) and low (L) expression were defined according to the median values; OVS was evaluated. The time scale refers to months from diagnosis.

### 3.1.2. Gene expression regulation of *ABCA6* and *ABCA7* by FoxOs and p53

*Gene expression of ABCA6 and ABCA7 in Ewing sarcoma models*

The gene expression of *ABCA6* and *ABCA7* was evaluated by RT-qPCR in a broad panel of Ewing sarcoma models, including eight patient-derived Ewing sarcoma cell lines, six patient-derived xenografts (PDX) and four PDX-derived cell lines. As showed in Figure 17, the level of expression of *ABCA6* and *ABCA7* was significantly lower in patient-derived cell lines compared to the 103 clinical samples, whereas no difference was found between PDX/PDX-derived cell lines and the clinical samples. Therefore, the PDX models offered a more faithful representation of clinical setting compared with standard cell lines. Moreover, half of the eight patient-derived cell lines of Ewing sarcoma included in the study had mutated *TP53*, whereas only 7-10% of clinical samples carry *TP53* mutations, thereby, we considered these cell models not entirely representative of clinical settings. The four PDX-derived cell lines had wild-type *TP53*, according to the faithful representation of the genetic features of the original tumor of these preclinical models [247].

Nevertheless, the different mutational status of *TP53* among the patient-derived cell lines was useful to investigate transcriptional mechanisms of regulation of the ABCAs.

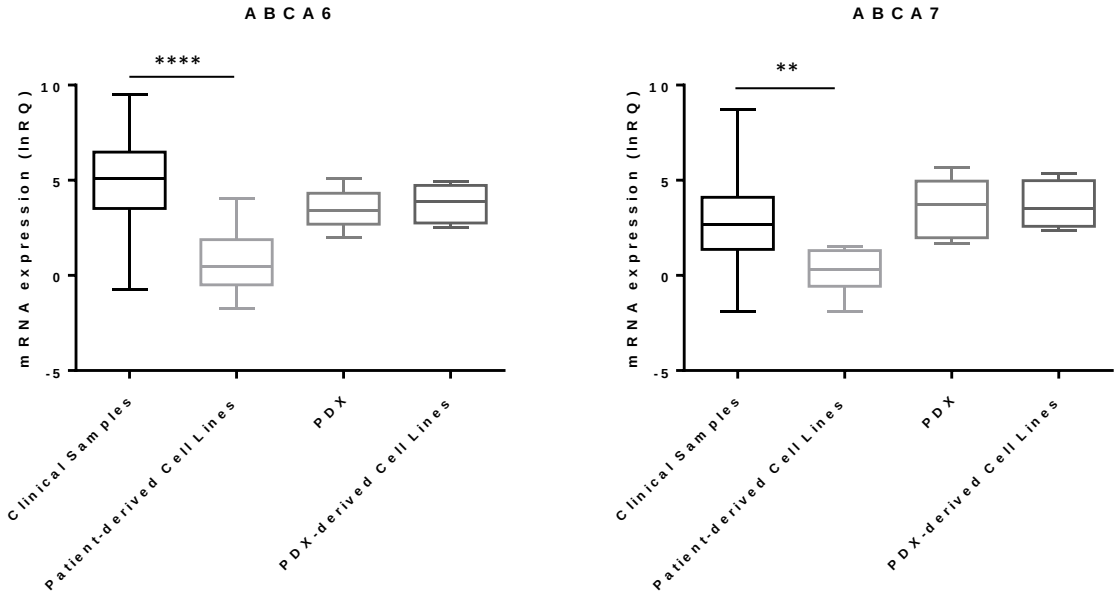


**Figure 17.** Expression level of *ABCA6* and *ABCA7* in Ewing Sarcoma models. The expression was analyzed by qRT-PCR and the cell line HSSC195 was used as calibrator. Patient-derived cell lines expressed *ABCA6* and *ABCA7* transporters at significantly lower levels than clinical samples (One-way ANOVA: P <0.0001 for ABCA6 and P=0.0023 for ABCA7).

*ABCA7 gene expression is regulated by p53 in Ewing sarcoma cells*

In the panel of patient-derived cell lines, the gene expression levels of *ABCA7* were associated with the mutational status of *TP53*, indeed cells with wild-type *TP53* (wt) expressed significantly higher levels of *ABCA7* compared to the cell lines with mutated *TP53* (mut) (p = 0.003; Student's t test) (Table 3). No difference was found between the two groups (wt *TP53* vs mut *TP53*) considering *ABCA6* gene expression (p = ns; Student's t test).

| Cell Lines | TP53 status | ABCA6 gene expression (RQ) | ABCA7 gene expression (RQ) |
|---|---|---|---|
| 6647 | Point Mutation (p.Ser241Phe) | 1.986 ± 0.541 | 0.153 ± 0.074 |
| SK-ES-1 | Point Mutation (p.Cys176Phe) | 0.789 ± 0.037 | 0.517 ± 0.097 |
| SK-N-MC | Major Mutation (c.170_572del) | 1.303 ± 1.024 | 0.751 ± 0.575 |
| TC-71 | Major Mutation (p.Arg213X) | 0.176 ± 0.051 | 0.824 ± 0.102 |
| IOR/GAC | *wt* | 0.562 ± 0.121 | 2.187 ± 0.247 |
| IOR/BRZ_2010 | *wt* | 7.602 ± 0.572 | 2.751 ± 0.436 |
| H1474-p2 | *wt* | 4.270 ± 0.147 | 4.049 ± 0.220 |
| H825 | *wt* (Silent Mutation: p.Arg213Arg) | 57.899 ± 24.440 | 4.592 ± 1.065 |

**Table 3.** Relationship between *TP53* mutational status and *ABCA6* and *ABCA7* gene expression in Ewing sarcoma patient-derived cell lines.

To evaluate the possibility of a transcriptional regulation of *ABCA7* expression by p53 in Ewing sarcoma cells, the promoter of *ABCA7* gene and the 5' flanking sequence were analyzed *in silico* in order to identify putative p53 binding sites. We confirmed the presence of binding sites for p53 and design primers to amplify the specific promoter region.

To confirm the transcriptional regulation of *ABCA7* by p53, experiments of Chromatin immunoprecipitation (ChIP) and RT-qPCR were performed to monitor, respectively, the binding of p53 to *ABCA7* promoter and the simultaneous variations in *ABCA7* gene expression level in a panel of four patient-derived cell lines. Two wt *TP53* cell lines (IOR/BRZ_2010 and IOR/GAC) and two mut *TP53* (SK-N-MC and TC-71, as negative controls) have been used for the experiment. Cells were treated for 24 hours with doxorubicin (DX), in order to induce activation of p53, which was verified as phosphorylation of the protein in serine 15 by Western Blotting (Figure 18A). Anti-p53 ChIP assay demonstrated a significant increased recruitment of p53 to the *ABCA7* promoter region after DX

treatment compared to untreated control (CTR), only in the two cell lines presenting wt TP53 (Figure 18B and C).

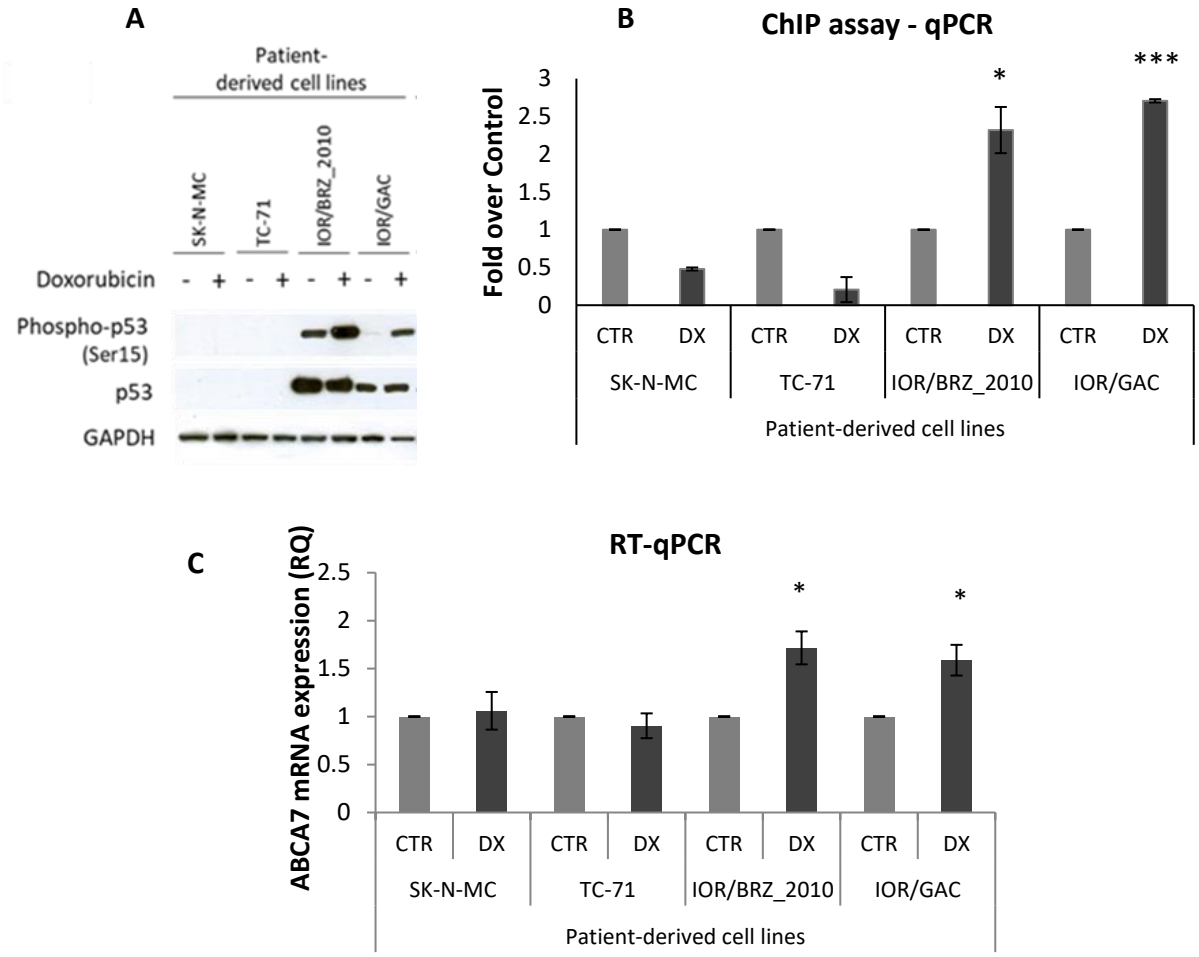


**Figure 18.** Transcriptional regulation of *ABCA7* expression by p53 in patient-derived cell lines. A) Representative western blotting showing the expression of phospho-p53 (ser15) and total p53 in four Ewing sarcoma patient-derived cell lines after 24 hours of treatment with doxorubicin (DX); B) anti-p53 chromatin immunoprecipitation (ChIP) was performed on the Ewing sarcoma patient-derived cell lines with and without DX. The results were obtained by qPCR. The data represent the recovery of each DNA fragment relative to the total input DNA and are plotted as fold over the untreated control (CTR); C) *ABCA7* mRNA expression was analyzed by RT-qPCR in four Ewing sarcoma patient-derived cell lines. *GAPDH* was used as a housekeeping gene. The DX concentration used in the experiments was the $IC_{50}$ x2 for each cell line calculated after 72 h of treatment. Data are mean ± SE from at least three experiments. *P < 0.05, ***P < 0.001, Student's t-test (DX versus CTR).

The result of increased recruitment of p53 to the *ABCA7* promoter, together with induced gene expression of the *ABCA* after DX, was further confirmed in two PDX-derived cell lines expressing wt *TP53* (Figure 19).

Taken together, the data supported the hypothesis of a transcriptional regulation of *ABCA7* gene expression mediated by p53 in Ewing sarcoma cells.

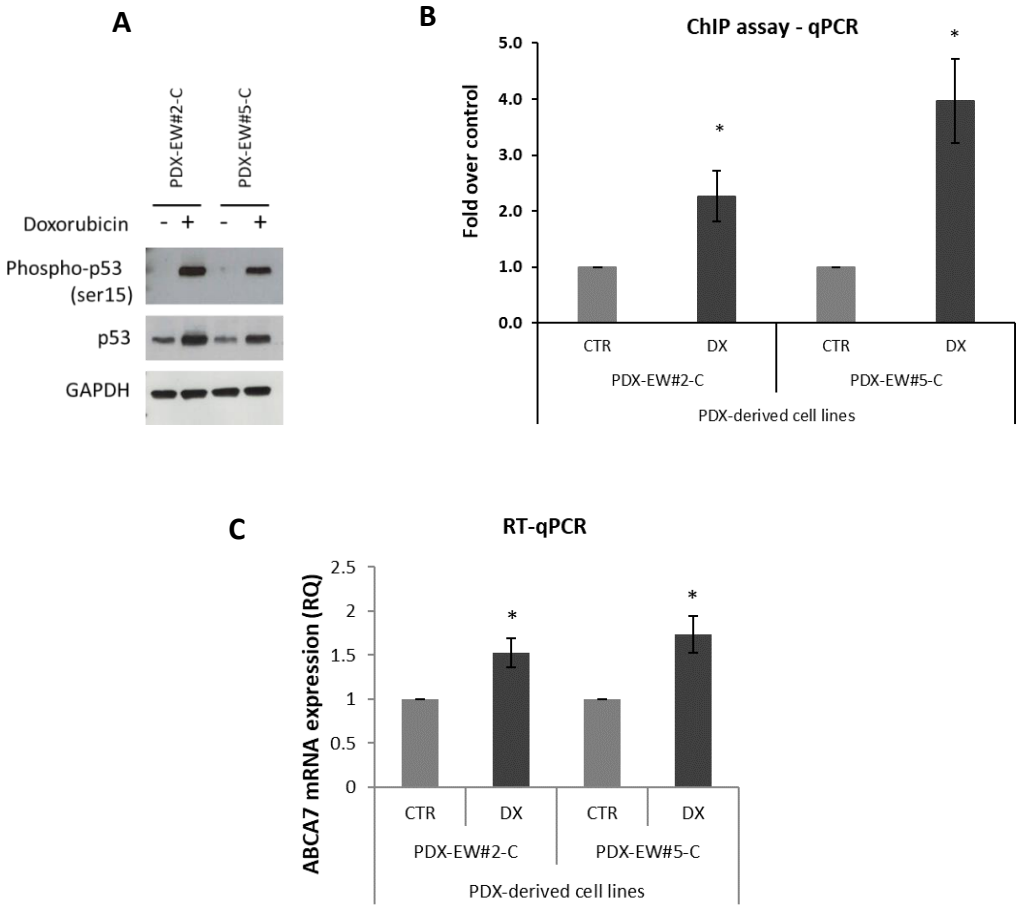


**Figure 19.** Transcriptional regulation of *ABCA7* expression by p53 in PDX-derived cell lines. A) Representative western blotting showing the expression of phospho-p53 (ser15) and total p53 in two Ewing sarcoma PDX-derived cell lines after 24 hours of treatment with doxorubicin (DX); B) anti-p53 chromatin immunoprecipitation (ChIP) was performed on the Ewing sarcoma PDX-derived cell lines with and without DX. The results were obtained by qPCR. The data represent the recovery of each DNA fragment relative to the total input DNA and are plotted as fold over the untreated control (CTR); C) *ABCA7* mRNA expression was analyzed by RT-qPCR in the Ewing sarcoma PDX-derived cell lines. *GAPDH* was used as a housekeeping gene. The DX concentration used in the experiments was the $IC_{50}$ x2 for each cell line calculated after 72 h of treatment. Data are mean ± SE from at least three independent experiments. *P < 0.05, Student's t-test (DX versus CTR).

*ABCA6 gene expression is regulated by FoxO transcription factors and repressed by IGF1R/Akt signaling*

Similarly to *ABCA7*, the gene expression of *ABCA6* significantly increased after treatment with DX compared to CTR, but this effect occurred in all the Ewing sarcoma cell lines tested independently from the mutational status of *TP53*, suggesting a different mechanism of regulation for this gene (Figure 20).

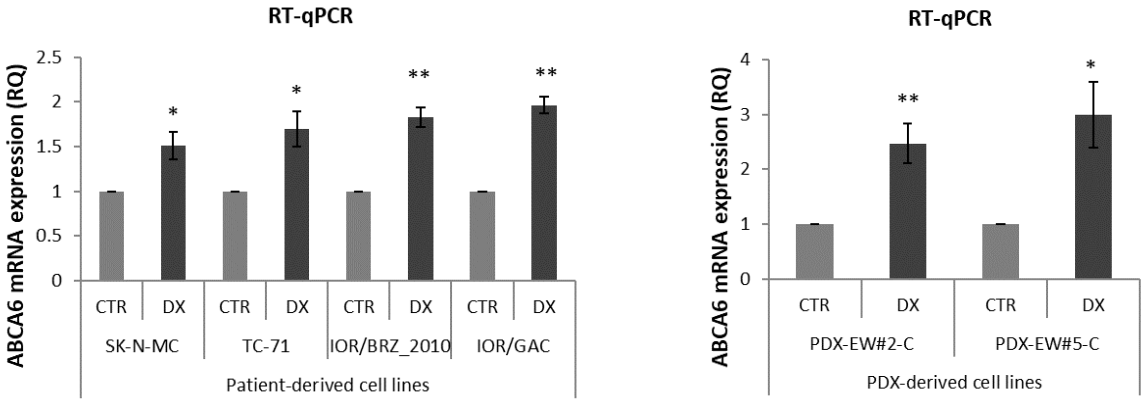


**Figure 20.** *ABCA6* gene expression in Ewing sarcoma patient-derived cell lines (left) and PDX-derived cell lines (right) after 24 hours treatment with doxorubicin (DX). *ABCA6* mRNA expression was analyzed by RT-qPCR. *GAPDH* was used as a housekeeping gene. The DX concentration used in the experiments was the $IC_{50}$ x2 for each cell line calculated after 72 h of treatment. Data are mean ± SE from at least three independent experiments. *P < 0.05, **P < 0.01, Student's t-test (DX versus CTR).

Considering that Gai J et al. identified two functional Forkhead box O (FoxO)-responsive elements in *ABCA6* promoter and consequently demonstrated the role of FoxO proteins in the transcription of the *ABCA* in human vascular endothelial cells [248], the hypothesis of a similar mechanism of regulation was evaluated in Ewing sarcoma cells. With an experimental design similar to the one previously reported, PDX-derived cell lines were treated for 24 hours with DX, then anti-FoxO1 ChIP assay was performed and *ABCA6* gene expression levels were monitored by RT-qPCR. In parallel, phosphorylation of FoxO1 at serine 256 was evaluated in order to verify activation of transcriptional activity of this factor; indeed, in its unphosphorylated state, FoxO1 localized into the nucleus where can activates transcription of target genes, while in its phosphorylated form at serine 256, FoxO1 is maintained inactive in the cytoplasm [249]. The data demonstrated that FoxO1 was phosphorylated, after DX treatment, and increasingly recruited on *ABCA6* promoter compared to CTR in both the Ewing sarcoma PDX-derived cell lines (Figure 21).

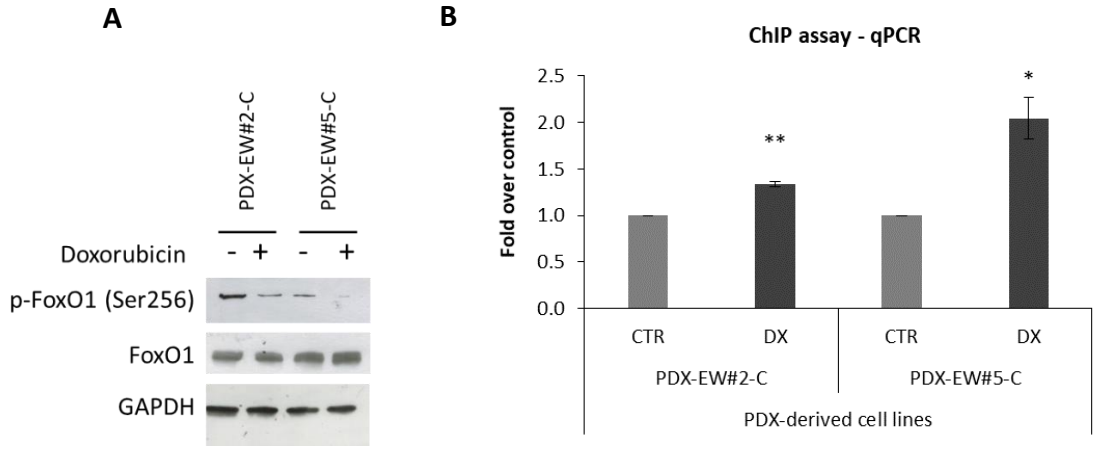


**Figure 21.** Transcriptional regulation of *ABCA6* expression by FoxO1. A) Representative western blotting showing the expression of phospho-FoxO1 (ser256) and total FoxO1 in Ewing sarcoma PDX-derived cell lines after 24 hours of treatment with doxorubicin (DX); B) anti-FoxO1 chromatin immunoprecipitation (ChIP) was performed on the Ewing sarcoma PDX-derived cell lines with and without DX. The results were obtained by qPCR. The data represent the recovery of each DNA fragment relative to the total input DNA. The DX concentration used in the experiments was the $IC_{50}$ x2 for each cell line after72 h of treatment. Data are mean ± SE from at least three independent experiments. *P < 0.05, **P < 0.01, Student's t-test (DX versus CTR).

Additionally, we evaluated the binding of FoxO1 and also FoxO3a on *ABCA6* promoter in three cell lines (TC-71 and two PDX-derived cells) under basal condition, without any treatment. ChIP assay, followed by PCR amplification of *ABCA6* promoter region, confirmed the recruitment of both FoxO1 and, to a lesser extent, FoxO3a on *ABCA6* promoter; the binding of the RNA Polymerase II demonstrated the functionality of the interaction in activating the gene transcription (Figure 22).

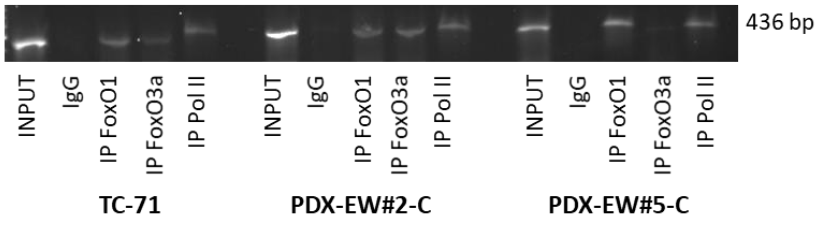


**Figure 22.** Transcriptional regulation of *ABCA6* expression by FoxO1 and FoxO3a. ChIP assay was carried out in TC71, PDX-EW#2-C and PDX-EW#5-C cells by using anti-FoxO1 and FoxO3a antibodies. The *ABCA6* promoter regions containing the putative binding sequence for FoxOs were amplified, after immunoprecipitation, by PCR with specific primers. The PCR products were detected by agarose gel electrophoresis. Input was amplified as control. Anti-mouse IgG immunoprecipitation was used as negative CTR. *IP, immunoprecipitation; Pol II, RNA Polymerase II.*

Interestingly, transcription factors of FoxO family are downstream targets of the IGF1R/PI3K/Akt signaling, which is a major autocrine loop that sustains cell growth and malignant behavior of Ewing sarcoma [44], as described in the introduction section. Therefore, we investigated by RT-qPCR if gene expression of *ABCA6* was downregulated by IGF1R/Akt signaling, through FoxO1 inactivation, in Ewing sarcoma cells (Figure 23). When starved TC-71 and PDX-EW5#C cells were stimulated by IGF1 (50 ng/ml) exposure for 24 hours, Akt resulted highly phosphorylated in ser473 and thus activated, FoxO1 was instead inactivated by phosphorylation at ser256 (Figure 23A), and *ABCA6* gene expression was significantly decreased in comparison with CTR (Figure 23B). On the other hand, the opposite findings were obtained when cells were treated with an anti-IGF1R monoclonal antibody (100 ng/ml) or the inhibitor of PI3K LY294002 (10 μM). An intermediate situation, similar to CTR, was found when cells were pretreated with an inhibitor (anti-IGF1R or LY294002) and further exposed to IGF1 (Figure 23 A and B).

These data offer a plausible explanation for the general low gene expression of *ABCA6* in Ewing sarcoma cells due to the constitutive activation of IGF1R/Akt signaling.

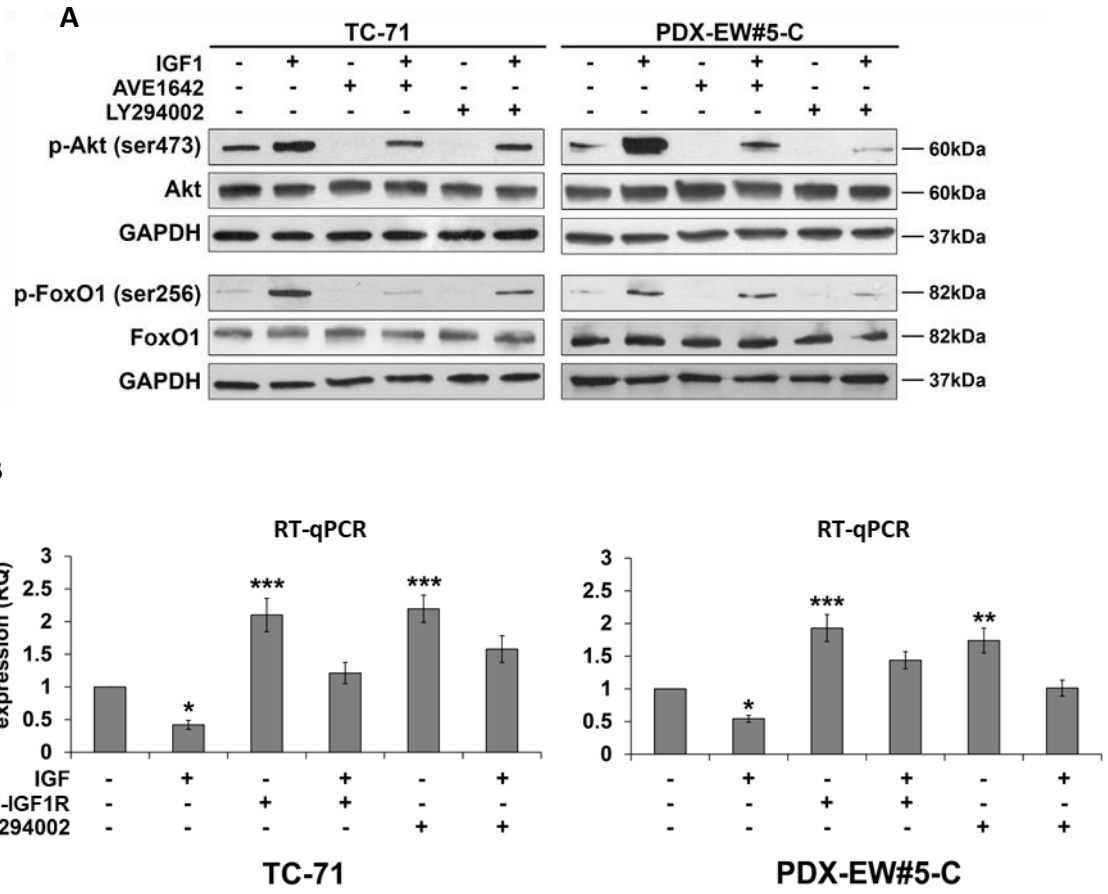

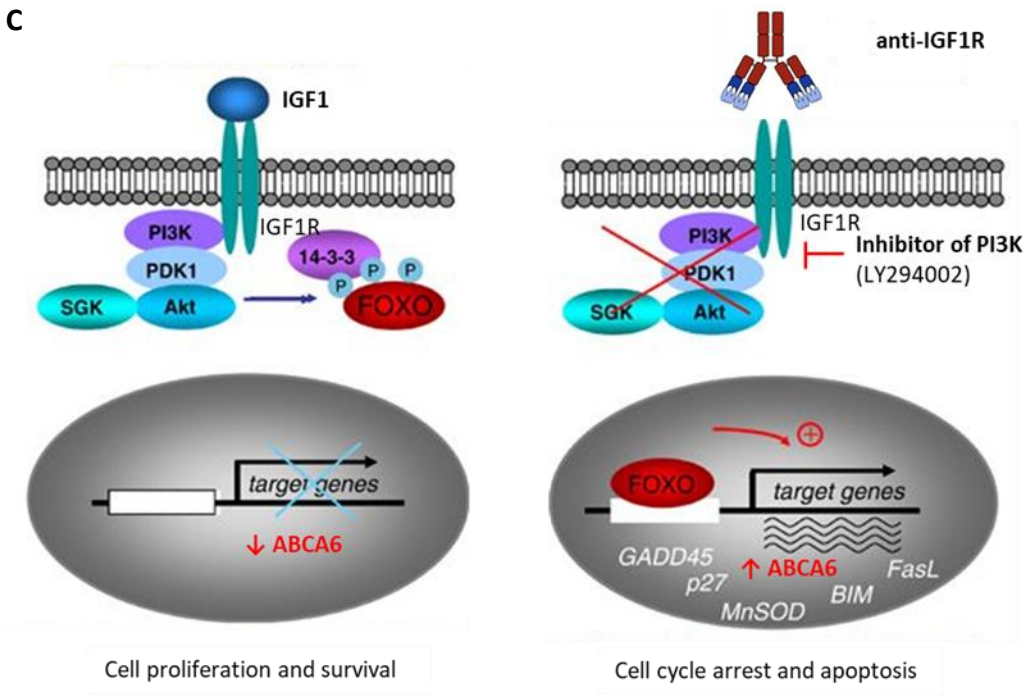


**Figure 23.** *ABCA6* gene expression is downregulated by IGF1R/Akt signaling through FoxO1 inactivation. A) Representative western blotting of three experiments showing the expression of phospho-Akt (ser473), phospho-FoxO1 (ser256), FoxO1 and Akt in TC-71 and PDX-EW#5-C cells. GAPDH was used for normalization. Cells were cultured in medium at 1% serum for 18 h and then exposed to IGF-1 (50 ng/mL) for 24 h in the presence or absence of an anti-IGF1R mAb (100 ng/mL) or LY294002 (10 μmol/L) (after pre-treatment of 3 h or 2h respectively); B) In the same experiments the *ABCA6* mRNA expression was evaluated by RT-qPCR. *GAPDH* was used as a housekeeping gene. Data are presented as mean ± SE from at least three independent experiments. *P < 0.05; **P < 0.01; ***P < 0.001, one-way ANOVA (versus CTR); C) schematic representation of *ABCA6* transcription regulation mediated by IGF1R/Akt/FoxO in different cellular context: after IGF1 stimulation (left) or after inhibition by anti-IGF1R/PI3K inhibitor (right). Picture adapted from Gai J et al., 2013 [248].

### 3.1.3. High expression of ABCA6 and ABCA7 affected *in vitro* malignancy and increased chemosensitivity

*Characterization of Ewing sarcoma PDX-derived cell lines with differential expression of ABCA6/7*

Accordingly with the previous data of gene expression levels of *ABCA6/7* in Ewing sarcoma models (Figure 17) and considering that PDXs are more representative of the genetic and phenotypic heterogeneity of the original tumor [247], PDX-derived cell lines were employed to further investigate the role of these transporters in Ewing sarcoma. The four PDX-derived cell lines available in our laboratory were characterized in terms of expression of ABCA6 and ABCA7, both at gene and protein levels (Figure 24A and B, respectively).

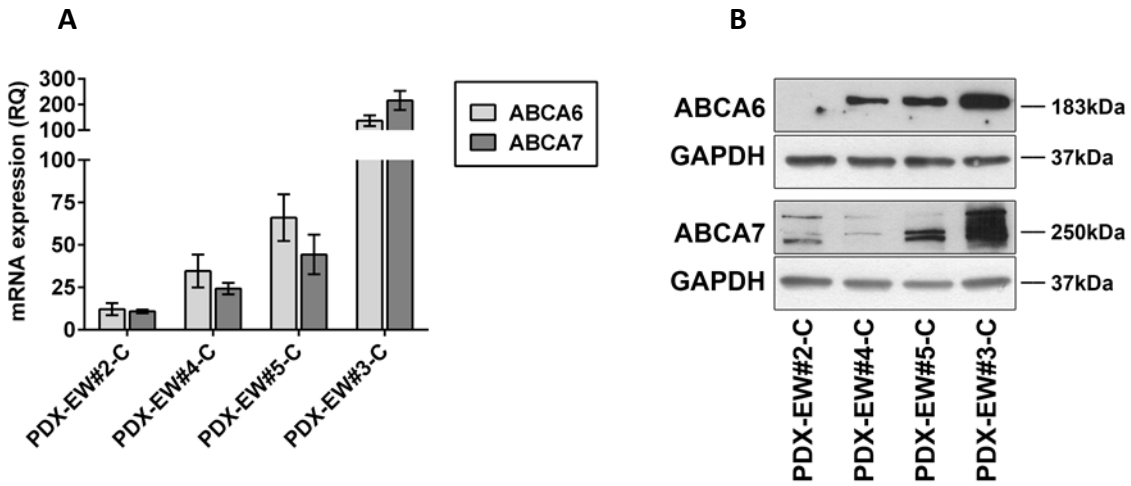


**Figure 24.** ABCA6 and ABCA7 expression in a panel of four Ewing sarcoma PDX-derived cell lines at mRNA (A) and protein level (B). Gene expression was evaluated by RT-qPCR using *GAPDH* as housekeeping gene. Protein expression was evaluated by western blotting; equal sample loading was monitored by blotting for GAPDH.

The levels of expression of the two transporters were different among the four PDX-derived cell lines, making them suitable models to find out functional differences associated with differential ABCA expression levels. PDX-EW#2-C and PDX-EW#4-C showed low expression of both ABCA6 and ABCA7, whereas PDX-EW#5-C and PDX-EW#3-C expressed the ABCAs at high levels. Accordingly with the data of correlation between *ABCA6* and *ABCA7* in the clinical set of 103 tumor samples, the same was found in PDX-derived cell lines where the levels of expression of both the ABCAs correlated with each other.

The four PDX-derived cell lines were further characterized in terms of *in vitro* parameters of malignancy, evaluated as anchorage-independent growth and migration ability, and sensitivity to conventional chemotherapy drugs used in Ewing sarcoma treatment.

We found out that the two cell lines with high expression of ABCA6 and ABCA7 displayed an attenuated phenotype, as demonstrated by the reduced number and dimension of colonies growth on soft-agar assay, and a decreased migration capability when compared to the cell lines with low ABCAs expression (Figure 25A and B, respectively).

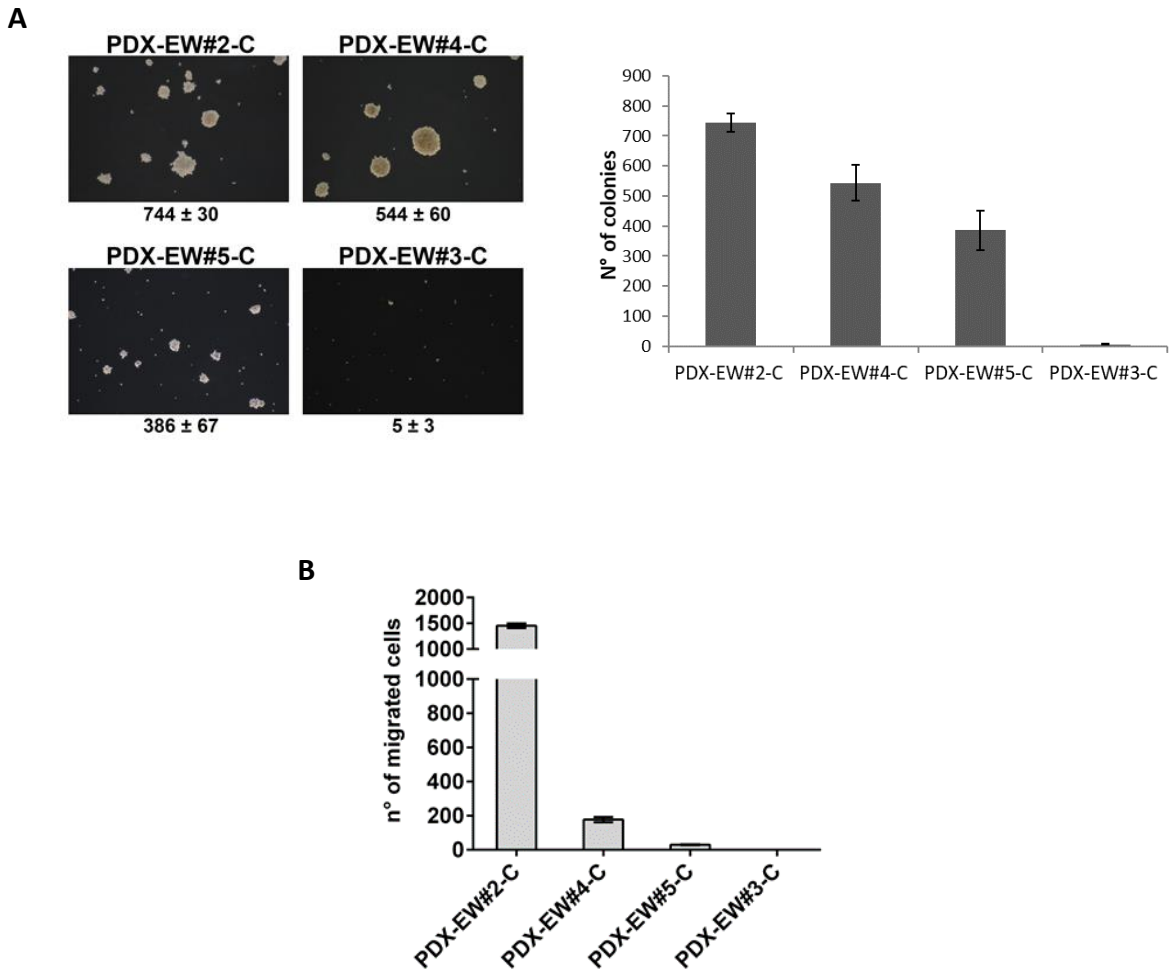


**Figure 25.** The expression of ABCA6 and ABCA7 influences malignancy in PDX-derived Ewing sarcoma cell lines. A) Soft-agar growth of four Ewing sarcoma PDX-derived cell lines; B) Migration ability of four Ewing sarcoma PDX-derived cell lines evaluated by motility assay. The mean ± SE of at least two independent experiments is reported.

Data of *in vitro* chemosensitivity, obtained by MTT assay after 72 hours of treatments, demonstrated a significantly enhanced sensitivity of PDX-EW#5-C cells (ABCA6/7 high) to the DNA damaging chemotherapeutics doxorubicin ($p = 0.002$; Student's t test), etoposide ($p = 0.004$; Student's t-test) and ifosfamide ($p = 0.029$, t-test). No difference was observed with respect to vincristine, whereas an opposite trend between the two cell lines was found for the actinomycin D (Figure 26 A).

The sensibility to DX-induced apoptosis was additionally evaluated in the two PDX-derived cell lines after 24 hours of treatment; in keeping with the prior data, the PDX-EW#5-C cells (ABCA6/7 high) displayed an increased susceptibility to the early apoptotic event of mitochondrial depolarization induced by DX when compared to PDX-EW#2-C cells (ABCA6/7 low). A lower range of concentrations of DX was used for the PDX-EW#5-C cells (ABCA6/7 high) according to the

difference in terms of IC50 values between the two cell lines (Figure 26B). The caspase-3 and PARP cleavage were also evaluated by western blotting, confirming the previous observations (Figure 26C). Notably, DX at concentration of 25 ng/ml induced an evident activation of both Caspase-3 and PARP by cleavage in PDX-EW#5-C cells but not in PDX-EW#2-C cells.

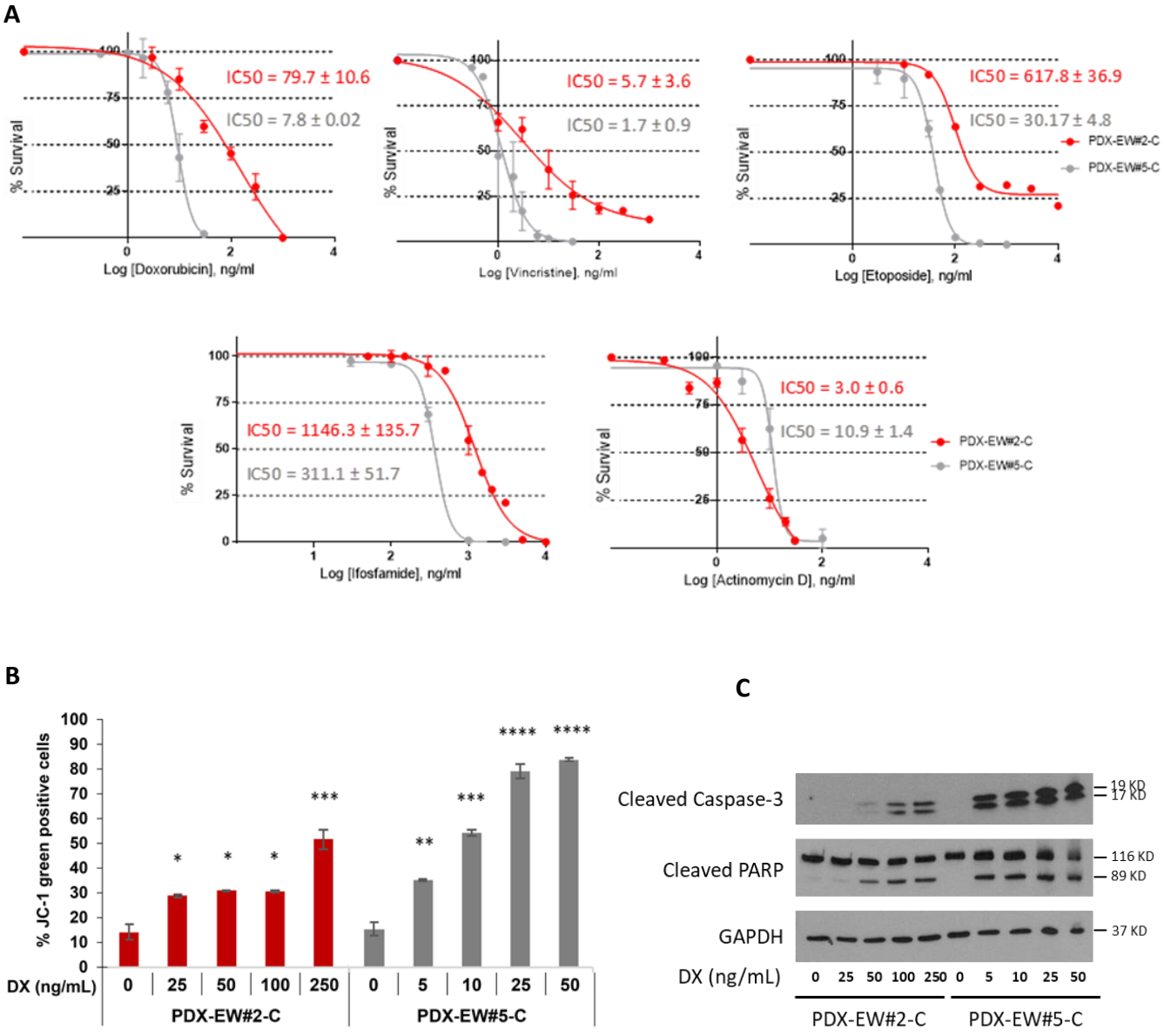


**Figure 26.** The expression of ABCA6 and ABCA7 influences chemosensitivity in PDX-derived Ewing sarcoma cell lines. A) Chemosensitivity of two PDX-derived cell lines with differential expression of ABCA6/7 to standard chemotherapy drugs for Ewing sarcoma treatment. Chemosensitivity was evaluated by MTT assay after 72 hours of treatment with doxorubicin, vincristine, etoposide, ifosfamide and actinomycin D. The mean ± SE of at least three independent experiments is reported for each point; B) Sensitivity to apoptosis induced by doxorubicin (DX) was determined as mitochondrial depolarization in the two Ewing sarcoma PDX-derived cell lines. The cells were treated for 24 h with different concentrations of DX. Columns represent the mean values ± SE of three independent experiments, *P < 0.05; **P < 0.01; ***P < 0.001; ****P<0.0001, one-way ANOVA (versus CTR); C) Representative western blotting of three experiments showing the expression of cleaved caspase 3 and cleaved PARP in the Ewing sarcoma PDX-derived cell lines. Equal sample loading was monitored by blotting for GAPDH.

*Overexpression of ABCA6 and ABCA7 by transient transfection*

The data reported thus far are in accordance with the positive prognostic role emerged for *ABCA6* and *ABCA7* by the clinical data of correlations with favorable outcome of patients. For a comprehensive evaluation of the plausible tumor suppressor role of ABCA6 and ABCA7 in Ewing sarcoma, the PDX-EW#2-C cells, characterized by low basal expression of ABCAs, were transiently transfected to overexpress one among *ABCA6* and *ABCA7* or both, in order to define individual and combined contributions of the transporters to Ewing sarcoma malignancy and chemosensitivity. 48 hours after transfection, the overexpression was verified by evaluating gene and protein expression levels of the ABCAs (Figure 27A); in parallel, migratory ability (Figure 27B) and chemosensitivity to DX (expressed as IC50) after 24 hours of treatment were evaluated (Figure 27C).

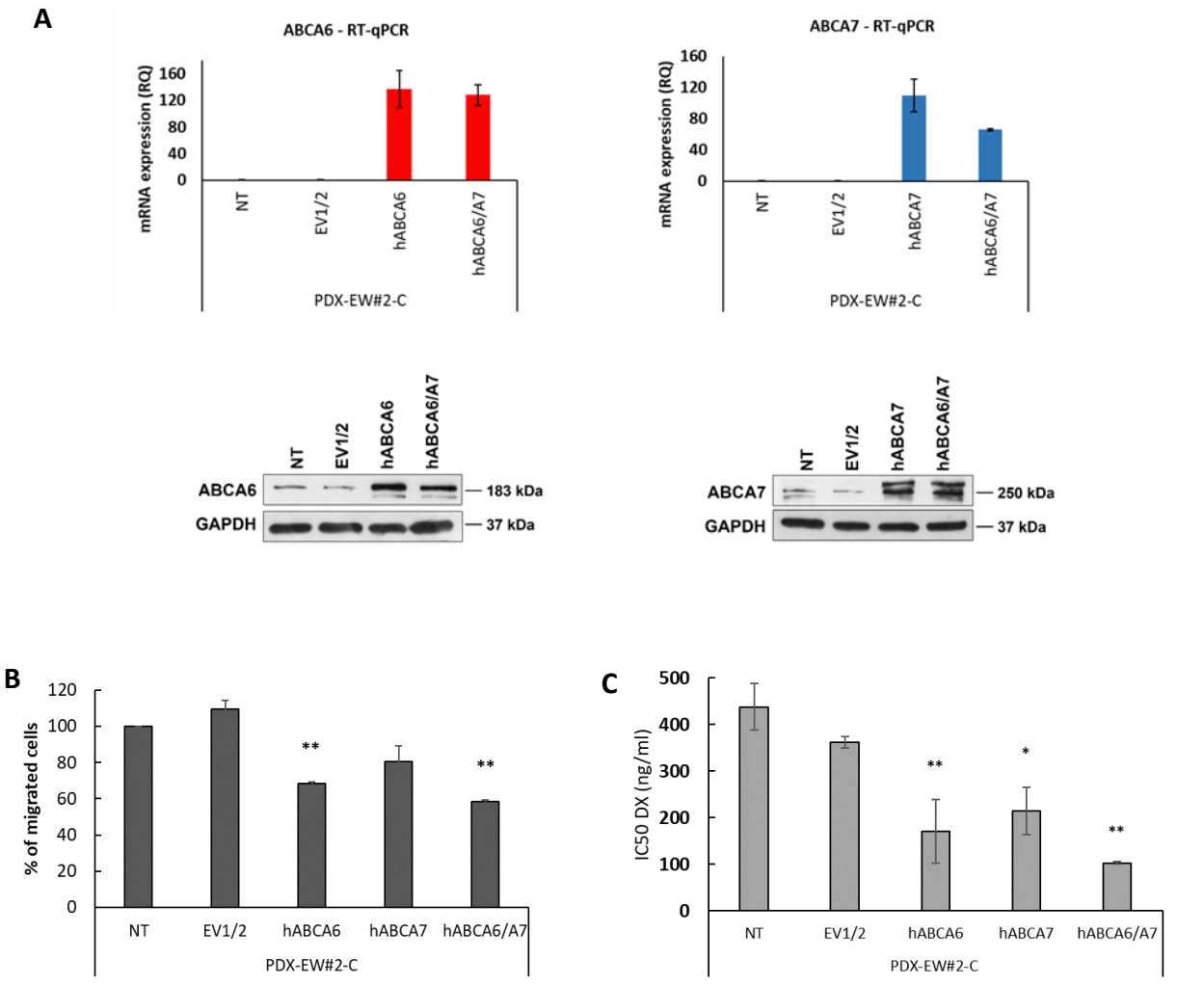


**Figure 27.** Effects of overexpression of *ABCA6*, *ABCA7* or both on *in vitro* malignancy and chemosensitivity. A) Expression of ABCA6 and ABCA7 was evaluated at mRNA and protein levels after 48 hours of transient transfection in Ewing sarcoma PDX-EW#2-C cells. Relative mRNA expression levels of *ABCA6* and *ABCA7* compared with that of the empty vector (EV1/2: 2^(-ΔΔCt) = 1). *GAPDH* was used as a housekeeping gene. Representative western blotting showing ABCA6 and ABCA7 expression is reported, in which equal sample loading was monitored by blotting for GAPDH; B) migratory ability of PDX-EW#2-C cells after transient

overexpression of ABCA6, ABCA7 or both; C) sensitivity to doxorubicin (DX), expressed as IC50, after 24 h of treatment of PDX-EW#2-C cells after transient overexpression of ABCA6, ABCA7 or both. Columns represent the mean ± SE of three independent experiments; * $P < 0.05$, ** $P < 0.01$, One –way ANOVA (vs NT, non-transfected cells).

According with the previous data, overexpression of ABCA6, ABCA7 or both affected significantly the migratory ability of cells and increased the sensitivity to doxorubicin (reduced IC50 value) when compared with non-transfected cells (NT) or empty vector-transfected cells (EV1/2). In particular, the comprehensive effect of modulation of malignancy and chemosensitivity can be mainly attributed to ABCA6, however the co-transfection with both the ABCAs impacted slightly more on decreasing DX IC50 than individual transfections with one among ABCA6 or ABCA7, supporting the stronger prognostic value of the combined expression of the two transporters.

### 3.1.4. Altered cholesterol levels and distribution in cells mediated the effects of low expression of ABCA6/7 on a more malignant phenotype

The last section of this part of results is dedicated to the understanding of the mechanisms which underlie the effects of reduced malignancy and increased susceptibility to DX in Ewing sarcoma cells expressing high levels of ABCA6 and ABCA7. Unfortunately, as extensively described in the introduction section, the information available for these two transporters are scarce; the endogenous ligands as well as the exact physiological functions are not univocally understood, however an increasing number of evidences indicate a role in cholesterol, ceramide and phospholipids homeostasis in cells, particularly for ABCA7.

Ceramide is a sphingolipid acting as second messenger for multiple extracellular stimuli including growth factors stimulation, chemotherapeutic agents and cellular stress. Ceramide is recognized as tumor-suppressor lipid, because a variety of stimuli which trigger apoptosis, such as DX, increase intracellular ceramide to initiate apoptotic signaling.

Therefore, levels of ceramide were evaluated by flow cytometry in PDX-EW#2-C cells after overexpression of ABCA6 or ABCA7 and treatment with DX for 24 hours (Figure 28). A trend of increased ceramide accumulation in cells overexpressing ABCA6 after DX treatment (50 ng/ml or 250 ng/ml) was found when compared with non-transfected (NT) cells or transfected-empty vector cells treated with the same concentration of DX. The data suggest that the sphingolipid may be

partially involved in increased susceptibility to apoptosis induced by DX in cells with high expression of ABCA6.

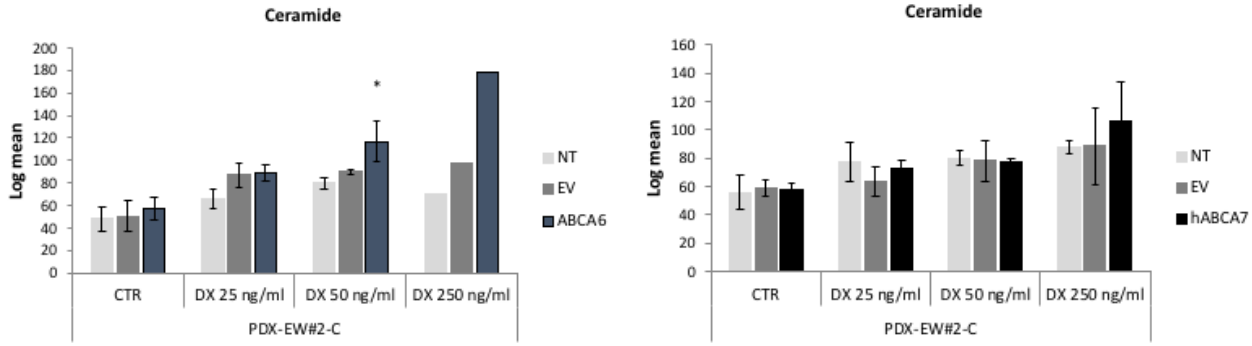


**Figure 28.** Ceramide levels after ABCA6 or ABCA7 transient overexpression. The total levels of ceramide were evaluated and quantified in PDX-EW#2-C cells, 48 hours after transfection, by flow cytometry after staining with an anti-ceramide monoclonal antibody and anti-mouse FITC as secondary antibody. Columns represent the mean ± SE of two independent experiments (one experiment after ABCA6 transfection and treatment with 250 ng/ml of doxorubicin (DX) has been performed); * $P < 0.05$, One –way ANOVA (vs NT and EV treated with the same concentration of DX).

Considering the role of ABCAs in cholesterol transport and homeostasis, intracellular **cholesterol** levels and distribution were evaluated in PDX-derived cells with differential expression of ABCAs by total cholesterol quantification with a colorimetric assay and filipin III staining, respectively (Figure 29). The PDX-EW#5-C cells, with high levels of both ABCA transporters, exhibited a diffuse localization of cholesterol in cellular membranes and, in general, a lower fluorescence compared to that in PDX-EW#2-C cells (ABCA6 and ABCA7 low), which were indeed characterized by intense intracellular accumulation of cholesterol particularly in the perinuclear region and plasma membrane (Figure 29A). The lower cellular cholesterol level in PDX-EW#5-C cells, compared to that of PDX-EW#2-C cells, was also confirmed by total cholesterol quantification (Figure 29B).

The hypothesis was that cells with low expression of ABCA6/7 accumulated cholesterol and underwent an unbalanced cholesterol distribution, which consequently determined the more aggressive tumor behavior. To verify this aspect, PDX-EW#2-C cells (ABCA6 and ABCA7 low) and PDX-EW#5-C cells (ABCA6 and ABCA7 high) were treated for 72 hours with cholesterol-lowing drug simvastatin or exogenous cholesterol, respectively. Change in intracellular cholesterol levels and distribution were monitored together with parameters of *in vitro* malignancy of anchorage-independent growth and migration ability.

Accordingly to the hypothesis, when PDX-EW#2-C cells (ABCA6/7 low and high cholesterol levels) were exposed to subtoxic doses of simvastatin, cellular cholesterol levels significantly decreased (Figure 29A and B) and growth in anchorage independent conditions as well as cell migratory ability were impaired (Figure 29C and D). The opposite effects were observed when PDX-EW#5-C cells (ABCA6/7 high and low cholesterol levels) were exposed to exogenous cholesterol, as demonstrated by enhanced clonogenic capacity, migratory ability and scratch wound closure (Figure 29 C and D).

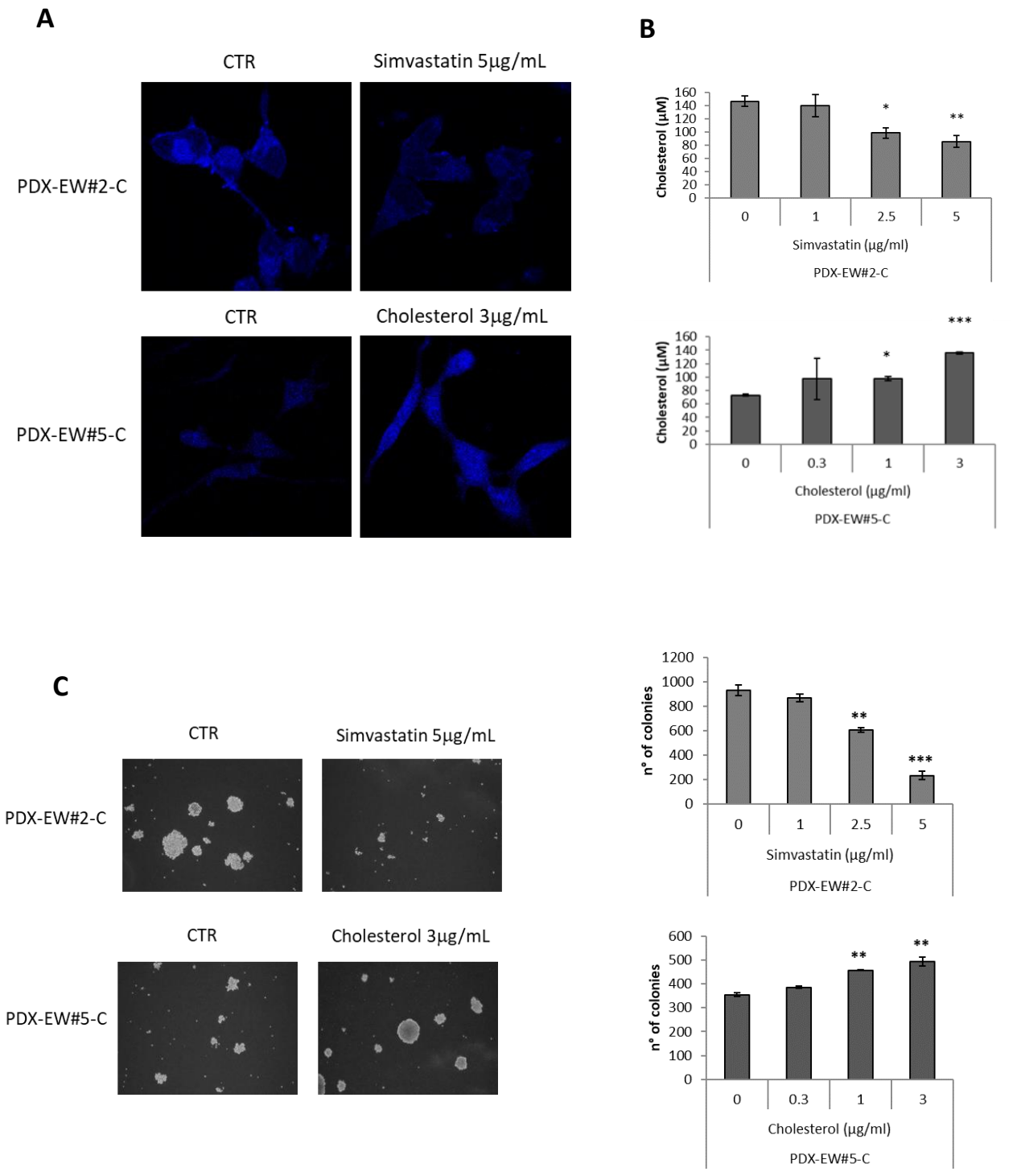

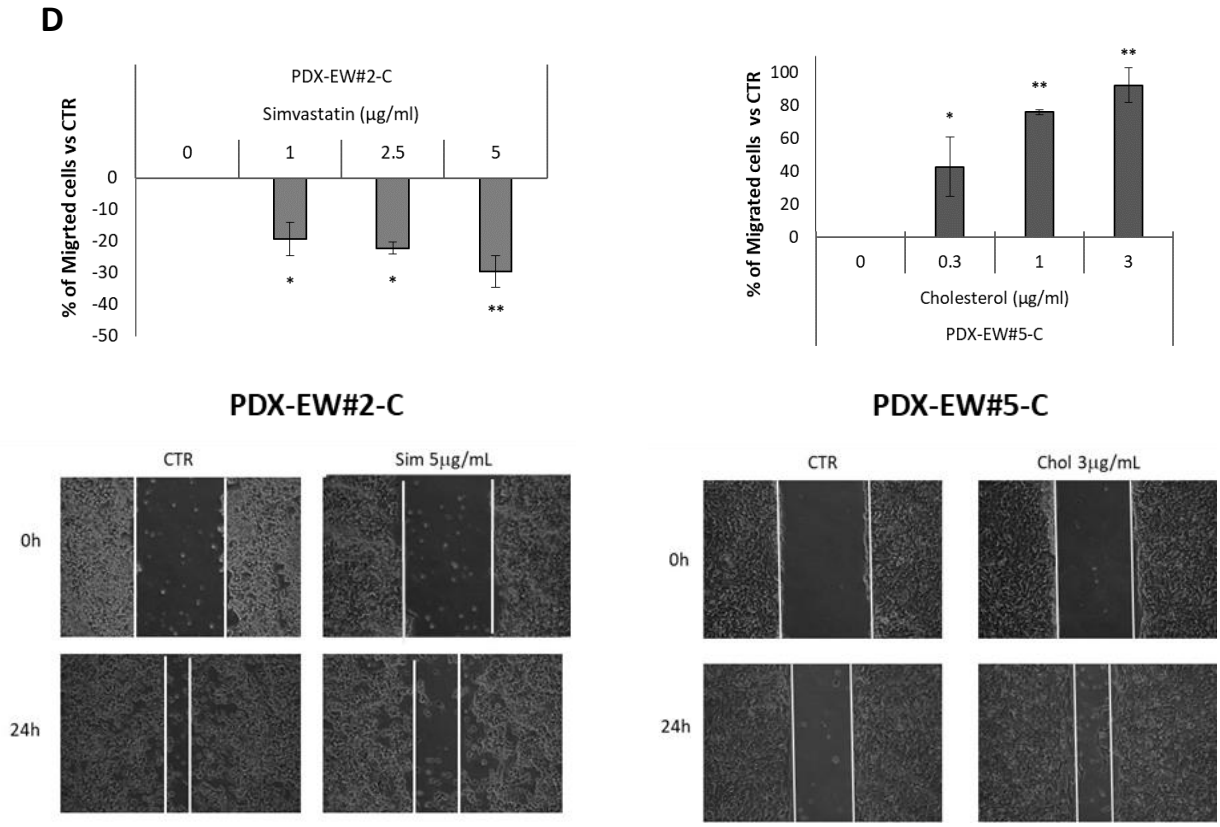


**Figure 29.** Effects of cholesterol modulation on Ewing sarcoma *in vitro* malignancy. Confocal microscopy after Filipin III staining (A) or total cholesterol quantification (B) of PDX-EW#2-C cells (ABCA6/7 low) or PDX-EW#5-C cells (ABCA6/7 high) after 72 hours of treatment with simvastatin or cholesterol, respectively. C) Soft-agar growth; D) Migration ability evaluated as motility assay (top of the figure D) or wound healing assay (bottom of the figure D). All the experiments were performed on PDX-EW#2-C cells (ABCA6/7 low) or PDX-EW#5-C cells (ABCA6/7 high) with and without simvastatin or cholesterol, respectively, after 72 hours of pre-treatment. Columns represent the mean values ± SE of at least two independent experiments, *P < 0.05; **P < 0.01; ***P < 0.001; one-way ANOVA (versus CTR). *Sim, simvastatin; Chol, cholesterol.*

In addition, the sensitivity to simvastatin was compared between the two cell lines with differential ABCA6/7 expression, and notably the cell line with low ABCA levels, PDX-EW#2-C, was more sensitive (IC50 = 63.65 +/- 5.47 µg/mL) to the cholesterol-lowering drug than PDX-EW#5-C with high ABCA levels (IC50 = 188.99 +/- 16.82 µg/ml) (p = 0.002; Student's t-test).

The therapeutic potential of simvastatin was also evaluated in combination with DX in PDX-EW#2-C cells, which were the most resistant among the two cell lines. The simvastatin increased the sensitivity to DX with a concentration-dependent effect and the combination of the two drugs resulted in a synergistic effect, as indicated by the combination index (CI) of 0.673 (Figure 30).

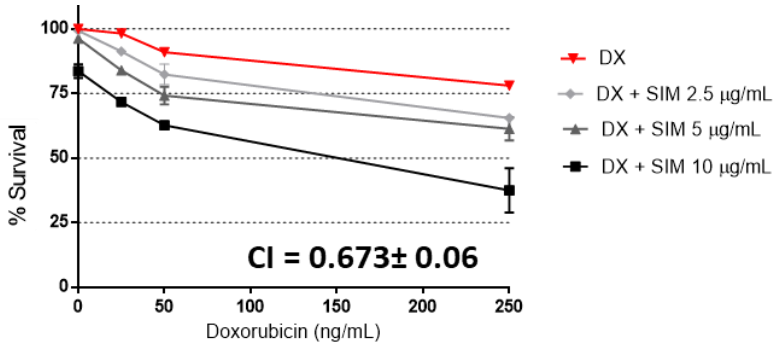


**Figure 30.** Combination treatment of simvastatin (SIM) with doxorubicin (DX) in PDX-EW#2-C cells. Cells were treated with SIM or SIM+DX for 24 hours after 72 hours of pre-treatment with SIM. Cells treated only with DX were used to determine the effect of the single drug. After the treatment, vital cells were counted by Trypan blue staining. Combination index (CI) was calculated with an isobologram equation using CalcuSyn software (Biosoft). Each point represents the mean value ± SE obtained from three independent experiments.

Proving the linkage between ABCA6, ABCA7 expression and cellular cholesterol accumulation, when PDX-EW#2-C cells over-expressing ABCA6 and ABCA7 were treated with exogenous cholesterol, the effect of reduced migration ability was completely reverted, as demonstrated by motility assays (Figure 31B).

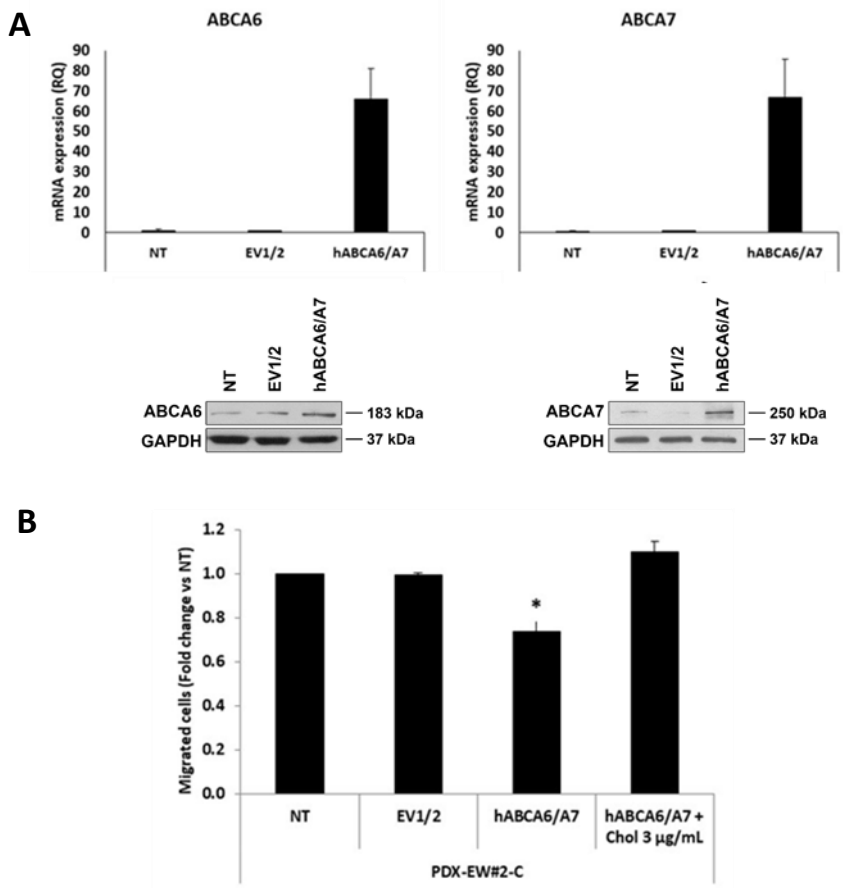


**Figure 31.** Treatment with cholesterol reverted the effect of reduced migration ability after ABCA6 and ABCA7 overexpression in PDX-EW#2-C. A) mRNA (top of the figure) and protein expression (bottom) of

ABCA6 and ABCA7 after 6 days of transient overexpression of both ABCAs. Relative mRNA expression levels of ABCA6/7 were compared with that of the empty vector (EV1/2; 2DDCt = 1). GAPDH was used as a housekeeping gene. Representative western blotting showing ABCA6 and ABCA7 expression. Equal sample loading was monitored by blotting for GAPDH; B) Migration ability evaluated by motility assay after overexpression of both ABCA6 and ABCA7 with and without cholesterol (Chol) for 72 hours. Columns represent the mean ± SE values of three independent experiment; *$P < 0.05$, one-way ANOVA (vs NT and EV1/2).

## 3.2. Generation of a novel synthetic human antibody phage-display library

### 3.2.1. Rationale for library design

To generate a large, highly diverse, naïve synthetic library of functional antibody in the scFv format, we cloned scFv fragments with sequence diversity restricted to the CDR3 loops of both the VH and VL chains into a phagemid vector.

Based on experience from previous highly functional synthetic libraries (ETH2-Gold, Philo1 and 2 libraries), the scFv antibody scaffold was constructed by choosing the DP47 germline sequence as VH domain and either DPK22/DPK9 or DPL16 as germline genes for the VL domain, Vκ and Vλ, respectively. These germlines dominate the functional repertoire in humans and represent 12% (DP47), 25% (DPK22) and 16% (for both DPK9 and DPL16) of the *in vivo* antibody repertoire in humans [204, 233]. Using the DP47 VH germline segment offers several further advantages, such as a higher thermodynamic stability and Protein A binding properties, which facilitate antibody purification and detection [185, 250]. Thus, in addition to the germline segments used in previously described libraries [234-236], the second most used Vκ germline in the human repertoire, DPK9 (Griffith AD et al., 1994), was added to maximize the functional diversity of the library. Furthermore, residue 90 of DPL16 was designed to be alanine, instead of serine, to abolish a potential N-glycosylation site (*i.e.*, the NXS/T amino acid sequence, where N is asparagine, X is any amino acid except proline, and S/T is serine/threonine). Indeed, glycosylation sites are usually removed from CDRs or their proximity because they may lead to heterogeneity during the manufacturing process as biopharmaceuticals [251]. A similar strategy of abrogation of N-glycosylation sites was adopted to develop the HuCAL PLATINUM library, which generated approximately 4-fold more unique sequences and higher affinity antibodies compared to those isolated from the HuCAL GOLD library in which the NXS/T pattern was maintained [232].

The scFv antibodies of the new library described in this thesis are essentially based on three alternative antibody scaffolds resulting from the combination of the germline VH segment DP47 with either a Vκ segment, among DPK9 and DPK22, or the Vλ segment DPL16. Combinatorial mutagenesis at the level of the CDR3 loops of both heavy and light chain was performed (Figure 32).

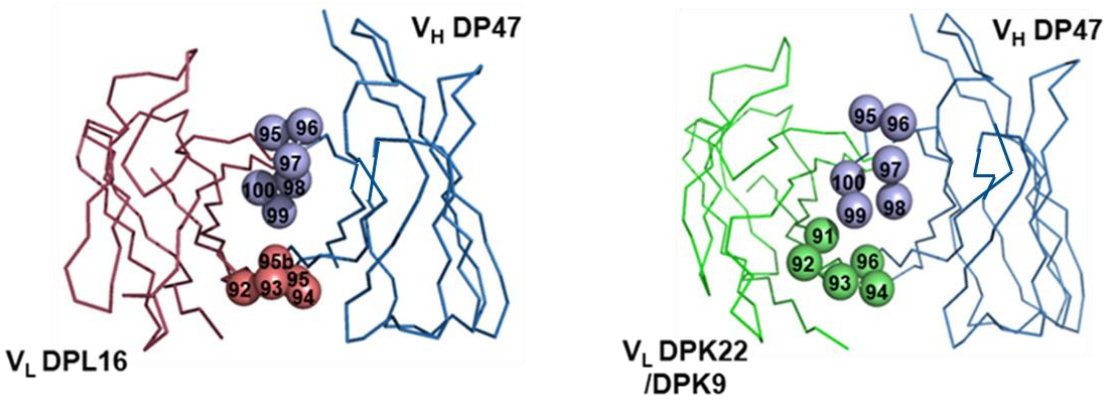


**Figure 32.** Design of antibody library. ScFv antibody fragment structures. On the left panel, the DPK22/DPK9 (Vk) backbone is represented in green and the DP47 (VH) in blue. Right panel: DPL16 (Vλ) backbone is depicted in dark red and DP47 (VH) in blue. Residue subject to random mutation are DP47 CDR3 position 95, 96, 97, 98, 99 and 100 (light blue specefill representation), DPK22/DPK9 CDR3 position 91, 92, 93, 94 and 96 (green spacefill representation) and DPL16 CDR3 position 92, 93, 94, 95, 95a and 95b (dark red spacefill representation). Using the program PyMol the structure of the scFvs were modulated from the protein data base (Brookhaven Protein Data Bank) files 1igm and 8FAB for DP47-DPK22 and DP47-DPL16, respectively. The residue numbers are according to Tomlinson IM et al., 1996 and Williams SC et al., 1996 [228, 252].

Variability was confined to the CDR3 amino acid positions with a major role in antigen contact and where high variability naturally occurs [253]. Particularly, combinatorial mutagenesis was introduced into the CDR3 of VH (DP47) with completely randomized sequence of four to seven residues (instead of a maximum of six as in ETH2-Gold library), whereas CDR3s in VL segments were partially randomized in six amino acid residues, including at least one proline. The randomized amino acid positions are shown in Figure 33.

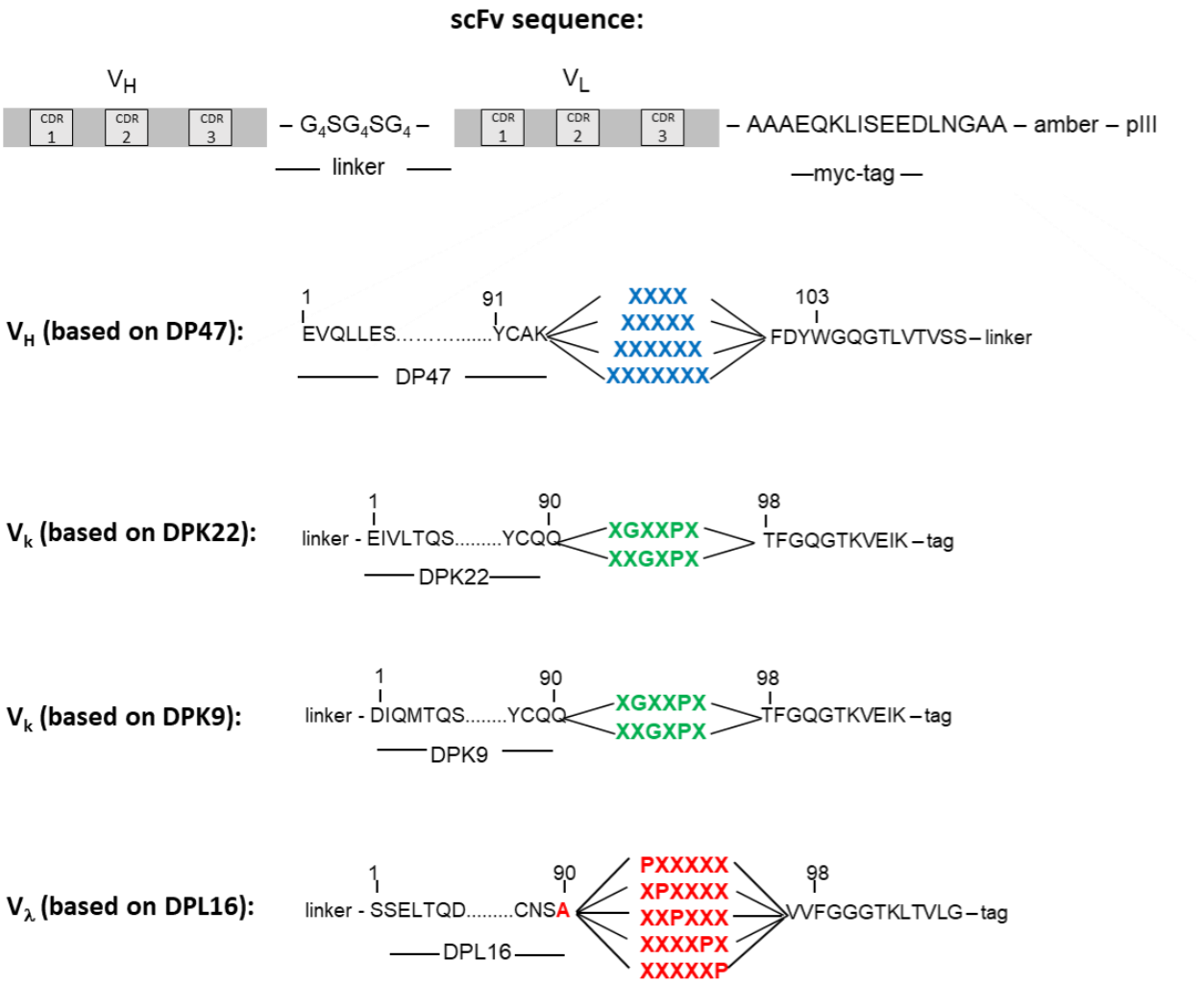


**Figure 33.** Sequences of relevant amino acid residues of the variable heavy (VH) and light (Vκ or Vλ) chains, together with the human antibody germline segments from which they are derived. Single amino acid codes are used according to standard IUPAC nomenclature.

In the natural human repertoire, the length of CDR3 can vary from a few residues to more than 20 residues [204]. The choice to confine the diversity to sequences of four to seven residues into the CDR3 loops was made according the evidence that short CDR3s in the VH and VL domains are generally associated with better antibody stability to proteolysis, reduced immunogenicity, improved affinity and bacterial expression [183, 254, 255]. Furthermore, the short CDRs used in our library design may facilitate the modeling of antigen recognition by the antibody using computational approaches [256].

The flexible polypeptide linker $Gly_4SerGly_4SerGly_4$ was used to connect VH and VL in the scFv antibody format [234, 235].

### 3.2.2. Cloning strategy and library construction

For library construction, the CDR3 regions were randomized by PCR using partially degenerated primers (Figure 34). After this amplification step, the resulting VH-VL segments were assembled by PCR. All the primers used in the amplification and assembly steps are listed in Table 8 of the material and methods section. A total of 105 µg of NotI-NcoI double-digested insert was ligated into double-digested phagemid pHEN1 vector [185], which appended a short peptidic myc-tag at C-terminus of recombinant antibodies. The ligation products for each sub-library were electroporated into freshly prepared electrocompetent *E. Coli* TG1. Seven different sub-libraries containing a total of 3.1 x $10^9$ individual clones were obtained (Table 4). For each sub-library, the cells were stored as glycerol stocks at -80°C and were super-infected with helper phage VCSM13 for phage production. The sub-libraries could be used together for selections against antigens of interest by mixing the corresponding phage preparations.

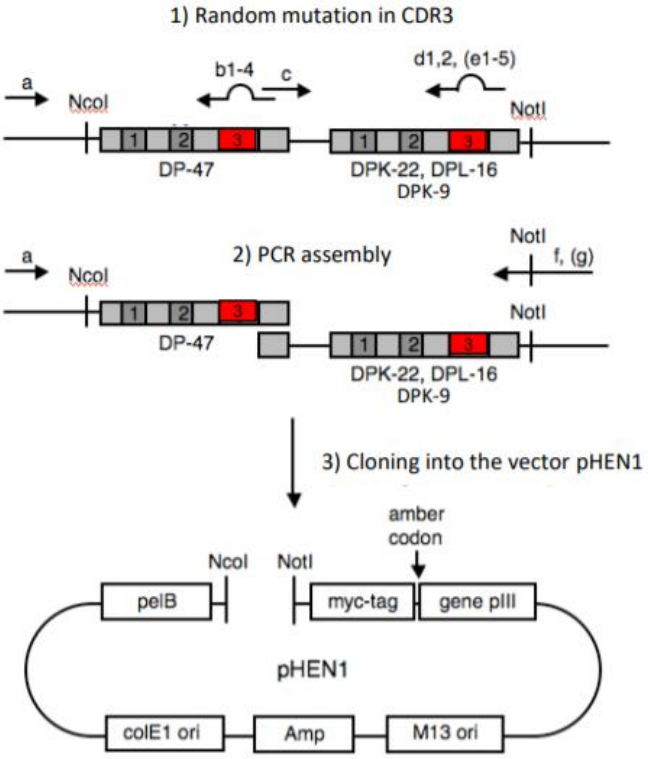


**Figure 34.** Libraries cloning strategy. Mutations were introduced in the CDR3 regions by PCR using partially degenerate primers, named b1-4 (for CDR3 of VH), d1,2 (for CDR3 of Vκ) and e1-5 (for CDR3 of Vλ). Genes are indicated as rectangles and CDRs as numbered boxes, among which the CDR3 is depicted in red. The VH and VL segments were then assembled by PCR and cloned into the pHEN1 vector [185].

| Sub-library | Amount of DNA insert ligated | Number of individual antibody clones |
|---|---|---|
| L16_1 | 15 µg | $3.2 \times 10^8$ |
| L16_2 | 15 µg | $6.4 \times 10^8$ |
| L16 sub-library | 30 µg | $9.6 \times 10^8$ |
| K22_3 | 15 µg | $6.5 \times 10^8$ |
| K22_4 | 15 µg | $6.2 \times 10^8$ |
| K22 sub-library | 30 µg | $1.4 \times 10^9$ |
| K9_1 | 15 µg | $7.6 \times 10^7$ |
| K9_2 | 15 µg | $6.5 \times 10^7$ |
| K9_3 | 15 µg | $6.1 \times 10^8$ |
| K9 sub-library | 45 µg | $7.5 \times 10^8$ |
| **Library total** | 105 µg | **$3.1 \times 10^9$** |

**Table 4.** Titers and total amount of double-digested DNA insert used for each sub-library.

### 3.2.3. Characterization of the new antibody library

The quality and functionality of the library were verified by PCR colony screening and DNA sequencing of randomly picked clones.

PCR screening analysis revealed that 100% of the tested individual clones (n=96), which were randomly picked from different sub-libraries, contained an insert of the right size of approximately 1000 bp (Figure 35). All the randomly picked clones that were sequenced (n=50) revealed that all amino acid sequences in the CDR3 region of both VH and VL were diverse (Table 5).

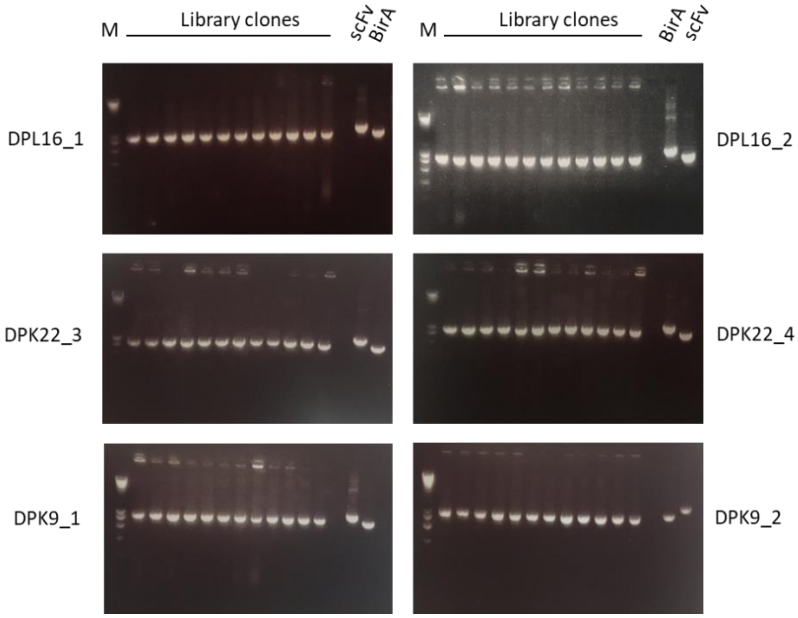


**Figure 35.** Characterization of the new antibody library. PCR colony screening of 12 randomly picked clones of each sub-library. As negative control a BirA insert (1200 bp) of a pHEN1 vector was amplified. All the tested clones showed an insert with the correct size of approximately 1000 bp.

| Sub-library | Clone | $V_H$ | $V_L$ |
|---|---|---|---|
| | | 95 – 100 | 91 – 96 |
| DPL16 | DPL-16_1#1 | A K V Q L A S - - F D | S A R E V R H **P** V V |
| | DPL-16_1#2 | A K T Q T G - - - F D | S A T Q T N **P** F V V |
| | DPL-16_1#3 | A K K V R R V F - N F D | S A S V **P** M S F V V |
| | DPL-16_2#1 | A K N I N R - - - F D | S A **P** F V Y W E V V |
| | DPL-16_2#2 | A K W L W W H R S F D | S A R M **P** F S P V V |
| | DPL-16_2#3 | A K N A R D P - - F D | S A H N L H Q **P** V V |
| DPK22 | DPL-22_3#1 | A K S T L H I R Q F D | Q Q V R **G** I **P** N T F |
| | DPL-22_3#2 | A K R H K D - - - F D | Q Q Q H **G** F **P** Y T F |
| | DPL-22_3#3 | A K W L R I I M - F D | Q Q L **G** S T **P** H T F |
| | DPK-22_4#1 | A K R W N G R - - F D | Q Q H F **G** P **P** N T F |
| | DPK-22_4#2 | A K P Q S V - - - F D | Q Q Y F **G** S **P** I T F |
| | DPK-22_4#3 | A K S G H D P F – D | Q Q L H **G** I **P** T T F |
| DPK9 | DPK-9_1#1 | A K R F F W K Y N F D | Q Q A A **G** Y **P** A T F |
| | DPK-9_1#2 | A K Y H L H F P - F D | Q Q N H **G** K **P** K T F |
| | DPK-9_1#3 | A K S T Q S - - - F D | Q Q A Q **G** K **P** P T F |
| | DPK-9_2#1 | A K P P N A S A - F D | Q Q T **G** P Q **P** L T F |
| | DPK-9_2#2 | A K N S Q Q S W L F D | Q Q L M **G** L **P** P T F |
| | DPK-9_2#3 | A K S D Y P - - - F D | Q Q N **G** D I **P** K T F |

**Table 5.** Randomized positions in CDR3 sequences of randomly selected library antibody clones. Positions that are randomly mutated are underlined. Mutation in position 90 (introducing alanine instead of serine) of the DPL16 was verified and is highlighted in red. Single amino acid codes are used according to standard IUPAC nomenclature. Numbering is according to Tomlinson et al., 1996 [228].

## 3.3. Generation of an Ewing sarcoma-specific phage-display antibody library

A new disease-specific antibody library, using the antibody genes repertoire of Ewing sarcoma patients, is currently being developed in our laboratory. The rationale for the creation of this new antibody library was that it may present the benefit of an enrichment in antibodies specific for Ewing sarcoma-associated antigens, which can be isolate after cycles of panning exposing the library to tumor cell lines.

In order to amplify the V sequences of antibody repertoire from Ewing sarcoma patients, peripheral blood mononuclear cells (PBMCs) were collected from blood samples of patients before chemotherapy treatment. During the PhD, ten samples of PBMCs from patients treated at Rizzoli Institute of Bologna have been collected. Total RNA was extracted from each sample and converted to cDNA by reverse transcription. In a first step of PCR, the VH and VL (λ and κ) coding sequences were amplified using partially degenerated primers. The primers, adapted from Sblattero D, 1998 [257] and further modified by Pasello M et al., 2016 [224], were sufficient to recognize and amplify all the functional human V genes. To amplify the V genes, 76 individual PCR reactions were performed separately (42 different primer combination for VH, 16 for Vκ, 18 for Vλ) for each cDNA sample (Figure 36).

A second step of PCR has been used for the assembly of the scFv. Equimolar amounts for each chain have been made pooling samples of three different donors, and subsequently used to join the heavy and light chains through the overlapping ends of the linker.

The assembled scFvs will be subsequently used for ligation in a phagemid pDNS vector [224] and electroporation in electrocompetent *E. coli* cells, according to the methods that we described in Pasello M. et al, 2018 [258].

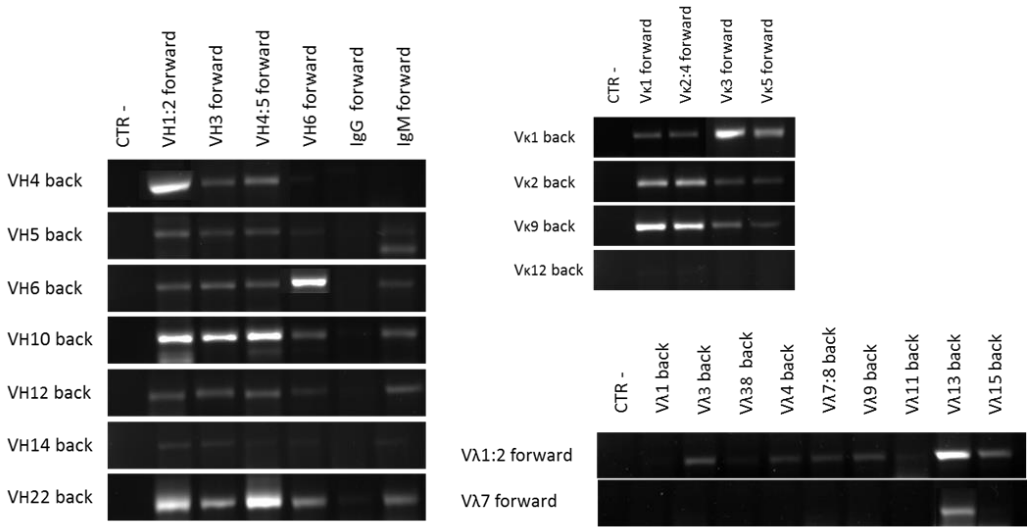


**Figure 36.** PCR amplification of V genes derived from the different 76 primer combinations. A) VH combinations; B) Vκ combinations; C) Vλ combinations.

# 4. Discussion

Conventional ABC transporters, including ABCB1, ABCC1 and ABCG2, have been extensively investigated as one of the causes of MDR in a plethora of tumors. To date, only associations of these ABC transporters with clinical outcome have been examined in Ewing Sarcoma, resulting in contradictory and not convincing evidences in favour of a prognostic value [155-158].
Nevertheless, beyond the well-established role of canonical ABCs in MDR, a less known but recently emerging theme is the drug efflux-independent contribution of ABC transporters in cancer biology; this particularly concerns some neglected members of ABC family, such as those of A subfamily [98, 105].

In our study, we described for the first time the impact of various transporters on the prognosis of Ewing sarcoma by assessment of their gene expression in two independent cohorts of patients with primary localized tumors. Therefore, the correlations with prognosis emerged from the explorative study in the cohort of 27 retrospective samples, were further validated in the larger clinical setting of 103 patients. The study was not limited to the conventional ABCs transporters involved in MDR, but inclusive of ABCs belonging to other subfamilies not typically involved in drug-efflux phenomenon.
According to previous studies, no associations with prognosis were identified for the conventional ABC transporters in the explorative study on 27 samples, whereas unexpected associations with favourable outcomes were observed for *ABCA6, ABCA7* and *ABCB9*. The prognostic value was validated in the larger cohort of 103 samples for the two *ABC* transporters belonging to A subfamily, *ABCA6* and *ABCA7*, but not for *ABCB9*.
In contrast with expectation, the higher expression of these two transporters is positively correlated with good prognosis; and interestingly, the combined low expression of *ABCA6* and *ABCA7* represented an independent marker of worse prognosis.
The clinical data suggested a protective and drug-efflux independent contribution for these ABCAs in cancer, rather than an involvement in malignancy and tumor progression. However, the available information about the physiological cell function of ABCA6 and ABCA7 are scarce, therefore their roles and functions in Ewing sarcoma have been further investigated *in vitro*.
Interestingly, ABCA6 mRNA was found to be inhibited by IGF1 in endothelial cells through inactivation of FoxOs [248]. FoxO proteins are transcriptional factors acting as key downstream regulators in IGF1/PI3K/Akt signaling pathway, and have been implicated in a range of cellular functions including the regulation of glucose and cholesterol homeostasis, stress responses, apoptosis and cell proliferation (schematic representation in Figure 23C) [259]. FoxO factors are also suggested to play a pivotal functional role as a tumor suppressor in a wide range of cancers [260]. Activation of

the IGF1/PI3K pathway blocks the transcriptional activity of FoxO factors by Akt-dependent phosphorylation, which leads to nuclear exclusion, sequestration in the cytoplasm and inhibition of binding to the promoter of target genes. The dephosphorylation of FoxOs, on the contrary, induces the nuclear localization of the factors leading to activation of their transcriptional function on target genes [261]. In our experimental model, we demonstrated that *ABCA6* is a gene target of both FoxO1 and FoxO3a, as reported by ChIP assay experiments. We paid particular attention to FoxO1 for its involvement in IGF1/Akt axis, considering that IGF1 is autocrinely produced by Ewing sarcoma cells and has a major role in sustaining tumor cell malignancy [44]. IGF1 treatment induced phosphorylation of FoxO1 in ser256 and consequently down-modulated *ABCA6* gene expression. Conversely, *ABCA6* gene expression was upregulated by treatment with the PI3K inhibitor LY294002 or with an anti-IGF1R monoclonal antibody. The negative regulation of *ABCA6* gene expression downstream of IGF1/Akt signaling may contribute to the general low expression of the transporter in Ewing sarcoma, in keeping with the tumor suppressor role of ABCA6 transporter.

Regarding *ABCA7*, we demonstrated for the first time that its gene expression is transcriptionally regulated by p53, as proved by ChIP assay and further confirmed by the association between *ABCA7* gene expression and *TP53* mutational status. Interestingly, in our experimental models, the treatment with doxorubicin increased the gene expression of both *ABCA6* and *ABCA7*, by inducing the recruitment of FoxO1 or p53, respectively, on the gene promoters, suggesting a virtuous circle of positive feedback regulation induced by the treatment. Besides inducing DNA damage and cell death, doxorubicin treatment can indeed increase the expression of *ABCA6* and *ABCA7*, which in turn by affecting cholesterol levels may further enhance the pro-apoptotic effects of the drug.

The data described thus far support a tumor suppressor role for ABCA6 and ABCA7, which was confirmed *in vitro* in Ewing sarcoma PDX-derived cell lines. The overexpression of ABCA6, ABCA7 or both impaired the *in vitro* migratory ability of Ewing sarcoma cells and increased the chemosensitivity to doxorubicin. The effect of tumor malignancy modulation and enhanced drug sensitivity was higher when both ABCAs were simultaneously overexpressed in cells, supporting the hypothesis that they may act in concert to contribute to a less malignant phenotype.

To date very little is known about the mechanisms underlying the drug efflux-independent role of ABC transporters in cancer biology. An increasing number of studies have reported that the loss or inhibition of several ABC transporters affects differentiation, migration/invasion and malignant potential in a variety of cancers [108, 262]. These effects are likely related to their normal physiological function of exporting endogenous metabolites as well as signaling molecules, such as lipids [89, 110].

Among the multiple physiological pathways in which ABCA transporters are implicated, lipid transport is one of the most established and studied due to its high impact on human health. Consistently, mutations in ABC transporters of the A-subfamily have been identified as the cause of severe disorders associated with altered lipid transport [113, 114]. Notably, ABCA6 is potentially involved in macrophage lipid homeostasis, as supported by its structural features and its cholesterol-responsive mRNA expression [248, 263]. ABCA7 is a member of the group of ABCA transporters associated with cholesterol and lipid homeostasis and may be involved in cholesterol/phospholipids transport at the plasma membrane level [129]. In support of ABCA7 function in cholesterol homeostasis, this transporter shows the highest amino acid homology with ABCA1, the main mediator of cholesterol and phospholipids efflux from cells *via* HDL formation.

The tumor suppressor role described in this thesis for ABCA6 and ABCA7 may be a consequence of their capabilities to export and/or flop signaling lipids, thereby affecting cholesterol and lipid metabolism in Ewing sarcoma cells. We demonstrated that cells with low ABCA6/7 expression displayed an increased intracellular cholesterol accumulation and were sensitive to the treatment with the cholesterol-lowering compound simvastatin, which significantly impaired cellular migration and clonogenic abilities of cells. The opposite effects were indeed found when cells with high ABCA6/7 expression and low cholesterol levels were exposed to exogenous cholesterol.

These observations were consistent with the growing body of evidence supporting the role of deregulated cholesterol and lipid homeostasis in the progression of numerous cancers, supporting the accumulation/altered distribution of cholesterol at plasma membrane as general feature of tumor cells. Membrane cholesterol negatively regulates cell membrane fluidity thus leading to increased epithelial–mesenchymal transition and cell migration in breast cancer [264]. In addition, membrane cholesterol may also indirectly regulate cancer cell migration through the modulation of functionality of growth factor receptors (e.g. IGF1R, EGFR and HER2), integrins and cell surface glycoproteins (e.g. CD44) [140]. In Ewing sarcoma, previous studies from our laboratory have shown that arachidonic acid metabolism and fatty acid biosynthesis pathways are associated with poor prognosis [240]. In addition, cholesterol biosynthesis has been demonstrated to be one of the significantly enriched pathways in Ewing sarcoma cell lines resistant to IGF1R-targeted therapies [265], indicating that lipid metabolism may have an important role in the resistance of Ewing sarcoma cells to either conventional or targeted therapies.

Taken together the data point out to ABCA6 and ABCA7 as potential markers of favorable prognosis in Ewing sarcoma patients and suggest the IGF1/ABCA/cholesterol axis as intriguing therapeutic target. The direct inhibition of cell cholesterol biosynthesis with statins or aminobiphoshonates, despite preclinical promising results in inhibiting tumor growth and synergistic effects with certain

chemotherapeutic agents, have shown controversial results in clinical studies. Therefore, targeting ABCA6/7 with agonist monoclonal antibodies to modulate intracellular cholesterol and lipid content may be a promising alternative strategy. Further investigation for combination therapies of cholesterol-lowering drugs or ABCA6/7 modulators with conventional chemotherapy for Ewing sarcoma patients who express low levels of both the transporters is needed.

The second part of the project has been dedicated to the generation of human antibodies phage-display libraries as tools for selecting mAbs in scFv format towards antigens of interest in Ewing sarcoma. Phage display libraries can differ in terms of antibody sequence source (naïve, immune, synthetic), randomization strategy as well as library size and functionality. In this thesis, (i.) a novel synthetic naïve human antibody phage-display library has been designed, cloned and characterized; whereas (ii.) a disease-specific library using the antibody genes repertoire of Ewing sarcoma patients is currently being developed in our laboratory.

(i.) We have described the design, construction and characterization of the new synthetic human antibody library, containing more than three billion antibody clones. The library was generated in collaboration with Philochem AG in Otelfingen (Zurich, Switzerland). We capitalize on the experience gained from previous highly functional synthetic libraries constructed over the years by the Neri group at ETH Zurich and Philochem, such as ETH2-Gold library [234], PHILO library [235], PHILODiamond [236]. The new library design, similarly to the previous libraries, incorporated germline sequences which are often found in the human antibody repertoire, the DP47 as VH in combination with one among DPL16 or DPK22 as VL. In order to try to expand the structural features that can be recognized using monoclonal antibodies, we introduced some modifications as compared to the ETH2-Gold library: the addition of the alternative Vκ segment DPK9 (the second most recurrent Vκ germline in human repertoire), the maximum length of the completely randomized sequence into the CDR3 of the VH up to seven residues (instead of six in the ETH2-Gold) and the residue 90 of DPL16 designed to be an alanine instead of a serine. The mutation on this residue was performed in order to abolish a potential N-glycosylation site (*i.e.* NXS/T amino acid sequence) in proximity to the CDR3.

The quality of the library was successfully assessed by PCR colony screening and DNA sequencing of randomly picked clones from different sub-libraries. All the amino acid sequences in the CDR3 region of both VH and VL were diverse and the mutation in position 90 of the DPL16 was verified. Overall, this library may represent a useful source for the isolation of binding specificities against a large variety of different target antigens. Next step will be to perform selection experiments through

rounds of panning on different types of antigens, including ABCA6 and ABCA7, followed by subsequent characterization of the identified binders.

# 5. Materials and methods

## 5.1. Clinical and *in vitro* preclinical studies of ABC transporters in Ewing sarcoma

### 5.1.1. Patient selection and tumor tissue sample processing

Patients with localized Ewing sarcoma who were enrolled in prospective neoadjuvant studies [266] [267] and treated at the Rizzoli Institute were included in the present retrospective analysis. Based on biobank availability and after tissue and quality control checks a total of 130 primary tumors were studied (27 as "training set"; 103 as "validation set"). The clinicopathological features of the patients are reported in Table 6. In the choice of the two experimental sets, we considered homogeneity of the clinical-pathological characteristics (chemotherapy regimens and surgical and local treatments).

| | TRAINING SET (27 CASES) | VALIDATION SET (103 CASES) |
|---|---|---|
| **Characteristics** | *n* | *n* |
| **Gender** | | |
| Female | 9 (33.3%) | 29 (28.2%) |
| Male | 18 (66.7%) | 74 (71.8%) |
| **Age** | | |
| ≤ 14 years | 8 (29.6%) | 40 (38.8%) |
| > 14 years | 19 (70.4%) | 63 (61.2%) |
| **Location** | | |
| Extremity | 21 (77.8%) | 80 (77.7%) |
| Others | 6 (22.2%) | 23 (22.3%) |
| **LDH*** | | |
| Normal | 10 (66.7%) | 68 (73.9%) |
| High | 5 (33.3%) | 24 (26.1%) |
| **Surgery** | | |
| YES | 22 (81.5%) | 91 (88.3%) |
| NO | 5 (18.5%) | 12 (11.7%) |
| **Local Treatment** | | |
| RxT | 5 (18.5%) | 12 (11.7%) |
| RxT + Surgery | 5 (18.5%) | 15 (14.6%) |
| Surgery | 17 (63%) | 76 (73.8%) |
| **Response to chemotherapy**** | | |
| Good | 9 (40.9%) | 33 (36.3%) |
| Poor | 13 (59.1%) | 58 (63.7%) |
| **Type of translocation** | | |
| EWS/Fli-1 type I | 18 (66.7%) | 49 (47.6%) |
| EWS/Fli1-1 non-type I | 9 (33.3%) | 54 (52.4%) |
| **RFS (Status)** | | |
| NED | 11 (40.7%) | 66 (64.1%) |
| REL | 16 (59.3%) | 37 (35.9%) |
| **OS (Status)** | | |
| Alive | 14 (51.9%) | 73 (70.9%) |
| Dead | 13 (48.1%) | 30 (29.1%) |

**Table 6.** Clinicopathological features of patients affected by Ewing sarcoma included in the retrospective analysis.

All patients had a diagnosis of Ewing sarcoma based on representative specimens from open or needle biopsies and on histological, cytological, and immunohistochemical features as well as the molecular

presence of the chimeric product derived from Ewing sarcoma-specific chromosomal translocations. Local treatment, performed after induction chemotherapy, consisted of radiation therapy, surgery or surgery followed by radiation therapy. In patients locally treated by surgery, the histologic response to chemotherapy was evaluated according to the method proposed by Picci et al [268]. For the training set, the median follow-up was 72 months (range 10–263 months). For the validation set, the median follow-up was 89 months (range 9–263 months). The clinical endpoint was the occurrence of adverse events (defined as recurrence or metastases for EFS or cancer-related death for OVS).

### 5.1.2. Sample processing for molecular analysis

Total RNA from snap-frozen tissue samples and cell lines was isolated using TRIzol Reagent (Invitrogen). RNA quality and quantity were assessed by NanoDrop analysis (Nanodrop ND-1000, ThermoFisher Scientific) and/or by electrophoresis. To check whether the extracted RNA was representative of Ewing sarcoma, tissue sections from the same snap-frozen tissue samples subjected to RNA extraction were morphologically analyzed with hematoxylin-eosin staining, and the slides were evaluated by a pathologist who certified the high-density cancer areas (> 70%) before any processing as previously reported [269]. Tissues nonrepresentative of Ewing sarcoma were excluded. Total RNA was reverse transcribed to cDNA using the High Capacity cDNA Reverse Transcription Kit (Applied Biosystems) according to the manufacturer's instructions. Reverse transcription quantitative realtime (RT-qPCR) was performed on ViiA7 (Life Technologies) using TaqMan PCR Master Mix (Life Technologies). Predesigned TaqMan probes were used for the target gene of ABC transporters. The relative quantification analysis was performed on the basis of the ΔΔCT method and the expression levels of each ABC were normalized to that of GAPDH. Human bone marrow CD34+ cells or human-derived mesenchymal stem cells HSSC195 were used as normal calibrators.

### 5.1.3 Ethical statement

The ethical committee of the Rizzoli Institute approved the study on clinical samples (21637/2013) and the establishment of PDX models (0009323/2016). The study was conducted in accordance with the Declaration of Helsinki ethical guidelines, and patient informed consent forms were obtained.

### 5.1.4 Statistical analysis

The association between ABC transporter expression and EFS or OS was estimated by Cox proportional hazards regression analysis. EFS and OS were plotted using the Kaplan-Meier method,

while the log-rank test was used to calculate univariate statistical significance of observed differences. Survivors or patients who were lost to follow-up were censored at the last contact date. All factors significantly associated with EFS and/or OS in univariate analysis were entered into a Cox proportional hazards model using stepwise selection multivariate analysis. Values of 95% confidence intervals (CIs) of hazard ratios (HRs) were provided [270].

Differences among means were analyzed using Student's t-test. Experimental data including more than two groups were analyzed using one-way ANOVA. Fisher's exact test was used for association data, and the Spearman rank test was used for correlations. IC50 values were calculated from linear transformation of dose–response curves using the CalcuSyn software (Biosoft). To define drug-drug interactions, the combination index (CI) was calculated with an isobologram equation using CalcuSyn software (Biosoft) to identify synergistic ($CI < 0.9$), additive ($0.9 \leq CI \geq 1.1$), or antagonistic ($CI > 1.1$) effects according to Chou et al. [271]. All P values were two-sided and a P value $< 0.05$ was considered statistically significant. Statistical analyses were performed with SPSS software, version 22.0 and GraphPad Prism 6 (GraphPad Prism). Statistical power and adequate sample size were calculated by PS Calculations free software (version 3.1.2).

### 5.1.5. Cell lines

The cell lines PDX-EW#2-C, PDX-EW#3-C, PDX-EW#4-C and PDX-EW#5-C were obtained by the respective Ewing sarcoma PDX after the first passage in animal. The human Ewing sarcoma TC-71 and 6647 cell lines were kindly provided by T. J. Triche (Children's Hospital, Los Angeles, CA) whereas the H825 and H1474-p2 cell lines were kindly provided by Prof Llombart-Bosch (University of Valencia, Spain). The human Ewing sarcoma cell lines SK-ES-1 and SK-N-MC were obtained from the American Type Culture Collection (Rockville, MD). The patient-derived Ewing sarcoma cell lines IOR/BRZ_2010 and IOR/GAC were established at Rizzoli Institute from a primary and metastastic lesion, respectively.

All cell lines were tested for Mycoplasma contamination (Mycoalert Mycoplasma Detection Kit, Lonza Cat#LT07-118) before use and authenticated by short tandem repeat PCR analysis for AMEL, D3S1358, TH01, D21S11, D18S51, D10S1248, D1S1656, D2S1338, D16S539, D22S1045, VWA, D8S1179, FGA, D2S441, D12S391, D19S433 and SE33 (last control December 2017 and July 2018; GenePrint® 10 System or POWERPLEX ESX 17 Fast System, Promega). All cell lines were immediately amplified to constitute liquid nitrogen stocks and were never passaged for more than 1 month upon thawing. Cells were maintained in Iscove's modified Dulbecco's medium (IMDM) (Euroclone) supplemented with 10% heat-inactivated fetal bovine serum (FBS) (Euroclone),

penicillin (20 U/mL) and streptomycin (100 μg/mL) (BioReagent) in a 37°C humidified environment at 5% CO2.

### 5.1.6. Chromatin immunoprecipitation (ChIP)

ChIP assays were performed as previously described [48] using the following antibodies for immunoprecipitation: anti-p53 (Santa Cruz Biotechnology) anti-FoxO1 (Thermo Fisher Scientific), anti-FoxO3a (Thermo Fisher Scientific), anti-RNA polymerase II CTD repeat YSPTSPS (phospho S5)(Abcam) and anti-mouse IgG negative control (Diagenode). ChIP assays were carried out in cell lines under basal conditions and after 24 h of treatment with doxorubicin (for each cell line, the corresponding 2xIC50 value was used).

The promoter of *ABCA7* and the 5' flanking sequence were analyzed and detected (sequence considered from -2500 to 100 bps; http://www.ensembl.org). The PROMO version 3.0.2 free software was used to predict the binding sites of TP53 in the promoter of the *ABCA7* gene and the sequence spanning from -1769 bps to -1763 bps was identified as the best. Primer3web version 4.1.0 was used to design the primers (Forward: 5'-TTTCTATGCCCGCAAGTTTC-3' and Reverse: 5'-GCAGGTCTGAGGGTCTGAAG-3').

The binding sites of FoxO1 and FoxO3a in the promoter of *ABCA6* and the primers spanning these sequences were reported by Gai J. et al [248].

For both ChIP analyses, the primers were used in realtime PCR with the SYBR Green method and the quantification analysis was calculated with the following formula: % recruitment = $2\Delta Ct \times$ input chromatin percentage where $\Delta Ct$ = Ct (INPUT) - Ct (IP).

The enrichment of *ABCA6* promoter sequence after immunoprecipitation in cell lines under basal conditions was also evaluated with standard PCR using the primers reported above. The obtained amplification products were observed on a 1.5% agarose gel with Gel Red (Biotium) staining.

### 5.1.7. hABCA6 and hABCA7 transfection

$1\times10^6$ PDX-EW#2-C cells/well were seeded in 6-well plates coated with fibronectin from bovine plasma (3 μg/cm2; Sigma). 24 h after seeding, cells were transfected with the expression vector pCMV6-AC-GFP containing the full-length hABCA6 (Origene), the expression vector pcDNA 3.1 containing the full length hABCA7 (kindly provided by Dr. Kazumitsu Ueda; Abe-Dohmae S, J Biol

Chem 2004) or co-transfected with both vectors. Non transfected cells or empty vector-transfected cells were used as controls.
Transfections were performed using TransIT-X2 (Mirus) according to the manufacturers' protocols. The expression level of ABCA6, ABCA7 or both were determined by RT-qPCR and Western Blotting analysis after transfection when functional studies were performed.

### 5.1.8. Treatment with IGF1 and inhibitors

To evaluate the effects of the IGF1/PI3K/Akt/FOXO signaling on ABCA6 gene expression, TC-71 ($3x10^5$/well) or PDX-EW#5-C cells ($5x10^5$/well) were seeded in IMDM 10% FBS in six-wells plate, serum starved in IMDM 1% FBS for 16 h and then treated with IGF1 (50 ng/mL; Millipore) or phosphatidylinositol 3-kinase inhibitor LY294002 (10 μmol/L; Calbiochem) or anti-IGF1R monoclonal antibody (100 ng/mL) for 24 h. Combined treatment of 24 h of IGF1 (50 ng/mL) with or without pretreatment of 2 h with LY294002 (10 μmol/L) or 3 h with anti-IGF1R monoclonal antibody (100 ng/mL) were also performed.

### 5.1.9. Treatments with Simvastatin or Cholesterol

To evaluate the effect of Simvastatin or Cholesterol on the parameters of malignancy and drug sensitivity, cells were pre-treated with simvastatin (Sigma) or cholesterol (Sigma) for 72 h as follows. PDX-EW#2-C or PDX-EW#5-C cells were seeded ($5\times10^5$ cells/well) in IMDM 10% FBS in 6-well plates. PDX-EW#5-C cells were serum starved for 24 h, by replacing medium with IMDM 1% FBS, and then exposed to cholesterol (0.3 μg/mL, 1 μg/mL, 3 μg/mL) for 72 h. For PDX-EW#2-C cells, 24 h after seeding, the medium was supplemented with Simvastatin (1 μg/mL, 2.5 μg/mL, 5 μg/mL). After 72 h of pre-treatment, cells were harvested and used for the evaluation of in vitro parameters of malignancy, drug sensitivity and cholesterol detection.

### 5.1.10. *In vitro* parameters of malignancy

Anchorage-independent growth was determined in 0.33% SeaPlaque Agarose (Lonza) with a 0.5% agarose underlay. To evaluate the effect of Simvastatin or Cholesterol on anchorage-independent growth, $10x10^4$ pre-treated PDX-EW#2-C or PDX-EW#5-C cells were plated in semisolid medium

supplemented with simvastatin (5 μg/mL) or cholesterol (3 μg/mL) respectively. Colonies were counted after 16 days.

Motility assay was performed using Transwell chambers (Costar). Cells ($1\times10^5$/well) were seeded in the upper compartment in IMDM 10% FBS, and incubated for 18 h in a humidified 5% CO2 atmosphere at 37°C. To evaluate the effect of simvastatin or cholesterol on cellular migration, $1\times10^4$ pre-treated PDX-EW#2-C or PDX-EW#5-C cells were seeded in the upper compartment of the chamber in IMDM 10% FBS supplemented with simvastatin (1 μg/mL, 2.5 μg/mL, 5 μg/mL) or cholesterol (0.3 μg/mL, 1 μg/mL, 3 μg/mL); IMDM 10% FBS supplemented with the respective concentration of simvastatin or cholesterol was placed in the lower compartment. The migrated cells were fixed in absolute methanol, counterstained with Giemsa (CARLO ERBA Reagents S.A.S) and counted.

Wound healing assay was performed seeding PDX-EW#2-C or PDX-EW#5-C cells ($1.5\times10^6$/well) in IMDM 10% FBS in 60 cm diameter petri dishes coated with fibronectin (3 μg/cm2) (Sigma-Aldrich Cat#F1141-5MG). Cells were allowed to grow until 100% confluence was achieved. A sterile 200 μl pipette tip was used to obtain the cell free lane and the medium was renewed with IMDM 10% FBS supplemented with simvastatin (5 μg/mL) or cholesterol (3 μg/mL). Images were obtained at time 0 and after 24 h under an inverted microscope (Zeiss, Inc., Thornwood, NY).

### 5.1.11. *In vitro* drug sensitivity

Sensitivity to conventional chemotherapeutics and simvastatin was assessed by 3-(4,5-dimethylthiazol-2-yl)-2,5-diphenyltetrazolium bromide (MTT) assay (TACS MTT Cell Proliferation Assays, Trevigen) after 72 h of treatment to estimate the percentage of growth inhibition when compared to controls. A total of $4\times10^4$ cells/well were seeded in 96-wells plates in IMDM 10% FBS. After 24 h, the medium was changed with IMDM 10% FBS containing different concentrations of doxorubicin (1-100 ng/mL; Pfizer), vincristine (0.1-1000 ng/mL; Pfizer), ifosfamide (10-3000 ng/mL; Baxter Oncology Cat#1118563), etoposide (10-3000 ng/mL; Sandoz), actinomicina D (0.1-100 ng/mL; Sigma) or simvastatin (1-250μg/mL; Sigma). Sensitivity to different drugs was expressed as IC50 (drug concentration resulting in 50% inhibition of cell growth).

In combination experiments, a total of $5\times10^5$ PDX-EW#2-C cells, pre-treated with Simvastatin (2.5 μg/mL, 5 μg/mL, 10 μg/mL) for 72 h, were seeded in IMDM 10% FBS in six-wells plate and treated for additional 24 hours with simvastatin alone (2.5 μg/mL, 5 μg/mL, 10 μg/mL) or in combination with doxorubicin (25 ng/mL, 50 ng/mL, 250 ng/mL). In addition, the same amount of PDX-EW#2-C

cells, without pre-treatment, were seeded and treated for 24 h with doxorubicin alone (25 ng/mL, 50 ng/mL, 250 ng/mL, 500 ng/mL) as control. After 24 h, cells were harvested and counted by Trypan blue vital cell count (Sigma). Sensitivity to different drugs combination was expressed as % survival.

### 5.1.12. Mitochondrial membrane potential assay

Changes in mitochondrial membrane potential were assessed by measuring the 1,1′,3,3′-tetraethylbenzimidazolcarbocyanine iodide (JC-1) (Sigma) red and green fluorescence intensity. PDX-EW#2-C and PDX-EW#5-C cells ($5\times10^5$/well) were seeded in 60 cm diameter petri dishes; doxorubicin (5-50 ng/mL or 25-250 ng/mL, respectively) was added after 24 h.
Otherwise, PDX-EW#2-C ($1x10^6$/well) were seeded in six-wells plate coated with fibronectin, after 24 h transiently transfected for the overexpression of ABCA6, ABCA7 or both and then treated with doxorubicin (50-250 ng/mL). After 24 h of treatment, cells were harvested and pre-incubated with 5 μg/ml JC-1 in IMDM 10% FBS for 15 minutes. The resulting fluorescence was measured by flow-cytometry (Becton Dickinson), and the results are presented as percentages of cell green fluorescence. In addition, sensitivity to doxorubicin after 24 h of treatment of PDX-EW#2-C cells, transfected for the overexpression of ABCA6, ABCA7 or both, was also estimated by Trypan blue vital cell count and expressed as IC50.

### 5.1.13. Western blotting

Western blot experiments were performed according to standard protocols. Subconfluent cells were treated as described above and cell lysates were prepared using NP40 1% lysis buffer (10 mM Tris–HCl pH 7.4, 150 nM NaCl, 50 mM EDTA, IGEPAL 1%, with protease and phosphatase inhibitors). Equal amounts of protein were analyzed by gel electrophoresis with a 4-15% separation gel (Mini-PROTEAN™ TGX Stain-Free™ Protein Gels, Biorad) or 10% gel and transferred to nitrocellulose or PVDF sheets. The membranes were incubated overnight with the following primary antibodies: anti–hABCA7 (Bethyl), anti-hABCA6 (Abcam), anti-Phospho-p53 (Ser15) (Cell Signaling Technology), anti-p53 (Bio-Rad), anti-Phospho-FoxO1 (Ser256) (Cell Signaling Technology), anti-FoxO1 (C29H4) (Cell Signaling Technology), anti-Cleaved Caspase-3 (Asp175) (Cell Signaling Technology), anti-Cleaved PARP (Asp214) (Cell Signaling Technology), anti-Phospho-Akt (Ser473) (736E11) (Cell Signaling Technology), anti-AKT (Cell Signaling Technology), and anti-GAPDH (Santa Cruz Biotechnology). Anti-rabbit (GE Healthcare) or anti-mouse GE (Healthcare) antibodies

conjugated to horseradish peroxidase were used as secondary antibodies. The proteins were visualized with an ECL Western Blotting Detection System (Euroclone).

### 5.1.14. Flow cytometry

Total ceramide levels after ABCA6 or ABCA7 overexpression were quantified by flow cytometry. PDX-EW#2-C cells were harvested after 48 hours of transient transfection and counted, $1\times10^6$ cells were fixed with 4% p-formaldehyde in PBS for 15 min at room temperature, permeabilized with Triton X and then washed three times with PBS. Fixed cells were incubated with anti-ceramide monoclonal antibody (MID 15B4) for 1 hour. After washing with PBS, cells were stained with anti-mouse FITC as a secondary antibody and analyzed on the flow cytometer.

### 5.1.15. Cholesterol detection and quantification

A total of $3x10^5$ pre-treated PDX-EW#2-C or PDX-EW#5-C cells were seeded on coverslips coated with fibronectin (3 μg/cm2; Sigma-Aldrich) in IMDM 10% FBS supplemented with simvastatin (5 μg/mL) or cholesterol (3 μg/mL). After 72 hours, cells were rinsed with PBS and fixed with 4% paraformaldehyde for 15 min at room temperature. Cells were rinsed with PBS and incubated with glycine (1.5 mg/mL) for 10 minutes at room temperature and stained with filipin (0.05 mg/mL in PBS/10% FBS; Sigma) for 2 h at room temperature. The fluorescence signals of the stained cells were detected using a fluorescent or confocal microscope (Nikon) with 340–380 nm excitation.

Quantification of total cholesterol was performed using Total Cholesterol Assay Kit (Colorimetric) (Cell Biolabs). Lipid extracts were obtained from $1x10^6$ cells using 200 μL of a chloroform: isopropanol: NP-40 (7:11:0.1, v:v:v) mixture and further processed accordingly to the manufacturers' protocol.

## 5.2. Construction of a synthetic antibody phage-display library

### 5.2.1. Media, buffers, bacterial strains

Media:

2xTY: 16g/l bacto-tryptone, 10g/l bacto-yeast extract, 5g/l NaCl pH 7.4;

2xTY agar plates Amp-Glu: 2xTY medium + 15 g/l agar. Autoclave, and add ampicillin 100 µg/l, glucose1% w/v only when the medium temperature is 50°C.

Buffers:

PBS (phosphate buffered saline): 100 mM NaCl, 20 mM NaH2 PO4 monohydrate, 30mM Na2 HPO4 dodecahydrate, pH 7.4;

TBS (Tris buffered saline): 50mM Tris Base, 100mM NaCl, pH 7.4;

Bacterial strains:

E. Coli TG1 (K12, D(lac-pro), supE, thi, hsdD5/F'traD36, $proA^+$ $B^+$, $laqI^q$, lacZDM15);

Helper phage:

VCSM13 (Strategene).

### 5.2.2. Cloning strategy for library construction

The sequences of ETH2-Gold clones [234] were used as template for the design of GeneStrands corresponding to the heavy chain DP47, the light chains DPK22 and the DPL16. Ser90Ala mutation was introduced in the DPL16 sequence. GeneStrand for the DPK9 was synthetized based on the sequence from V-BASE database (www.vbase.mrc-cpe.cam.ac.uk). All the germline sequences were verified by alignment with the corresponding human germline variable region sequences from V-BASE. The three alternative templates (DP47-DPK9, DP47-DPK22, DP47-DPK22) were assembled by PCR and cloned into pHENI vector [185]. The linker (Gly4Ser Gly4Ser Gly4) was kept constant between DP47/DPK22 and DP47/DPL16 as in the ETH2-Gold and PHILO libraries [234, 235]. In the antibody library, residues are numbered according to Tomlinson et al. [227]and are indicated in Figure 32. Sequence variability in the CDR3 of VH and VL chains of the library was introduced by PCR using partially degenerate primers (Figure 33 and Table 8) as follows: DP47-based VH domains were randomly mutated from residue 95 to 100 and this CDR3 loop was designed to be 4–7 amino acids long; DPK22-based VL domains were randomized between residues 91 - 96, with a fixed proline at position 95 and a glycine either at position 92 or at position 93. DPL16-based VL domains were randomized between residues 91 - 96, with a proline at position 91, 92, 93, 95 or 96.

VH-VL combinations were assembled in scFv format by PCR assembly (Figure 34 and Table 8), using gel-purified VH and VL segments as templates. The assembled VH-VL fragments were double-digested with NcoI/NotI and cloned into NcoI/NotI double-digested pHEN1 phagemid vector (Figure 34).

The resulting ligation product was purified and electroporated into electrocompetent E. Coli TG1 cells (see the section 4.2.3.). The different sub-libraries were electroporated on different days. Electroporated cells were spread on 2xTY-agar plates with ampicillin and glucose and incubated at 30°C overnight. On the next day, cells were rescued (with 2xTY - 10% glycerol), stored as glycerol stocks and used for phage production according to standard protocol [171] (see the section 4.2.4.). Sub-library sizes are reported in Table 4.

**Synthetic antibody library primers**

| Name | Sequence |
|---|---|
| (a1) LMB3long | 5′ CAG GAA ACA GCT ATG ACC ATG ATT AC 3′ |
| (b1) DP47_CDR3_01 | 5′ GT GCC CTG GCC CCA GTA GTC AAA MNN MNN MNN MNN TTT CGC ACA GTA ATA TAC GGC C 3′ |
| (b2) DP47_CDR3_02 | 5′ GT GCC CTG GCC CCA GTA GTC AAA MNN MNN MNN MNN MNN TTT CGC ACA GTA ATA TAC GGC C 3′ |
| (b3) DP47_CDR3_03 | 5′ GT GCC CTG GCC CCA GTA GTC AAA MNN MNN MNN MNN MNN MNN TTT CGC ACA GTA ATA TAC GGC C 3′ |
| (b4) DP47_CDR3_04 | 5′ GT GCC CTG GCC CCA GTA GTC AAA MNN MNN MNN MNN MNN MNN MNN TTT CGC ACA GTA ATA TAC GGC C 3′ |
| (c) DP47_FR4 | 5′ TTT GAC TAC TGG GGC CAG GGC AC 3′ |
| (e1) DPL16_CDR3_01 | 5′ CTT GGT CCC TCC GCC GAA TAC CAC MNN MNN MNN MNN MNN GGG **AGC** GGA GTT ACA GTA ATA GTC 3′ |
| (e2) DPL16_CDR3_02 | 5′ CTT GGT CCC TCC GCC GAA TAC CAC MNN MNN MNN MNN GGG MNN **AGC** GGA GTT ACA GTA ATA GTC 3′ |
| (e3) DPL16_CDR3_03 | 5′ CTT GGT CCC TCC GCC GAA TAC CAC MNN MNN MNN GGG MNN MNN **AGC** GGA GTT ACA GTA ATA GTC 3′ |
| (e4) DPL16_CDR3_04 | 5′ CTT GGT CCC TCC GCC GAA TAC CAC MNN GGG MNN MNN MNN MNN **AGC** GGA GTT ACA GTA ATA GTC 3′ |
| (e5) DPL16_CDR3_05 | 5′ CTT GGT CCC TCC GCC GAA TAC CAC GGG MNN MNN MNN MNN MNN **AGC** GGA GTT ACA GTA ATA GTC 3′ |
| (d1) DPK9_CDR3_01 | 5′ CAC CTT GGT CCC TTG GCC GAA CGT MNN CGG MNN MNN ACC MNN CTG TTG ACA GTA GTA AGT TGC 3′ |
| (d2) DPK9_CDR3_02 | 5′ CAC CTT GGT CCC TTG GCC GAA CGT MNN CGG MNN ACC MNN MNN CTG TTG ACA GTA GTA AGT TGC 3′ |
| (d1) DPK22_CDR3_01 | 5′ CAC CTT GGT CCC TTG GCC GAA CGT MNN CGG MNN MNN ACC MNN CTG CTG ACA GTA ATA CAC TGC 3′ |
| (d2) DPK22_CDR3_02 | 5′ CAC CTT GGT CCC TTG GCC GAA CGT MNN CGG MNN ACC MNN MNN CTG CTG ACA GTA ATA CAC TGC 3′ |
| (g) DPL16_FR4_NotI | 5′ TTT TCC TTT TGC GGC CGC GCC TAG GAC GGT CAG CTT GGT CCC TCC GCC GAA 3′ |
| (f) DPK22_FR4_NotI | 5′ TTT TCC TTT TGC GGC CGC TTT GAT TTC CAC CTT GGT CCC TTG GCC GAA CG 3′ |
| fdseqlong | 5′ GAC GTT AGT AAA TGA ATT TTC TGT ATG AGG 3′ |

**Table 8.** Nucleotide sequences of the primers used for the construction of the synthetic antibody library. M and N are defined according to the IUPAC nomenclature (M = A/C, N = A/C/G/T)

### 5.2.3. TG1 electroporation and quality control

*Fresh Electro-Competent TG1 preparation*

Electro-competent TG-1 cells were prepared by washing the cells, which are in exponential growing phase, twice with cold sterile autoclaved 1 mM HEPES/5% glycerol (pH 7) and twice with cold sterile 10% glycerol in water. Washing steps were performed at 4°C. Finally, cells were resuspended in 10% glycerol to a density of approximately $10^{11}$ cells /ml.

*Electroporation*

10µl of ligated and purified DNA (about 0.5µg) were incubated with 190µl of fresh electro-competent TG1 bacteria. Electroporation was performed in a 0.2 cm cuvette (E. Coli Pulser® cuvette, Bio-Rad) on an Electro cell manipulator 600 (BTX) with 2.5 kV, 50µF and 129Ω. After electroporation, 200µl 2xTY media was added and plated on an agar plate containing 2xTY, ampicillin and glucose.

*Titer Calculation and PCR-Screening*

Dilutions of the electroporated cells were performed and the titer calculated. Randomly picked clones were screened by PCR using primers LMB3long and fdseqlong (Table 8) to verify the correct insert size. Cycling parameters: 94°C-10min, (94°C-1min, 50°C-1min, 72°C-90sec) x30, 72°C-10min. PCR performed with RedTaq ReadyMix (SIGMA). The insert DNA was purified from gel and used for Sanger-sequencing.

### 5.2.4. Phage production

All electroporated clones were rescued from the agar plates using 2xTY-10% glycerol. A small culture was inoculated and grown until the exponential growth phase was reached. Superinfection with helper phage VCSM13 (stratagene, Agilent Technologies inc., USA) was performed. After incubation overnight at 30°C, phages were purified using PEG-NaCl as described earlier [234].

## 5.3. Construction of a human Ewing sarcoma-specific antibody library

### 5.3.1. PBMCs isolation, RNA extraction and cDNA synthesis

PBMCs were isolated from peripheral blood samples from 10 Ewing sarcoma patients using Ficoll-Paque density gradient centrifugation. Total RNA was extracted using TRIzol Reagent (Invitrogen, California,USA), and the cDNA was synthesized using the High Capacity cDNA Archive kit (Applied Biosystem; California, USA).The quality of cDNA was controlled by the amplification of the β actin gene.

### 5.3.2. Amplification of VH and VL genes by PCR

In this first step of PCR, the VH and VL (λ and κ) human coding sequences were amplified using partially degenerated primers. The primers, adapted from Sblattero D, 1998 [257] and further modified by Pasello M et al., 2016 [224] are listed in Table 9. They were able to recognize and amplify all the functional human V genes. To amplify the V genes, 76 individual PCR reactions were performed separately (42 different primer combination for VH, 16 for Vκ, 18 for Vλ) for each cDNA sample. The PCR products were separated by agarose gel electrophoresis and further purified and quantified in order to perform the next step pf PCR assembly.

| Primer | 5′ to 3′ sequence |
|---|---|
| Antibody gene PCR VH | |
| VH1:2 forward | ***gcctgagccgccgccgccaga****tccacctccacc***TGA GGA GAC RGT GAC CAG GGT G** |
| VH4:5 forward | ***gcctgagccgccgccgccaga****tccacctccacc***TGA GGA GAC GGT GAC CAG GGT T** |
| VH3 forward | ***gcctgagccgccgccgccaga****tccacctccacc***TGA AGA GAC GGT GAC CAT TGT** |
| VH6 forward | ***gcctgagccgccgccgccaga****tccacctccacc***TGA GGA GAC GGT GAC CGT GGT CC** |
| IgM forward | ***gcctgagccgccgccgccaga****tccacctccacc***GGT TGG GGC GGA TGC ACT CC** |
| IgG forward | ***gcctgagccgccgccgccaga****tccacctccacc***SGA TGG GCC CTT GGT GGA RGC** |
| VH4 back | gatgctttagCCATGGcc**CAG GTG CAG CTG CAG GAG TCS G** |
| VH5 back | gatgctttagCCATGGcc**CAG GTA CAG CTG CAG CAG TCA** |
| VH6 back | gatgctttagCCATGGcc**CAG GTG CAG CTA CAG CAG TGG G** |
| VH10 back | gatgctttagCCATGGcc**GAG GTG CAG CTG KTG GAG WCY** |
| VH12 back | gatgctttagCCATGGcc**CAG GTC CAG CTK GTR CAG TCT GG** |
| VH14 back | gatgctttagCCATGGcc**CAG RTC ACC TTG AAG GAG TCT G** |
| VH22 back | gatgctttagCCATGGcc**CAG GTG CAG CTG GTG SAR TCT GG** |
| Antibody gene PCR V lambda | |
| Vλ1:2 forward | gatgctttagGCGGCCGCtag**GAC GGT SAS CTT GGT CC** |
| Vλ7 forward | gatgctttagGCGGCCGCgag**GAC GGT CAG CTG GGT GC** |
| Vλ1 back | ***tctggcggcggcggctcaggc****ggaggaggttcc***CAG TCT GTS BTG ACG CAG CCG CC** |
| Vλ3 back | ***tctggcggcggcggctcaggc****ggaggaggttcc***TCC TAT GWG CTG ACW CAG CCA C** |
| Vλ38 back | ***tctggcggcggcggctcaggc****ggaggaggttcc***TCC TAT GAG CTG AYR CAG CYA CC** |
| Vλ4 back | ***tctggcggcggcggctcaggc****ggaggaggttcc***CAG CCT GTG CTG ACT CAR YC** |
| Vλ7:8 back | ***tctggcggcggcggctcaggc****ggaggaggttcc***CAG DCT GTG GTG ACY CAG GAG CC** |
| Vλ9 back | ***tctggcggcggcggctcaggc****ggaggaggttcc***CAG CCW GKG CTG ACT CAG CCM CC** |
| Vλ11 back | ***tctggcggcggcggctcaggc****ggaggaggttcc***TCC TCT GAG CTG AST CAG GAS CC** |
| Vλ13 back | ***tctggcggcggcggctcaggc****ggaggaggttcc***CAG TCT GYY CTG AYT CAG CCT** |
| Vλ15 back | ***tctggcggcggcggctcaggc****ggaggaggttcc***AAT TTT ATG CTG ACT CAG CCC C** |
| Antibody gene PCR V kappa | |
| Vκ1 forward | gatgctttagGCGGCCGCttt**GAT TTC CAC CTT GGT CC** |
| Vκ2:4 forward | gatgctttagGCGGCCGCttt**GAT CTC CAS CTT GGT CC** |
| Vκ3 forward | gatgctttagGCGGCCGCttt**GAT ATC CAC TTT GGT CC** |
| Vκ5 forward | gatgctttagGCGGCCGCttt**AATCTC CAG TCG TGT CC** |
| Vκ1 back | ***tctggcggcggcggctcaggc****ggaggaggttcc***GAC ATC CRG DTG ACC CAG TCT CC** |
| Vκ2 back | ***tctggcggcggcggctcaggc****ggaggaggttcc***GAA ATT GTR WTG ACR CAG TCT CC** |
| Vκ9 back | ***tctggcggcggcggctcaggc****ggaggaggttcc***GAT ATT GTG MTG ACB CAG WCT CC** |
| Vκ12 back | ***tctggcggcggcggctcaggc****ggaggaggttcc***GAA ACG ACA CTC ACG CAG TCT C** |

**Table 9.** Primers for amplification of VH and VL genes. Uppercase bold text: sequence for the amplification of VH, VL. Downcase italic text: linker sequence (in bold overlapping regions). Uppercase text: sequence for NcoI or NotI.

# 6. References


1. Siegel, R.L., K.D. Miller, and A. Jemal, *Cancer statistics, 2015.* CA Cancer J Clin, 2015. **65**(1): p. 5-29.
2. Stiller, C.A., et al., *Descriptive epidemiology of sarcomas in Europe: report from the RARECARE project.* Eur J Cancer, 2013. **49**(3): p. 684-95.
3. Valery, P.C., M. Laversanne, and F. Bray, *Bone cancer incidence by morphological subtype: a global assessment.* Cancer Causes Control, 2015. **26**(8): p. 1127-39.
4. Casali, P.G., et al., *Bone sarcomas: ESMO-PaedCan-EURACAN Clinical Practice Guidelines for diagnosis, treatment and follow-up.* Ann Oncol, 2018. **29**(Suppl 4): p. iv79-iv95.
5. Lessnick, S.L. and M. Ladanyi, *Molecular pathogenesis of Ewing sarcoma: new therapeutic and transcriptional targets.* Annu Rev Pathol, 2012. **7**: p. 145-59.
6. Ewing, J., *Classics in oncology. Diffuse endothelioma of bone. James Ewing. Proceedings of the New York Pathological Society, 1921.* CA Cancer J Clin, 1972. **22**(2): p. 95-8.
7. Kovar, H., *Progress in the molecular biology of ewing tumors.* Sarcoma, 1998. **2**(1): p. 3-17.
8. de Alava, E. and W.L. Gerald, *Molecular biology of the Ewing's sarcoma/primitive neuroectodermal tumor family.* J Clin Oncol, 2000. **18**(1): p. 204-13.
9. Doyle, L.A., *Sarcoma classification: an update based on the 2013 World Health Organization Classification of Tumors of Soft Tissue and Bone.* Cancer, 2014. **120**(12): p. 1763-74.
10. Watson, S., et al., *Transcriptomic definition of molecular subgroups of small round cell sarcomas.* J Pathol, 2018. **245**(1): p. 29-40.
11. Sankar, S. and S.L. Lessnick, *Promiscuous partnerships in Ewing's sarcoma.* Cancer Genet, 2011. **204**(7): p. 351-65.
12. Antonescu, C.R., et al., *Sarcomas With CIC-rearrangements Are a Distinct Pathologic Entity With Aggressive Outcome: A Clinicopathologic and Molecular Study of 115 Cases.* Am J Surg Pathol, 2017. **41**(7): p. 941-949.
13. Gambarotti, M., et al., *CIC-DUX4 fusion-positive round-cell sarcomas of soft tissue and bone: a single-institution morphological and molecular analysis of seven cases.* Histopathology, 2016. **69**(4): p. 624-34.
14. Kao, Y.C., et al., *BCOR-CCNB3 Fusion Positive Sarcomas: A Clinicopathologic and Molecular Analysis of 36 Cases With Comparison to Morphologic Spectrum and Clinical Behavior of Other Round Cell Sarcomas.* Am J Surg Pathol, 2018. **42**(5): p. 604-615.
15. Jawad, M.U., et al., *Ewing sarcoma demonstrates racial disparities in incidence-related and sex-related differences in outcome: an analysis of 1631 cases from the SEER database, 1973-2005.* Cancer, 2009. **115**(15): p. 3526-36.
16. Khoury, J.D., *Ewing sarcoma family of tumors.* Adv Anat Pathol, 2005. **12**(4): p. 212-20.
17. Buckley, J.D., et al., *Epidemiology of osteosarcoma and Ewing's sarcoma in childhood: a study of 305 cases by the Children's Cancer Group.* Cancer, 1998. **83**(7): p. 1440-8.
18. Novakovic, B., et al., *Increased risk of neuroectodermal tumors and stomach cancer in relatives of patients with Ewing's sarcoma family of tumors.* J Natl Cancer Inst, 1994. **86**(22): p. 1702-6.
19. McKeen, E.A., et al., *Birth defects with Ewing's sarcoma.* N Engl J Med, 1983. **309**(24): p. 1522.
20. Fraumeni, J.F., Jr. and A.G. Glass, *Rarity of Ewing's sarcoma among U.S. Negro children.* Lancet, 1970. **1**(7642): p. 366-7.
21. Jensen, R.D. and R.M. Drake, *Rarity of Ewing's tumour in Negroes.* Lancet, 1970. **1**(7650): p. 777.
22. Worch, J., et al., *Racial differences in the incidence of mesenchymal tumors associated with EWSR1 translocation.* Cancer Epidemiol Biomarkers Prev, 2011. **20**(3): p. 449-53.
23. Grunewald, T.G.P., et al., *Ewing sarcoma.* Nat Rev Dis Primers, 2018. **4**(1): p. 5.
24. Helman, L.J. and P. Meltzer, *Mechanisms of sarcoma development.* Nat Rev Cancer, 2003. **3**(9): p. 685-94.
25. Turc-Carel, C., et al., *[Chromosomal translocation (11; 22) in cell lines of Ewing's sarcoma].* C R Seances Acad Sci III, 1983. **296**(23): p. 1101-3.
26. Delattre, O., et al., *Gene fusion with an ETS DNA-binding domain caused by chromosome translocation in human tumours.* Nature, 1992. **359**(6391): p. 162-5.

27. May, W.A., et al., *Ewing sarcoma 11;22 translocation produces a chimeric transcription factor that requires the DNA-binding domain encoded by FLI1 for transformation.* Proc Natl Acad Sci U S A, 1993. **90**(12): p. 5752-6.
28. Janknecht, R., *EWS-ETS oncoproteins: the linchpins of Ewing tumors.* Gene, 2005. **363**: p. 1-14.
29. Toomey, E.C., J.D. Schiffman, and S.L. Lessnick, *Recent advances in the molecular pathogenesis of Ewing's sarcoma.* Oncogene, 2010. **29**(32): p. 4504-16.
30. Mackintosh, C., et al., *The molecular pathogenesis of Ewing's sarcoma.* Cancer Biol Ther, 2010. **9**(9): p. 655-67.
31. Jedlicka, P., *Ewing Sarcoma, an enigmatic malignancy of likely progenitor cell origin, driven by transcription factor oncogenic fusions.* Int J Clin Exp Pathol, 2010. **3**(4): p. 338-47.
32. Grohar, P.J. and L.J. Helman, *Prospects and challenges for the development of new therapies for Ewing sarcoma.* Pharmacol Ther, 2013. **137**(2): p. 216-24.
33. Hancock, J.D. and S.L. Lessnick, *A transcriptional profiling meta-analysis reveals a core EWS-FLI gene expression signature.* Cell Cycle, 2008. **7**(2): p. 250-6.
34. Riggi, N., et al., *EWS-FLI1 utilizes divergent chromatin remodeling mechanisms to directly activate or repress enhancer elements in Ewing sarcoma.* Cancer Cell, 2014. **26**(5): p. 668-681.
35. Tomazou, E.M., et al., *Epigenome mapping reveals distinct modes of gene regulation and widespread enhancer reprogramming by the oncogenic fusion protein EWS-FLI1.* Cell Rep, 2015. **10**(7): p. 1082-95.
36. Gonzalez, I., et al., *EWS/FLI-1 oncoprotein subtypes impose different requirements for transformation and metastatic activity in a murine model.* J Mol Med (Berl), 2007. **85**(9): p. 1015-29.
37. Ouchida, M., et al., *Loss of tumorigenicity of Ewing's sarcoma cells expressing antisense RNA to EWS-fusion transcripts.* Oncogene, 1995. **11**(6): p. 1049-54.
38. Kovar, H., et al., *EWS/FLI-1 antagonists induce growth inhibition of Ewing tumor cells in vitro.* Cell Growth Differ, 1996. **7**(4): p. 429-37.
39. Toretsky, J.A., et al., *Inhibition of EWS-FLI-1 fusion protein with antisense oligodeoxynucleotides.* J Neurooncol, 1997. **31**(1-2): p. 9-16.
40. Lambert, G., et al., *EWS fli-1 antisense nanocapsules inhibits ewing sarcoma-related tumor in mice.* Biochem Biophys Res Commun, 2000. **279**(2): p. 401-6.
41. Jacques, C., et al., *Small animal models for the study of bone sarcoma pathogenesis:characteristics, therapeutic interests and limitations.* J Bone Oncol, 2018. **12**: p. 7-13.
42. Lopez-Guerrero, J.A., et al., *Molecular analysis of the 9p21 locus and p53 genes in Ewing family tumors.* Lab Invest, 2001. **81**(6): p. 803-14.
43. Riggi, N. and I. Stamenkovic, *The Biology of Ewing sarcoma.* Cancer Lett, 2007. **254**(1): p. 1-10.
44. Mancarella, C. and K. Scotlandi, *IGF system in sarcomas: a crucial pathway with many unknowns to exploit for therapy.* J Mol Endocrinol, 2018. **61**(1): p. T45-T60.
45. Herrero-Martin, D., et al., *Stable interference of EWS-FLI1 in an Ewing sarcoma cell line impairs IGF-1/IGF-1R signalling and reveals TOPK as a new target.* Br J Cancer, 2009. **101**(1): p. 80-90.
46. Jayabal, P., P.J. Houghton, and Y. Shiio, *EWS-FLI-1 creates a cell surface microenvironment conducive to IGF signaling by inducing pappalysin-1.* Genes Cancer, 2017. **8**(11-12): p. 762-770.
47. Manara, M.C., M. Pasello, and K. Scotlandi, *CD99: A Cell Surface Protein with an Oncojanus Role in Tumors.* Genes (Basel), 2018. **9**(3).
48. Rocchi, A., et al., *CD99 inhibits neural differentiation of human Ewing sarcoma cells and thereby contributes to oncogenesis.* J Clin Invest, 2010. **120**(3): p. 668-80.
49. Ambros, I.M., et al., *MIC2 is a specific marker for Ewing's sarcoma and peripheral primitive neuroectodermal tumors. Evidence for a common histogenesis of Ewing's sarcoma and peripheral primitive neuroectodermal tumors from MIC2 expression and specific chromosome aberration.* Cancer, 1991. **67**(7): p. 1886-93.
50. Arndt, C.A. and W.M. Crist, *Common musculoskeletal tumors of childhood and adolescence.* N Engl J Med, 1999. **341**(5): p. 342-52.
51. Zambo, I. and K. Vesely, *[WHO classification of tumours of soft tissue and bone 2013: the main changes compared to the 3rd edition].* Cesk Patol, 2014. **50**(2): p. 64-70.

52. Baldauf, M.C., et al., *Robust diagnosis of Ewing sarcoma by immunohistochemical detection of super-enhancer-driven EWSR1-ETS targets.* Oncotarget, 2018. **9**(2): p. 1587-1601.
53. Sorensen, P.H., et al., *Reverse transcriptase PCR amplification of EWS/FLI-1 fusion transcripts as a diagnostic test for peripheral primitive neuroectodermal tumors of childhood.* Diagn Mol Pathol, 1993. **2**(3): p. 147-57.
54. Newman, E.N., R.L. Jones, and D.S. Hawkins, *An evaluation of [F-18]-fluorodeoxy-D-glucose positron emission tomography, bone scan, and bone marrow aspiration/biopsy as staging investigations in Ewing sarcoma.* Pediatr Blood Cancer, 2013. **60**(7): p. 1113-7.
55. Gaspar, N., et al., *Ewing Sarcoma: Current Management and Future Approaches Through Collaboration.* J Clin Oncol, 2015. **33**(27): p. 3036-46.
56. Stahl, M., et al., *Risk of recurrence and survival after relapse in patients with Ewing sarcoma.* Pediatr Blood Cancer, 2011. **57**(4): p. 549-53.
57. Meyers, P.A. and A.S. Levy, *Ewing's sarcoma.* Curr Treat Options Oncol, 2000. **1**(3): p. 247-57.
58. Erkizan, H.V., et al., *A small molecule blocking oncogenic protein EWS-FLI1 interaction with RNA helicase A inhibits growth of Ewing's sarcoma.* Nat Med, 2009. **15**(7): p. 750-6.
59. Theisen, E.R., et al., *Therapeutic opportunities in Ewing sarcoma: EWS-FLI inhibition via LSD1 targeting.* Oncotarget, 2016. **7**(14): p. 17616-30.
60. Sonnemann, J., et al., *Histone deacetylase inhibitors induce cell death and enhance the apoptosis-inducing activity of TRAIL in Ewing's sarcoma cells.* J Cancer Res Clin Oncol, 2007. **133**(11): p. 847-58.
61. Hurtubise, A., M.L. Bernstein, and R.L. Momparler, *Preclinical evaluation of the antineoplastic action of 5-aza-2'-deoxycytidine and different histone deacetylase inhibitors on human Ewing's sarcoma cells.* Cancer Cell Int, 2008. **8**: p. 16.
62. Manara, M.C., et al., *CD99 triggering induces methuosis of Ewing sarcoma cells through IGF-1R/RAS/Rac1 signaling.* Oncotarget, 2016. **7**(48): p. 79925-79942.
63. Guerzoni, C., et al., *CD99 triggering in Ewing sarcoma delivers a lethal signal through p53 pathway reactivation and cooperates with doxorubicin.* Clin Cancer Res, 2015. **21**(1): p. 146-56.
64. Scotlandi, K., et al., *Targeting CD99 in association with doxorubicin: an effective combined treatment for Ewing's sarcoma.* Eur J Cancer, 2006. **42**(1): p. 91-6.
65. Gellini, M., et al., *Generation of human single-chain antibody to the CD99 cell surface determinant specifically recognizing Ewing's sarcoma tumor cells.* Curr Pharm Biotechnol, 2013. **14**(4): p. 449-63.
66. Dworzak, M.N., et al., *CD99 expression in T-lineage ALL: implications for flow cytometric detection of minimal residual disease.* Leukemia, 2004. **18**(4): p. 703-8.
67. Seol, H.J., et al., *Overexpression of CD99 Increases the Migration and Invasiveness of Human Malignant Glioma Cells.* Genes Cancer, 2012. **3**(9-10): p. 535-49.
68. Celik, H., et al., *Clofarabine inhibits Ewing sarcoma growth through a novel molecular mechanism involving direct binding to CD99.* Oncogene, 2018. **37**(16): p. 2181-2196.
69. Gao, M., et al., *Discovery and optimization of 3-(2-(Pyrazolo[1,5-a]pyrimidin-6-yl)ethynyl)benzamides as novel selective and orally bioavailable discoidin domain receptor 1 (DDR1) inhibitors.* J Med Chem, 2013. **56**(8): p. 3281-95.
70. Friedbichler, K., et al., *Pharmacodynamic and antineoplastic activity of BI 836845, a fully human IGF ligand-neutralizing antibody, and mechanistic rationale for combination with rapamycin.* Mol Cancer Ther, 2014. **13**(2): p. 399-409.
71. Olmos, D., et al., *Safety, pharmacokinetics, and preliminary activity of the anti-IGF-1R antibody figitumumab (CP-751,871) in patients with sarcoma and Ewing's sarcoma: a phase 1 expansion cohort study.* Lancet Oncol, 2010. **11**(2): p. 129-35.
72. Tolcher, A.W., et al., *Phase I, pharmacokinetic, and pharmacodynamic study of AMG 479, a fully human monoclonal antibody to insulin-like growth factor receptor 1.* J Clin Oncol, 2009. **27**(34): p. 5800-7.
73. Olmos, D., et al., *Targeting the Insulin-Like Growth Factor 1 Receptor in Ewing's Sarcoma: Reality and Expectations.* Sarcoma, 2011. **2011**: p. 402508.
74. Garofalo, C., et al., *Identification of common and distinctive mechanisms of resistance to different anti-IGF-IR agents in Ewing's sarcoma.* Mol Endocrinol, 2012. **26**(9): p. 1603-16.

75. Tawbi, H.A., et al., *Pembrolizumab in advanced soft-tissue sarcoma and bone sarcoma (SARC028): a multicentre, two-cohort, single-arm, open-label, phase 2 trial.* Lancet Oncol, 2017. **18**(11): p. 1493-1501.
76. Spurny, C., et al., *Programmed cell death ligand 1 (PD-L1) expression is not a predominant feature in Ewing sarcomas.* Pediatr Blood Cancer, 2018. **65**(1).
77. Huang, X., et al., *IGF1R- and ROR1-Specific CAR T Cells as a Potential Therapy for High Risk Sarcomas.* PLoS One, 2015. **10**(7): p. e0133152.
78. Yarchoan, M., et al., *Targeting neoantigens to augment antitumour immunity.* Nat Rev Cancer, 2017. **17**(4): p. 209-222.
79. Higgins, C.F., *ABC transporters: from microorganisms to man.* Annu Rev Cell Biol, 1992. **8**: p. 67-113.
80. Shitan, N., et al., *Involvement of CjMDR1, a plant multidrug-resistance-type ATP-binding cassette protein, in alkaloid transport in Coptis japonica.* Proc Natl Acad Sci U S A, 2003. **100**(2): p. 751-6.
81. Quazi, F. and R.S. Molday, *Differential phospholipid substrates and directional transport by ATP-binding cassette proteins ABCA1, ABCA7, and ABCA4 and disease-causing mutants.* J Biol Chem, 2013. **288**(48): p. 34414-26.
82. Quazi, F., S. Lenevich, and R.S. Molday, *ABCA4 is an N-retinylidene-phosphatidylethanolamine and phosphatidylethanolamine importer.* Nat Commun, 2012. **3**: p. 925.
83. Ford, R.C. and K. Beis, *Learning the ABCs one at a time: structure and mechanism of ABC transporters.* Biochem Soc Trans, 2019. **47**(1): p. 23-36.
84. Dean, M., A. Rzhetsky, and R. Allikmets, *The human ATP-binding cassette (ABC) transporter superfamily.* Genome Res, 2001. **11**(7): p. 1156-66.
85. Jones, P.M. and A.M. George, *The ABC transporter structure and mechanism: perspectives on recent research.* Cell Mol Life Sci, 2004. **61**(6): p. 682-99.
86. Mohammad, I.S., W. He, and L. Yin, *Understanding of human ATP binding cassette superfamily and novel multidrug resistance modulators to overcome MDR.* Biomed Pharmacother, 2018. **100**: p. 335-348.
87. Falasca, M. and K.J. Linton, *Investigational ABC transporter inhibitors.* Expert Opin Investig Drugs, 2012. **21**(5): p. 657-66.
88. Bodo, A., et al., *The role of multidrug transporters in drug availability, metabolism and toxicity.* Toxicol Lett, 2003. **140-141**: p. 133-43.
89. Tarling, E.J., T.Q. de Aguiar Vallim, and P.A. Edwards, *Role of ABC transporters in lipid transport and human disease.* Trends Endocrinol Metab, 2013. **24**(7): p. 342-50.
90. Domenichini, A., A. Adamska, and M. Falasca, *ABC transporters as cancer drivers: Potential functions in cancer development.* Biochim Biophys Acta Gen Subj, 2019. **1863**(1): p. 52-60.
91. Sun, S., et al., *Prognostic Value and Implication for Chemotherapy Treatment of ABCB1 in Epithelial Ovarian Cancer: A Meta-Analysis.* PLoS One, 2016. **11**(11): p. e0166058.
92. Kim, H., et al., *Prognostic value of biomarkers related to drug resistance in patients with advanced epithelial ovarian cancer.* Anticancer Res, 2012. **32**(2): p. 589-94.
93. Zou, F., et al., *Prognostic significance of ABCB1 in stage I lung adenocarcinoma.* Oncol Lett, 2017. **14**(1): p. 313-321.
94. Wang, Y., et al., *Genetic variants in ABCG1 are associated with survival of nonsmall-cell lung cancer patients.* Int J Cancer, 2016. **138**(11): p. 2592-601.
95. Munoz, M., et al., *Role of the MRP1/ABCC1 multidrug transporter protein in cancer.* IUBMB Life, 2007. **59**(12): p. 752-7.
96. Ji, N., et al., *VS-4718 Antagonizes Multidrug Resistance in ABCB1- and ABCG2-Overexpressing Cancer Cells by Inhibiting the Efflux Function of ABC Transporters.* Front Pharmacol, 2018. **9**: p. 1236.
97. Allen, J.D., et al., *Potent and specific inhibition of the breast cancer resistance protein multidrug transporter in vitro and in mouse intestine by a novel analogue of fumitremorgin C.* Mol Cancer Ther, 2002. **1**(6): p. 417-25.
98. Fletcher, J.I., et al., *ABC transporters in cancer: more than just drug efflux pumps.* Nat Rev Cancer, 2010. **10**(2): p. 147-56.

99. Morris, M.E., V. Rodriguez-Cruz, and M.A. Felmlee, *SLC and ABC Transporters: Expression, Localization, and Species Differences at the Blood-Brain and the Blood-Cerebrospinal Fluid Barriers.* AAPS J, 2017. **19**(5): p. 1317-1331.
100. Lingineni, K., et al., *The role of multidrug resistance protein (MRP-1) as an active efflux transporter on blood-brain barrier (BBB) permeability.* Mol Divers, 2017. **21**(2): p. 355-365.
101. Kryczka, J. and J. Boncela, *Cell Migration Related to MDR-Another Impediment to Effective Chemotherapy?* Molecules, 2018. **23**(2).
102. Amiri-Kordestani, L., et al., *Targeting MDR in breast and lung cancer: discriminating its potential importance from the failure of drug resistance reversal studies.* Drug Resist Updat, 2012. **15**(1-2): p. 50-61.
103. Shaffer, B.C., et al., *Drug resistance: still a daunting challenge to the successful treatment of AML.* Drug Resist Updat, 2012. **15**(1-2): p. 62-9.
104. Fletcher, J.I., et al., *ABC transporters as mediators of drug resistance and contributors to cancer cell biology.* Drug Resist Updat, 2016. **26**: p. 1-9.
105. Pasello, M., A.M. Giudice, and K. Scotlandi, *The ABC subfamily A transporters: multifaceted players with incipient potentialities in cancer.* Semin Cancer Biol, 2019.
106. Copsel, S., et al., *Multidrug resistance protein 4 (MRP4/ABCC4) regulates cAMP cellular levels and controls human leukemia cell proliferation and differentiation.* J Biol Chem, 2011. **286**(9): p. 6979-88.
107. Hedditch, E.L., et al., *ABCA transporter gene expression and poor outcome in epithelial ovarian cancer.* J Natl Cancer Inst, 2014. **106**(7).
108. Henderson, M.J., et al., *ABCC multidrug transporters in childhood neuroblastoma: clinical and biological effects independent of cytotoxic drug efflux.* J Natl Cancer Inst, 2011. **103**(16): p. 1236-51.
109. Mochida, Y., et al., *The role of P-glycoprotein in intestinal tumorigenesis: disruption of mdr1a suppresses polyp formation in Apc(Min/+) mice.* Carcinogenesis, 2003. **24**(7): p. 1219-24.
110. Huls, M., F.G. Russel, and R. Masereeuw, *The role of ATP binding cassette transporters in tissue defense and organ regeneration.* J Pharmacol Exp Ther, 2009. **328**(1): p. 3-9.
111. Nigam, S.K., et al., *Handling of Drugs, Metabolites, and Uremic Toxins by Kidney Proximal Tubule Drug Transporters.* Clin J Am Soc Nephrol, 2015. **10**(11): p. 2039-49.
112. Albrecht, C. and E. Viturro, *The ABCA subfamily--gene and protein structures, functions and associated hereditary diseases.* Pflugers Arch, 2007. **453**(5): p. 581-9.
113. Akiyama, M., et al., *Mutations in lipid transporter ABCA12 in harlequin ichthyosis and functional recovery by corrective gene transfer.* J Clin Invest, 2005. **115**(7): p. 1777-84.
114. Akiyama, M., *ABCA12 mutations and autosomal recessive congenital ichthyosis: a review of genotype/phenotype correlations and of pathogenetic concepts.* Hum Mutat, 2010. **31**(10): p. 1090-6.
115. Allikmets, R., et al., *Mutation of the Stargardt disease gene (ABCR) in age-related macular degeneration.* Science, 1997. **277**(5333): p. 1805-7.
116. Tanna, P., et al., *Stargardt disease: clinical features, molecular genetics, animal models and therapeutic options.* Br J Ophthalmol, 2017. **101**(1): p. 25-30.
117. Fasano, T., et al., *Novel mutations of ABCA1 transporter in patients with Tangier disease and familial HDL deficiency.* Mol Genet Metab, 2012. **107**(3): p. 534-41.
118. Kruit, J.K., et al., *Loss of both ABCA1 and ABCG1 results in increased disturbances in islet sterol homeostasis, inflammation, and impaired beta-cell function.* Diabetes, 2012. **61**(3): p. 659-64.
119. Yan, H., et al., *ATP-binding cassette sub-family a member1 gene mutation improves lipid metabolic abnormalities in diabetes mellitus.* Lipids Health Dis, 2019. **18**(1): p. 103.
120. Zhao, Y., et al., *Role of ABC transporters in the pathology of Alzheimer's disease.* Rev Neurosci, 2017. **28**(2): p. 155-159.
121. Gabbi, C., M. Warner, and J.A. Gustafsson, *Action mechanisms of Liver X Receptors.* Biochem Biophys Res Commun, 2014. **446**(3): p. 647-50.
122. Goldstein, J.L., R.A. DeBose-Boyd, and M.S. Brown, *Protein sensors for membrane sterols.* Cell, 2006. **124**(1): p. 35-46.

123. Costet, P., et al., *Sterol-dependent transactivation of the ABC1 promoter by the liver X receptor/retinoid X receptor.* J Biol Chem, 2000. **275**(36): p. 28240-5.
124. Venkateswaran, A., et al., *Control of cellular cholesterol efflux by the nuclear oxysterol receptor LXR alpha.* Proc Natl Acad Sci U S A, 2000. **97**(22): p. 12097-102.
125. Zeng, L., et al., *Sterol-responsive element-binding protein (SREBP) 2 down-regulates ATP-binding cassette transporter A1 in vascular endothelial cells: a novel role of SREBP in regulating cholesterol metabolism.* J Biol Chem, 2004. **279**(47): p. 48801-7.
126. Tamehiro, N., et al., *Sterol regulatory element-binding protein-2- and liver X receptor-driven dual promoter regulation of hepatic ABC transporter A1 gene expression: mechanism underlying the unique response to cellular cholesterol status.* J Biol Chem, 2007. **282**(29): p. 21090-9.
127. Iwamoto, N., et al., *ABCA7 expression is regulated by cellular cholesterol through the SREBP2 pathway and associated with phagocytosis.* J Lipid Res, 2006. **47**(9): p. 1915-27.
128. Madison, B.B., *Srebp2: A master regulator of sterol and fatty acid synthesis.* J Lipid Res, 2016. **57**(3): p. 333-5.
129. Abe-Dohmae, S., et al., *Human ABCA7 supports apolipoprotein-mediated release of cellular cholesterol and phospholipid to generate high density lipoprotein.* J Biol Chem, 2004. **279**(1): p. 604-11.
130. Ishigami, M., et al., *Temporary sequestration of cholesterol and phosphatidylcholine within extracellular domains of ABCA1 during nascent HDL generation.* Sci Rep, 2018. **8**(1): p. 6170.
131. Jehle, A.W., et al., *ATP-binding cassette transporter A7 enhances phagocytosis of apoptotic cells and associated ERK signaling in macrophages.* J Cell Biol, 2006. **174**(4): p. 547-56.
132. Linsel-Nitschke, P., et al., *Potential role of ABCA7 in cellular lipid efflux to apoA-I.* J Lipid Res, 2005. **46**(1): p. 86-92.
133. Mack, J.T., et al., *The ABCA2 transporter: intracellular roles in trafficking and metabolism of LDL-derived cholesterol and sterol-related compounds.* Curr Drug Metab, 2007. **8**(1): p. 47-57.
134. van der Kant, R., et al., *Cholesterol-binding molecules MLN64 and ORP1L mark distinct late endosomes with transporters ABCA3 and NPC1.* J Lipid Res, 2013. **54**(8): p. 2153-65.
135. Trigueros-Motos, L., et al., *ABCA8 Regulates Cholesterol Efflux and High-Density Lipoprotein Cholesterol Levels.* Arterioscler Thromb Vasc Biol, 2017. **37**(11): p. 2147-2155.
136. Long, J., et al., *Lipid metabolism and carcinogenesis, cancer development.* Am J Cancer Res, 2018. **8**(5): p. 778-791.
137. Currie, E., et al., *Cellular fatty acid metabolism and cancer.* Cell Metab, 2013. **18**(2): p. 153-61.
138. Luo, X., et al., *Emerging roles of lipid metabolism in cancer metastasis.* Mol Cancer, 2017. **16**(1): p. 76.
139. Luo, X., et al., *The implications of signaling lipids in cancer metastasis.* Exp Mol Med, 2018. **50**(9): p. 127.
140. Mollinedo, F. and C. Gajate, *Lipid rafts as major platforms for signaling regulation in cancer.* Adv Biol Regul, 2015. **57**: p. 130-46.
141. Murai, T., et al., *Membrane cholesterol modulates the hyaluronan-binding ability of CD44 in T lymphocytes and controls rolling under shear flow.* J Cell Sci, 2013. **126**(Pt 15): p. 3284-94.
142. Xu, L., et al., *Lipid raft-regulated IGF-1R activation antagonizes TRAIL-induced apoptosis in gastric cancer cells.* FEBS Lett, 2013. **587**(23): p. 3815-23.
143. Irwin, M.E., et al., *Lipid raft localization of EGFR alters the response of cancer cells to the EGFR tyrosine kinase inhibitor gefitinib.* J Cell Physiol, 2011. **226**(9): p. 2316-28.
144. Orr, G., et al., *Cholesterol dictates the freedom of EGF receptors and HER2 in the plane of the membrane.* Biophys J, 2005. **89**(2): p. 1362-73.
145. Jeong, J. and A.P. McMahon, *Cholesterol modification of Hedgehog family proteins.* J Clin Invest, 2002. **110**(5): p. 591-6.
146. Huang, P., et al., *Cellular Cholesterol Directly Activates Smoothened in Hedgehog Signaling.* Cell, 2016. **166**(5): p. 1176-1187 e14.
147. Guixa-Gonzalez, R., et al., *Membrane cholesterol access into a G-protein-coupled receptor.* Nat Commun, 2017. **8**: p. 14505.

148. Rivel, T., C. Ramseyer, and S. Yesylevskyy, *The asymmetry of plasma membranes and their cholesterol content influence the uptake of cisplatin.* Sci Rep, 2019. **9**(1): p. 5627.
149. Yin, H.L. and P.A. Janmey, *Phosphoinositide regulation of the actin cytoskeleton.* Annu Rev Physiol, 2003. **65**: p. 761-89.
150. Padron, D., et al., *Phosphatidylinositol phosphate 5-kinase Ibeta recruits AP-2 to the plasma membrane and regulates rates of constitutive endocytosis.* J Cell Biol, 2003. **162**(4): p. 693-701.
151. Landry, Y.D., et al., *ATP-binding cassette transporter A1 expression disrupts raft membrane microdomains through its ATPase-related functions.* J Biol Chem, 2006. **281**(47): p. 36091-101.
152. Zha, X., J. Genest, Jr., and R. McPherson, *Endocytosis is enhanced in Tangier fibroblasts: possible role of ATP-binding cassette protein A1 in endosomal vesicular transport.* J Biol Chem, 2001. **276**(42): p. 39476-83.
153. Serra, M., et al., *Analysis of P-glycoprotein expression in osteosarcoma.* Eur J Cancer, 1995. **31A**(12): p. 1998-2002.
154. Liu, T., et al., *Targeting ABCB1 (MDR1) in multi-drug resistant osteosarcoma cells using the CRISPR-Cas9 system to reverse drug resistance.* Oncotarget, 2016. **7**(50): p. 83502-83513.
155. Roessner, A., et al., *Prognostic implication of immunodetection of P glycoprotein in Ewing's sarcoma.* J Cancer Res Clin Oncol, 1993. **119**(4): p. 185-9.
156. Perri, T., et al., *Effect of P-glycoprotein expression on outcome in the Ewing family of tumors.* Pediatr Hematol Oncol, 2001. **18**(5): p. 325-34.
157. Scotlandi, K., et al., *Prognostic and therapeutic relevance of HER2 expression in osteosarcoma and Ewing's sarcoma.* Eur J Cancer, 2005. **41**(9): p. 1349-61.
158. Roundhill, E. and S. Burchill, *Membrane expression of MRP-1, but not MRP-1 splicing or Pgp expression, predicts survival in patients with ESFT.* Br J Cancer, 2013. **109**(1): p. 195-206.
159. Zambo, I., et al., *Expression of nestin, CD133 and ABCG2 in relation to the clinical outcome in pediatric sarcomas.* Cancer Biomark, 2016. **17**(1): p. 107-16.
160. Schroeder, H.W., Jr. and L. Cavacini, *Structure and function of immunoglobulins.* J Allergy Clin Immunol, 2010. **125**(2 Suppl 2): p. S41-52.
161. Brekke, O.H. and I. Sandlie, *Therapeutic antibodies for human diseases at the dawn of the twenty-first century.* Nat Rev Drug Discov, 2003. **2**(1): p. 52-62.
162. Charles A Janeway, J., Paul Travers, Mark Walport, and Mark J Shlomchik, *Immunobiology: The Immune System in Health and Disease.* Immunobiology. 5th edition., 2001.
163. Ecker, D.M., S.D. Jones, and H.L. Levine, *The therapeutic monoclonal antibody market.* MAbs, 2015. **7**(1): p. 9-14.
164. Frenzel, A., et al., *Designing Human Antibodies by Phage Display.* Transfus Med Hemother, 2017. **44**(5): p. 312-318.
165. Emmons, C. and L.G. Hunsicker, *Muromonab-CD3 (Orthoclone OKT3): the first monoclonal antibody approved for therapeutic use.* Iowa Med, 1987. **77**(2): p. 78-82.
166. Kohler, G. and C. Milstein, *Continuous cultures of fused cells secreting antibody of predefined specificity.* Nature, 1975. **256**(5517): p. 495-7.
167. Hwang, W.Y. and J. Foote, *Immunogenicity of engineered antibodies.* Methods, 2005. **36**(1): p. 3-10.
168. Green, L.L., *Antibody engineering via genetic engineering of the mouse: XenoMouse strains are a vehicle for the facile generation of therapeutic human monoclonal antibodies.* J Immunol Methods, 1999. **231**(1-2): p. 11-23.
169. Harada, G., et al., *In vitro immunization of Epstein-Barr virus-immortalized B cells augments antigen-specific antibody production.* Cytotechnology, 2013. **65**(6): p. 979-83.
170. McCafferty, J., et al., *Phage antibodies: filamentous phage displaying antibody variable domains.* Nature, 1990. **348**(6301): p. 552-4.
171. Viti, F., et al., *Design and use of phage display libraries for the selection of antibodies and enzymes.* Methods Enzymol, 2000. **326**: p. 480-505.
172. Weiner, G.J., *Building better monoclonal antibody-based therapeutics.* Nat Rev Cancer, 2015. **15**(6): p. 361-70.

173. Mayes, P.A., K.W. Hance, and A. Hoos, *The promise and challenges of immune agonist antibody development in cancer.* Nat Rev Drug Discov, 2018. **17**(7): p. 509-527.
174. Neri, D., *Antibody-Cytokine Fusions: Versatile Products for the Modulation of Anticancer Immunity.* Cancer Immunol Res, 2019. **7**(3): p. 348-354.
175. Spadiut, O., et al., *Microbials for the production of monoclonal antibodies and antibody fragments.* Trends Biotechnol, 2014. **32**(1): p. 54-60.
176. Jefferis, R., *Recombinant antibody therapeutics: the impact of glycosylation on mechanisms of action.* Trends Pharmacol Sci, 2009. **30**(7): p. 356-62.
177. Jevsevar, S., M. Kusterle, and M. Kenig, *PEGylation of antibody fragments for half-life extension.* Methods Mol Biol, 2012. **901**: p. 233-46.
178. Andersen, J.T., et al., *Single-chain variable fragment albumin fusions bind the neonatal Fc receptor (FcRn) in a species-dependent manner: implications for in vivo half-life evaluation of albumin fusion therapeutics.* J Biol Chem, 2013. **288**(33): p. 24277-85.
179. Nelson, A.L., *Antibody fragments: hope and hype.* MAbs, 2010. **2**(1): p. 77-83.
180. Nelson, A.L., E. Dhimolea, and J.M. Reichert, *Development trends for human monoclonal antibody therapeutics.* Nat Rev Drug Discov, 2010. **9**(10): p. 767-74.
181. Bazin-Redureau, M.I., C.B. Renard, and J.M. Scherrmann, *Pharmacokinetics of heterologous and homologous immunoglobulin G, F(ab')2 and Fab after intravenous administration in the rat.* J Pharm Pharmacol, 1997. **49**(3): p. 277-81.
182. Li, Z., et al., *Influence of molecular size on tissue distribution of antibody fragments.* MAbs, 2016. **8**(1): p. 113-9.
183. Clackson, T., et al., *Making antibody fragments using phage display libraries.* Nature, 1991. **352**(6336): p. 624-8.
184. Marks, J.D., et al., *By-passing immunization. Human antibodies from V-gene libraries displayed on phage.* J Mol Biol, 1991. **222**(3): p. 581-97.
185. Hoogenboom, H.R. and G. Winter, *By-passing immunisation. Human antibodies from synthetic repertoires of germline VH gene segments rearranged in vitro.* J Mol Biol, 1992. **227**(2): p. 381-8.
186. Munster, P., et al., *Safety and pharmacokinetics of MM-302, a HER2-targeted antibody-liposomal doxorubicin conjugate, in patients with advanced HER2-positive breast cancer: a phase 1 dose-escalation study.* Br J Cancer, 2018. **119**(9): p. 1086-1093.
187. Fleuren, E.D., et al., *Theranostic applications of antibodies in oncology.* Mol Oncol, 2014. **8**(4): p. 799-812.
188. Freise, A.C. and A.M. Wu, *In vivo imaging with antibodies and engineered fragments.* Mol Immunol, 2015. **67**(2 Pt A): p. 142-52.
189. van Brussel, A.S., et al., *Hypoxia-Targeting Fluorescent Nanobodies for Optical Molecular Imaging of Pre-Invasive Breast Cancer.* Mol Imaging Biol, 2016. **18**(4): p. 535-44.
190. Kijanka, M.M., et al., *Optical imaging of pre-invasive breast cancer with a combination of VHHs targeting CAIX and HER2 increases contrast and facilitates tumour characterization.* EJNMMI Res, 2016. **6**(1): p. 14.
191. Viola-Villegas, N.T., et al., *Noninvasive Imaging of PSMA in prostate tumors with (89)Zr-Labeled huJ591 engineered antibody fragments: the faster alternatives.* Mol Pharm, 2014. **11**(11): p. 3965-73.
192. Maier, J., B. Traenkle, and U. Rothbauer, *Real-time analysis of epithelial-mesenchymal transition using fluorescent single-domain antibodies.* Sci Rep, 2015. **5**: p. 13402.
193. Smith, G.P., *Filamentous fusion phage: novel expression vectors that display cloned antigens on the virion surface.* Science, 1985. **228**(4705): p. 1315-7.
194. Bird, R.E., et al., *Single-chain antigen-binding proteins.* Science, 1988. **242**(4877): p. 423-6.
195. Skerra, A. and A. Pluckthun, *Assembly of a functional immunoglobulin Fv fragment in Escherichia coli.* Science, 1988. **240**(4855): p. 1038-41.
196. Barbas, C.F., 3rd, et al., *Assembly of combinatorial antibody libraries on phage surfaces: the gene III site.* Proc Natl Acad Sci U S A, 1991. **88**(18): p. 7978-82.

197. Hess, G.T., et al., *M13 bacteriophage display framework that allows sortase-mediated modification of surface-accessible phage proteins.* Bioconjug Chem, 2012. **23**(7): p. 1478-87.
198. Ledsgaard, L., et al., *Basics of Antibody Phage Display Technology.* Toxins (Basel), 2018. **10**(6).
199. Greenwood, J., A.E. Willis, and R.N. Perham, *Multiple display of foreign peptides on a filamentous bacteriophage. Peptides from Plasmodium falciparum circumsporozoite protein as antigens.* J Mol Biol, 1991. **220**(4): p. 821-7.
200. Frenzel, A., T. Schirrmann, and M. Hust, *Phage display-derived human antibodies in clinical development and therapy.* MAbs, 2016. **8**(7): p. 1177-1194.
201. Hanes, J. and A. Pluckthun, *In vitro selection and evolution of functional proteins by using ribosome display.* Proc Natl Acad Sci U S A, 1997. **94**(10): p. 4937-42.
202. Francisco, J.A., et al., *Production and fluorescence-activated cell sorting of Escherichia coli expressing a functional antibody fragment on the external surface.* Proc Natl Acad Sci U S A, 1993. **90**(22): p. 10444-8.
203. Beerli, R.R., et al., *Isolation of human monoclonal antibodies by mammalian cell display.* Proc Natl Acad Sci U S A, 2008. **105**(38): p. 14336-41.
204. Griffiths, A.D., et al., *Isolation of high affinity human antibodies directly from large synthetic repertoires.* EMBO J, 1994. **13**(14): p. 3245-60.
205. Hoogenboom, H.R., *Selecting and screening recombinant antibody libraries.* Nat Biotechnol, 2005. **23**(9): p. 1105-16.
206. Kabat, E.A. and T.T. Wu, *Identical V region amino acid sequences and segments of sequences in antibodies of different specificities. Relative contributions of VH and VL genes, minigenes, and complementarity-determining regions to binding of antibody-combining sites.* J Immunol, 1991. **147**(5): p. 1709-19.
207. Raghunathan, G., et al., *Antigen-binding site anatomy and somatic mutations in antibodies that recognize different types of antigens.* J Mol Recognit, 2012. **25**(3): p. 103-13.
208. Almagro, J.C., et al., *Phage Display Libraries for Antibody Therapeutic Discovery and Development.* Antibodies (Basel), 2019. **8**(3).
209. Shi, L., et al., *De novo selection of high-affinity antibodies from synthetic fab libraries displayed on phage as pIX fusion proteins.* J Mol Biol, 2010. **397**(2): p. 385-96.
210. Knappik, A., et al., *Fully synthetic human combinatorial antibody libraries (HuCAL) based on modular consensus frameworks and CDRs randomized with trinucleotides.* J Mol Biol, 2000. **296**(1): p. 57-86.
211. Lin, B., et al., *A step-wise approach significantly enhances protein yield of a rationally-designed agonist antibody fragment in E. coli.* Protein Expr Purif, 2008. **59**(1): p. 55-63.
212. Raybould, M.I.J., et al., *Five computational developability guidelines for therapeutic antibody profiling.* Proc Natl Acad Sci U S A, 2019.
213. Hulseweh, B., et al., *Human-like antibodies neutralizing Western equine encephalitis virus.* MAbs, 2014. **6**(3): p. 718-27.
214. Miethe, S., et al., *Development of Human-Like scFv-Fc Neutralizing Botulinum Neurotoxin E.* PLoS One, 2015. **10**(10): p. e0139905.
215. Miethe, S., et al., *Development of neutralizing scFv-Fc against botulinum neurotoxin A light chain from a macaque immune library.* MAbs, 2014. **6**(2): p. 446-59.
216. Pelat, T., M. Hust, and P. Thullier, *Obtention and engineering of non-human primate (NHP) antibodies for therapeutics.* Mini Rev Med Chem, 2009. **9**(14): p. 1633-8.
217. Rossant, C.J., et al., *Phage display and hybridoma generation of antibodies to human CXCR2 yields antibodies with distinct mechanisms and epitopes.* MAbs, 2014. **6**(6): p. 1425-38.
218. Cai, X. and A. Garen, *Anti-melanoma antibodies from melanoma patients immunized with genetically modified autologous tumor cells: selection of specific antibodies from single-chain Fv fusion phage libraries.* Proc Natl Acad Sci U S A, 1995. **92**(14): p. 6537-41.
219. Coomber, D.W., et al., *Generation of anti-p53 Fab fragments from individuals with colorectal cancer using phage display.* J Immunol, 1999. **163**(4): p. 2276-83.
220. Dantas-Barbosa, C., et al., *Isolation of osteosarcoma-associated human antibodies from a combinatorial Fab phage display library.* J Biomed Biotechnol, 2009. **2009**: p. 157531.

221. He, J., et al., *Construction and preliminary screening of a human phage single-chain antibody library associated with gastric cancer.* J Surg Res, 2002. **102**(2): p. 150-5.
222. Richard, G., et al., *In vivo neutralization of alpha-cobratoxin with high-affinity llama single-domain antibodies (VHHs) and a VHH-Fc antibody.* PLoS One, 2013. **8**(7): p. e69495.
223. Stewart, C.S., C.R. MacKenzie, and J.C. Hall, *Isolation, characterization and pentamerization of alpha-cobrotoxin specific single-domain antibodies from a naive phage display library: preliminary findings for antivenom development.* Toxicon, 2007. **49**(5): p. 699-709.
224. Pasello, M., et al., *Design and construction of a new human naive single-chain fragment variable antibody library, IORISS1.* J Biotechnol, 2016. **224**: p. 1-11.
225. de Kruif, J., E. Boel, and T. Logtenberg, *Selection and application of human single chain Fv antibody fragments from a semi-synthetic phage antibody display library with designed CDR3 regions.* J Mol Biol, 1995. **248**(1): p. 97-105.
226. Chothia, C., et al., *Structural repertoire of the human VH segments.* J Mol Biol, 1992. **227**(3): p. 799-817.
227. Tomlinson, I.M., et al., *The structural repertoire of the human V kappa domain.* EMBO J, 1995. **14**(18): p. 4628-38.
228. Tomlinson, I.M., et al., *The imprint of somatic hypermutation on the repertoire of human germline V genes.* J Mol Biol, 1996. **256**(5): p. 813-17.
229. Pini, A., et al., *Design and use of a phage display library. Human antibodies with subnanomolar affinity against a marker of angiogenesis eluted from a two-dimensional gel.* J Biol Chem, 1998. **273**(34): p. 21769-76.
230. Maruthachalam, B.V., et al., *A Single-Framework Synthetic Antibody Library Containing a Combination of Canonical and Variable Complementarity-Determining Regions.* Chembiochem, 2017. **18**(22): p. 2247-2259.
231. Nissim, A., et al., *Antibody fragments from a 'single pot' phage display library as immunochemical reagents.* EMBO J, 1994. **13**(3): p. 692-8.
232. Prassler, J., et al., *HuCAL PLATINUM, a synthetic Fab library optimized for sequence diversity and superior performance in mammalian expression systems.* J Mol Biol, 2011. **413**(1): p. 261-78.
233. Kirkham, P.M., et al., *Immunoglobulin VH clan and family identity predicts variable domain structure and may influence antigen binding.* EMBO J, 1992. **11**(2): p. 603-9.
234. Silacci, M., et al., *Design, construction, and characterization of a large synthetic human antibody phage display library.* Proteomics, 2005. **5**(9): p. 2340-50.
235. Villa, A., et al., *A novel synthetic naive human antibody library allows the isolation of antibodies against a new epitope of oncofetal fibronectin.* MAbs, 2011. **3**(3): p. 264-72.
236. Weber, M., et al., *A highly functional synthetic phage display library containing over 40 billion human antibody clones.* PLoS One, 2014. **9**(6): p. e100000.
237. Moghaddam, A., et al., *Identification of scFv antibody fragments that specifically recognise the heroin metabolite 6-monoacetylmorphine but not morphine.* J Immunol Methods, 2003. **280**(1-2): p. 139-55.
238. Breitling, F., et al., *A surface expression vector for antibody screening.* Gene, 1991. **104**(2): p. 147-53.
239. Hust, M., et al., *The production of a genus-specific recombinant antibody (scFv) using a recombinant potyvirus protease.* J Virol Methods, 2002. **106**(2): p. 225-33.
240. Schutte, M., et al., *Identification of a putative Crf splice variant and generation of recombinant antibodies for the specific detection of Aspergillus fumigatus.* PLoS One, 2009. **4**(8): p. e6625.
241. Noren, C.J., et al., *A general method for site-specific incorporation of unnatural amino acids into proteins.* Science, 1989. **244**(4901): p. 182-8.
242. Low, N.M., P.H. Holliger, and G. Winter, *Mimicking somatic hypermutation: affinity maturation of antibodies displayed on bacteriophage using a bacterial mutator strain.* J Mol Biol, 1996. **260**(3): p. 359-68.
243. Pfaffen, S., et al., *Isolation and characterization of human monoclonal antibodies specific to MMP-1A, MMP-2 and MMP-3.* Exp Cell Res, 2010. **316**(5): p. 836-47.

244. Ravenni, N., M. Weber, and D. Neri, *A human monoclonal antibody specific to placental alkaline phosphatase, a marker of ovarian cancer.* MAbs, 2014. **6**(1): p. 86-94.
245. Hawkins, R.E., S.J. Russell, and G. Winter, *Selection of phage antibodies by binding affinity. Mimicking affinity maturation.* J Mol Biol, 1992. **226**(3): p. 889-96.
246. Dubel, S., *Recombinant therapeutic antibodies.* Appl Microbiol Biotechnol, 2007. **74**(4): p. 723-9.
247. Patrizia Nanni, L.L., [...], and Katia Scotlandi, *Bone sarcoma patient-derived xenografts are faithful and stable preclinical models for molecular and therapeutic investigations.* Scientific Reports, 2019.
248. Gai, J., et al., *FoxO regulates expression of ABCA6, an intracellular ATP-binding-cassette transporter responsive to cholesterol.* Int J Biochem Cell Biol, 2013. **45**(11): p. 2651-9.
249. Greer, E.L. and A. Brunet, *FOXO transcription factors at the interface between longevity and tumor suppression.* Oncogene, 2005. **24**(50): p. 7410-25.
250. Ewert, S., et al., *Biophysical properties of human antibody variable domains.* J Mol Biol, 2003. **325**(3): p. 531-53.
251. Igawa, T., et al., *Engineering the variable region of therapeutic IgG antibodies.* MAbs, 2011. **3**(3): p. 243-52.
252. Williams, S.C., et al., *Sequence and evolution of the human germline V lambda repertoire.* J Mol Biol, 1996. **264**(2): p. 220-32.
253. Padlan, E.A., *Anatomy of the antibody molecule.* Mol Immunol, 1994. **31**(3): p. 169-217.
254. Castellani, P., et al., *The fibronectin isoform containing the ED-B oncofetal domain: a marker of angiogenesis.* Int J Cancer, 1994. **59**(5): p. 612-8.
255. Neri, D., et al., *Radioactive labeling of recombinant antibody fragments by phosphorylation using human casein kinase II and [gamma-32P]-ATP.* Nat Biotechnol, 1996. **14**(4): p. 485-90.
256. Helmer-Citterich, M. and A. Tramontano, *PUZZLE: a new method for automated protein docking based on surface shape complementarity.* J Mol Biol, 1994. **235**(3): p. 1021-31.
257. Sblattero, D. and A. Bradbury, *A definitive set of oligonucleotide primers for amplifying human V regions.* Immunotechnology, 1998. **3**(4): p. 271-8.
258. Pasello, M., et al., *Construction of Human Naive Antibody Gene Libraries.* Methods Mol Biol, 2018. **1827**: p. 73-91.
259. Lee, S.X., et al., *FoxO transcription factors are required for hepatic HDL cholesterol clearance.* J Clin Invest, 2018. **128**(4): p. 1615-1626.
260. Farhan, M., et al., *FOXO Signaling Pathways as Therapeutic Targets in Cancer.* Int J Biol Sci, 2017. **13**(7): p. 815-827.
261. Zhang, X., et al., *Phosphorylation of serine 256 suppresses transactivation by FKHR (FOXO1) by multiple mechanisms. Direct and indirect effects on nuclear/cytoplasmic shuttling and DNA binding.* J Biol Chem, 2002. **277**(47): p. 45276-84.
262. Sekine, Y., et al., *High-density lipoprotein induces proliferation and migration of human prostate androgen-independent cancer cells by an ABCA1-dependent mechanism.* Mol Cancer Res, 2010. **8**(9): p. 1284-94.
263. Kaminski, W.E., A. Piehler, and G. Schmitz, *Genomic organization of the human cholesterol-responsive ABC transporter ABCA7: tandem linkage with the minor histocompatibility antigen HA-1 gene.* Biochem Biophys Res Commun, 2000. **278**(3): p. 782-9.
264. Zhao, Z., et al., *CtBP promotes metastasis of breast cancer through repressing cholesterol and activating TGF-beta signaling.* Oncogene, 2019. **38**(12): p. 2076-2091.
265. Garofalo, C., et al., *Efficacy of and resistance to anti-IGF-1R therapies in Ewing's sarcoma is dependent on insulin receptor signaling.* Oncogene, 2011. **30**(24): p. 2730-40.
266. Bacci, G., et al., *Prognostic factors in non-metastatic Ewing's sarcoma tumor of bone: an analysis of 579 patients treated at a single institution with adjuvant or neoadjuvant chemotherapy between 1972 and 1998.* Acta Oncol, 2006. **45**(4): p. 469-75.
267. Ferrari, S., et al., *Nonmetastatic Ewing family tumors: high-dose chemotherapy with stem cell rescue in poor responder patients. Results of the Italian Sarcoma Group/Scandinavian Sarcoma Group III protocol.* Ann Oncol, 2011. **22**(5): p. 1221-7.

268. Picci, P., et al., *Chemotherapy-induced tumor necrosis as a prognostic factor in localized Ewing's sarcoma of the extremities.* J Clin Oncol, 1997. **15**(4): p. 1553-9.
269. Marino, M.T., et al., *Prognostic significance of miR-34a in Ewing sarcoma is associated with cyclin D1 and ki-67 expression.* Ann Oncol, 2014. **25**(10): p. 2080-6.
270. Bradburn, M.J., et al., *Survival analysis part II: multivariate data analysis--an introduction to concepts and methods.* Br J Cancer, 2003. **89**(3): p. 431-6.
271. Chou, T.C., et al., *Computerized quantitation of synergism and antagonism of taxol, topotecan, and cisplatin against human teratocarcinoma cell growth: a rational approach to clinical protocol design.* J Natl Cancer Inst, 1994. **86**(20): p. 1517-24.